

ROLE OF THE NUCLEAR ENVELOPE IN THE MECHANOREGULATION OF
ADIPOGENESIS

by

Matthew H. Goelzer



A dissertation

submitted in partial fulfillment

of the requirements for the degree of

Doctor of Philosophy in Material Science and Engineering

Boise State University

December 2021

© 2021

Matthew H. Goelzer

ALL RIGHTS RESERVED

BOISE STATE UNIVERSITY GRADUATE COLLEGE

DEFENSE COMMITTEE AND FINAL READING APPROVALS

of the dissertation submitted by

Matthew H. Goelzer

Dissertation Title: Role of the Nuclear Envelope in the Mechanoregulation of
 Adipogenesis

Date of Final Oral Examination: 30 November 2021

The following individuals read and discussed the dissertation submitted by student Matthew H. Goelzer, and they evaluated the student's presentation and response to questions during the final oral examination. They found that the student passed the final oral examination.

Gunes Uzer, Ph.D. Chair, Supervisory Committee

David Estrada, Ph.D. Member, Supervisory Committee

Eric Hayden, Ph.D. Member, Supervisory Committee

Andre van Wijnen, Ph.D. Member, Supervisory Committee

The final reading approval of the dissertation was granted by Gunes Uzer, Ph.D., Chair of the Supervisory Committee. The dissertation was approved by the Graduate College.

DEDICATION

This dissertation is dedicated to my parents whose sacrifices for me and my education I can never repay. May this dissertation be a testimony to their unending love and support.

ACKNOWLEDGMENTS

I would first like to thank Dr. Gunes Uzer for providing me an opportunity to work for him and be a part of his research. Without him I would not be the scientist I am today. He has made me a better communicator, researcher, and scientist. I am eternally grateful for the time and effort he has put into making me as a better scientist.

I would also like to thank my collaborators Dr. Janet Rubin, Dr. Amel Dudakovic, and Dr. Andre van Wijnen. All of them have provide new insights and ways to conduct better research and communicate my findings, all of which are part of the core of being an impactful scientist. Dr. Andre van Wijnen, who not only helped me through being a graduate advisory committee member, but has additionally given me his time and mentoring, making me think in new and creative ways that not only made the research better, but me better as well. I would like to also thank my other graduate advisory committee members Dr. David Estrada and Dr. Eric Hayden for guiding me through the process of graduate school and graduate research.

Lastly, I would like to thank my wife Dr. Julianna Goelzer. I would not have been able to survive the rigors and challenges of graduate school without her. Her undying support and encouragement kept me going. Not only did she support me through encouragement, but supported me through insightful discussions and suggestions on research techniques and directions. More can be said about her, but I will finish by saying that without her I would not be the person I am today.

ABSTRACT

Mechanical signals are known regulators of mesenchymal stem cell (MSC) fate, regulating their differentiation into osteoblasts, chondrocytes, and adipocytes. These relevant mechanical signals reach to nucleus through nuclear envelope proteins such as Lamin A/C and the Linker of the Nucleoskeleton and Cytoskeleton (LINC) complexes. Within the context of bone, clinically relevant mutations of Lamin A/C and the LINC complexes have been shown to alter adipogenic and osteogenic MSC differentiation patterns, suggesting that that nucleo-cytoskeletal connectivity provided by nuclear envelope is important in regulating MSC fate. Using MSC adipogenesis as a model of MSC mechanical regulation, the goal of this work is to further our understanding of how Lamin A/C and the LINC complex affect the mechanical regulation of MSC adipogenesis during application of mechanical forces. Investigation into the role of Lamin A/C in mechanoregulation revealed that activation of focal adhesions occurs independently from the loss of Lamin A/C. Additionally, Lamin A/C depletion and application daily mechanically challenge repress MSC adipogenesis independent of each other. Depletion of the LINC complex proteins Sun1/2 also significantly inhibited adipogenesis differentiation in MSCs. Depletion of Sun1/2 also increased heterochromatin marker H3K9me3 global levels, H3K9me3 foci count per nucleus, and increased enrichment in adipogenesis marker gene *Adipoq*. In contrast, expression of dominant-negative KASH domain, the cytoskeletal connector element of the LINC complex, resulted in accelerated MSC adipogenesis and no increased H3K9me3 foci count or enrichment on *Adipoq* gene.

Further research will utilize the dominant-negative KASH expression to investigate the role of the LINC complex in the mechanical regulation of adipogenesis and the spatio-temporal changes of adipogenic gene loci that occurs during adipogenesis and application of mechanical forces. Ultimately these studies will help to shed light into understanding the etiology of musculoskeletal problems in conditions that suffer from nuclear envelope instabilities including, aging, progeria, and microgravity.

TABLE OF CONTENTS

DEDICATION.....	iv
ACKNOWLEDGMENTS.....	v
ABSTRACT.....	vi
LIST OF PUBLICATIONS.....	xiii
LIST OF TABLES.....	xiv
LIST OF FIGURES.....	xv
LIST OF ABBREVIATIONS.....	xvii
CHAPTER ONE: NUCLEAR ENVELOPE MECHANOBIOLOGY: LINKING THE NUCLEAR STRUCTURE AND FUNCTION.....	1
Abstract.....	1
Introduction.....	2
Nuclear Structure and Mechanical Force.....	4
LINC Complex.....	4
Emerin.....	7
Spectrin, Intranuclear Actin, and Other Nuclear Proteins.....	9
Nuclear Lamins.....	11
Chromatin.....	14
Characterization of Nuclear Structure and Mechanics.....	17
Nuclear Structure.....	17
Intranuclear Strain.....	18

Intranuclear Stiffness	19
Linking Nuclear Mechanics and Mechanobiology	20
Visualizing Chromatin Dynamics in Living Cells.....	20
Fluorescence Imaging Techniques	21
Fluorescent Biomolecule Labeling.....	25
Conclusion.....	27
Study Objective and Hypotheses	40
Hypothesis 1.....	40
Hypothesis 2.....	40
CHAPTER TWO: LAMIN A/C FUNCTIONS INDEPENDENTLY FROM MECHANICAL SIGNALING DURING ADIPOGENESIS	41
Abstract	41
Introduction	42
Results	45
siRNA Depletion of Lamin A/C Weakens the Nuclear Elastic Modulus in MSCs	45
siRNA Depletion of Lamin A/C (LMNA) Increases Sun2 (SUN2) Nuclear Levels and Focal Adhesion Proteins	46
Focal Adhesions Maintain Response to Mechanical Stimulus in Lamin A/C Depleted MSCs	47
Application of Daily LIV Treatment Decreases Adipogenic Differentiation in MSCs	48
Differential Effect of Lamin A/C Depletion and LIV on mRNA Transcription during Adipogenic Differentiation	48
Lamin A/C Depletion Impedes Adipogenic Transcription in MSCs	49
LIV Decreases Interferon Signaling Pathway in siLMNA and siCnt1 Treated Cells	50

Materials and Methods	51
MSC Isolation.....	51
Cell Culture, Pharmacological Reagents, and Antibodies	52
LIV and Strain	53
Isolation of Focal Adhesions	53
siRNA Silencing Sequences	54
Isolation of Nuclei for Young's Modulus	54
RNA-Seq	54
Immunofluorescence.....	55
Nuclear Morphology.....	55
Western Blotting.....	56
Statistical Analysis.....	56
Discussion.....	57
Conclusion	61
CHAPTER THREE: DEPLETION OF SUN1/2 INDUCES HETEROCHROMATIN ACCRUAL IN MSCS.....	70
Abstract.....	70
Introduction.....	71
Materials and Methods	74
MSCs Isolation	74
dnKASH Cell Stable Cell Line.....	75
Cell Culture, Pharmacological Reagents, and Antibodies	75
siRNA Silencing Sequences	76
qPCR	76

RNA-Seq Analysis	76
Immunofluorescence	77
Image Analysis	78
Western Blotting	78
CUT&RUN	79
Statistical analysis and Reproducibility	79
Results	80
siSun and dnKASH Expression Alter Nuclear Morphology	80
Depletion of Sun1/2 Inhibits Adipogenesis	81
dnKASH Expression Induces Accelerated Adipogenesis in MSCs	81
Sun1/2 Depletion Decreases Adipogenesis and Lipid Metabolism Related Genes	82
Dominant-Negative KASH Expression Upregulates Adipogenesis Related Pathways	84
H3K9me3 Levels and Enrichment at Adipogenic Gene Adipoq Increases during Sun1/2 Depletion	85
H3K9me3 Levels and Enrichment at Adipogenic Gene Adipoq Remains Unaltered during dnKASH Disruption of the LINC Complex	86
Discussion and Conclusion	87
CHAPTER FOUR: FUTURE DIRECTIONS AND CONCLUSIONS	103
Introduction	103
Adipogenesis Commitment Depends upon Differentiation Time and Adipogenic Media Strength	104
Strain Induces Mechanoinhibition of Adipogenesis	106
Investigation Routes to Determine Mechanoregulatory Role of the LINC Complex	108

Conclusion	111
REFERENCES	112
APPENDIX	145

LIST OF PUBLICATIONS

List of Peer-Reviewed Publications

1. **Goelzer M**, Dudakovic A, Olcum M, Sen B, Ozcivici E, Rubin J, van Wijnen AJ, Uzer G. Lamin A/C Is Dispensable to Mechanical Repression of Adipogenesis. *Int J Mol Sci.* 2021 Jun 19;22(12):6580. doi: 10.3390/ijms22126580.
2. **Goelzer M**, Goelzer J, Ferguson ML, Neu CP, Uzer G. Nuclear envelope mechanobiology: linking the nuclear structure and function. *Nucleus.* 2021 Dec;12(1):90-114. doi: 10.1080/19491034.2021.1962610.
3. Kennedy Z, Newberg J, **Goelzer M**, Judex S, Fitzpatrick CK, Uzer G. Modeling stem cell nucleus mechanics using confocal microscopy. *Biomech Model Mechanobiol.* 2021 Aug 23. doi: 10.1007/s10237-021-01513-w.

List of Book Authorships

1. **Goelzer M**, Thompson W. R, Uzer G. in *Mechanobiology* (ed Glen L. Niebur) 79-98. Elsevier. 2020.

List of Conference Proceedings

1. **Goelzer M**, Olcum M, Bas G, Newberg J, Ozcivici E, Rubin J, Uzer G. Mechanotransduction In MSCs Is Not Dependent Upon Lamin A/C. Orthopedic Research Society. Austin, TX, USA. Feb 2nd 2019.
2. **Goelzer M**, Olcum M, Bas G, Newberg J, Ozcivici E, Rubin J, Uzer G. Lamin A/C Depletion Affects Chromatin Dynamics but Not Mechanoresponse in Mesenchymal Stem Cells. World Congress of Biomechanics. Dublin, Ireland. July 9th, 2018.
3. Bas G, **Goelzer M**, Pu S, Hayden E, Oxford J, Uzer G. Low Intensity Vibrations Augment Mechanoresponse in Aging Mesenchymal Stem Cells. World Congress of Biomechanics. Dublin, Ireland. July 9th, 2018.
4. Touchstone H, **Goelzer M**, Byrd R, Oxford J, Alwood J, Uzer G. Effects of Microgravity-induced Compromise of Cell Structure on MSC Mechanoresponse. World Congress of Biomechanics. Dublin, Ireland. July 9th, 2018.

LIST OF TABLES

Table 1.1	Common in vitro mechanical force simulation methods and their major studied outcomes.....	30
Table 1.2	Fluorescence Imaging Techniques.....	33
Table 1.3	Fluorescence Labeling Technologies and their benefits and drawbacks ..	36

LIST OF FIGURES

Figure 1.1	Nucleus is a mechanically-integrated mechanosignaling center.....	29
Figure 2.1	siRNA depletion of Lamin A/C weakens the nuclear elastic modulus in MSCs	62
Figure 2.2	siRNA depletion of Lamin A/C (LMNA) Increases Sun2 (SUN2) Nuclear Levels and Focal Adhesion Proteins	63
Figure 2.3	Focal adhesions maintain response to mechanical stimulus in Lamin A/C depleted MSCs	64
Figure 2.4	Application of daily LIV treatment decreases adipogenic differentiation in MSCs	65
Figure 2.5	Differential effect of Lamin A/C depletion and LIV on mRNA transcription during adipogenic differentiation.....	67
Figure 2.6	Lamin A/C depletion impedes adipogenic transcription in MSCs.....	68
Figure 2.7	LIV Decrease Interferon Signaling Pathway in siLMNA and siCntl Cells	69
Figure 3.1	Sun1/2 Depletion Alters Nuclear Morphology	92
Figure 3.2	Dominant-Negative KASH Disruption of the LINC Complex Reduces Nuclear Area	93
Figure 3.3	Depletion of Sun1/2 Inhibits Adipogenesis	94
Figure 3.4	dnKASH Expression Induces Accelerated Adipogenesis in MSCs	95
Figure 3.5	Sun1/2 Depletion Decreases Adipogenesis and Lipid Metabolism Related Genes	96
Figure 3.6	Dominant-Negative KASH Expression Upregulates Adipogenesis Related Pathways	97

Figure 3.7	Global levels of H3K9me3 and Enrichment on Adipoq increases during Sun1/2 depletion	99
Figure 3.8	H3K9me3 Levels Are Unaltered During dnKASH Disruption of the LINC Complex	101
Figure 4.1	Adipogenesis Markers Increased Due to Differentiation Duration and Indomethacin Amounts.	105
Figure 4.2	Strain Mechanoregulates Adipogenesis in MSCs.....	107
Figure 4.3	Loss of β -Catenin and Yap Nuclear functionality during loss of LINC Complex Function.....	109

LIST OF ABBREVIATIONS

MSCs	Mesenchymal stem cell
LINC	Linker of the Nucleoskeleton and Cytoskeleton
HGPS	Hutchens Gilford Progeria syndrome
FA	Focal Adhesion
LIV	Low intensity vibration
NPC	Nuclear Pore Complex
FAK	Focal Adhesion Kinase
GEFs	Guanine nucleotide exchange factors
GAPs	GTPase activation proteins
Larg	Leukemia-associated Rho guanine nucleotide exchange factor
WAS	Wiskott-Aldrich syndrome
FH1	Formin homology 1
FH2	Formin homology 2
ECM	Extracellular Matrix
NE	Nuclear Envelope
ONM	Outer nuclear membrane
INM	Inner nuclear membrane
ER	Endoplasmic reticulum
CH	Calponin homology
SR	Spectrin repeat

FHOD1	FH1/FH2 domain-containing protein 1
KASH	Klarsichtm ANC-1, Syne Homology
LAP-1	Latency associated polypeptide 1
VGLL4	Vestigial-Like 4
NLS	Nuclear localization signal
Ig	Immunoglobulin
LBR	Lamin B receptor
LAP	Latency associated polypeptides
MARs	Matrix associated regions
Arp	Actin related protein
PNS	Perinuclear space
BAF	Barrier-to-autointegration factor
YAP	Yes-associated-protein
LEM-domain	LAP2 β , Emerin, MAN1
FRAP	Fluorescence recovery after photobleaching
NM1	Nuclear myosin-1
HRR	Homologous recombination repair
NHEJ	Nonhomologous end-joining
NER	Nucleotide excision repair
MEF	Mouse embryonic fibroblasts
LAD	Lamin-associated domain
TAD	Topological-associated domain
CHO	Chinese hamster ovary

FRET	Förster Resonance Energy Transfer
FCS	Fluorescence Correlation Spectroscopy
FCCS	Fluorescence Cross Correlation Spectroscopy
SPT	Single Particle Tracking
TIRF	Total Internal Reflection Fluorescence
HILO	Highly inclined illuminated optical sheet
MSD	Mean squared displacement
dCas9	Deactivated Cas9
gRNA	Guide RNA
JF	Janelia Fluor
ESC	Embryonic stem cells
PPARG1	peroxisome proliferator-activated receptor gamma
siCntl	Control siRNA
siLMNA	Lamin A/C specific siRNA
pFAK	Phosphorylated focal adhesion kinase
TFAK	Total focal adhesion kinase
FPKM	Fragments per kilobase of transcript per million mapped reads
CEBPA	CCAAT/enhancer-binding protein alpha
mdMSC	Bone marrow derived mesenchymal stem cells
TEA	Triethanoe
siRNA	Small interfering RNA
AFM	Atomic Force Microscopy
PMSF	Phenylmethylsulfonylfluoride

PVDF

Polyvinylidene difluoride

dnKASH

Dominant-negative KASH

CHAPTER ONE: NUCLEAR ENVELOPE MECHANOBIOLOGY: LINKING THE NUCLEAR STRUCTURE AND FUNCTION

Abstract

Cellular responses rely on effective sensing and intra-cellular transduction of environmental information. This information is either coded in the extracellular matrix as biochemical cues or activated by mechanosensitive signaling cascades through dynamic environmental force gradients. The nucleus, central to cellular activity, relies on both direct mechanical input as well as its molecular transducers to sense external stimuli and respond by regulating intra-nuclear chromatin organization that determines cell function and fate. In mesenchymal stem cells of musculoskeletal tissues, changes in nuclear structures are emerging as a key modulator of their differentiation and proliferation programs. While significant advances were made in the understanding of nuclear structure and gene expression separately, studying the nuclear mechanics and gene transcription in tandem has been challenging. In this review we will first introduce the structural elements of the nucleoskeleton and discuss the current literature on how nuclear structure and signaling are altered in relation to environmental and tissue level mechanical cues. We will focus on state-of-the-art methods that can measure nuclear structure and mechanics of living nuclei with a particular emphasis on the methodologies that can be used in conjunction to visualize DNA, RNA, and protein dynamics in live cells in response to various forms of mechanical stimulation. Ultimately, combining real-time nuclear deformations and

chromatin dynamics can be a powerful tool to study mechanisms of how forces affect the dynamics of genome function.

Introduction

Cells both sense and adapt to dynamic mechanical environments in tissues. Cellular mechanosensation is accomplished through a variety of structures and proteins that reside within the plasma membrane, the cytoskeleton, and the nucleus. Depending on the type of sensory element and the external stimuli, mechanical signals are either converted into biochemical signaling cascades or physically transmitted to the intra-cellular structures (**Table 1.1**). This conversion of extracellular deformations into intra-cellular information is called mechanotransduction. For example, application of extracellular mechanical signals such as substrate strain first activates focal adhesions, protein plaques smaller than 200nm comprised of integrins, focal adhesion kinase (FAK), talin, paxilin, vinculin, and zyxin that enable direct connections between the extracellular matrix (ECM) and the cell¹. In stem cells, strain application recruits signaling complexes to focal adhesions, essentially turning them into intracellular signaling relays for extracellular mechanical information². Upon mechanical challenge, more structural elements, such as vinculin, paxilin and talin, as well as signaling molecules, including FAK, Src, and Akt, are recruited into focal adhesions³⁻⁷. These signaling events in focal adhesions in turn activate adaptations of cell cytoskeleton where compressive forces on microtubules balance the contractile pulling forces generated by F-actin stress fibers. Numerous proteins maintain the structural adaptation of the F-actin cytoskeleton, including actin related protein (Arp) 2/3 complexes that maintain branching⁸, formin homology 1 & 2 domain containing proteins that regulate the end-to-end actin formation⁹. Changes in the F-actin contractility and tension are largely

regulated by Rho GTPases, such as RhoA, Ras, and CDC42A¹⁰. RhoA for example, recruits myosin light chain kinase to F-actin fibers through its effector protein ROCK, which in turn activates the dimerized motor protein myosin II to generate tension by pulling F-actin bundles together¹¹. Not only these changes in cytoskeletal contractions are directly transmitted to cell nuclei through nuclear envelope proteins such as Linker of Nucleoskeleton and Cytoskeleton (LINC) complex¹², restructuring events also result in activation of a number of signaling molecules, most notably, β -catenin, and YAP/TAZ. Following strain application for example, both β -catenin and YAP are activated (dephosphorylated) in the cytoplasm^{13,14}. Following their activation by mechanical force both β -catenin^{15,16} and YAP/TAZ¹⁷⁻¹⁹ enter cell nuclei through nuclear pores to act as co-transcriptional factors for regulating cell function. Mechanical information, whether directly through cytoskeletal networks or through intermediate molecular transducers, has to be transmitted through the nuclear envelope and into the nucleus to direct cell function and fate.

The nucleus, long thought to be just a simple and isolated house for the DNA of the cell, is now emerging as a far more intricate organelle with dynamic skeletal proteins and active subunits. This new view not only makes the nucleus a complex system but also a vital component that is integral to the overall cell function and genome regulation. Investigations into nuclear structure and function revealed that the nucleus has its own structural network called the nucleoskeleton, which for the purposes of this review will be defined as the insoluble fraction of the nuclei including nucleoskeletal proteins and chromatin but not RNA²⁰. The nucleoskeleton component includes proteins such as the LINC complex, Lamin proteins, emerin, and spectrins to name a few. The nucleoskeleton

proteins are vital for the mechanical sensing of the cell and are the means by which the mechanical signal is transduced into the nucleus and ultimately to the chromatin regulating genome expression and chromosomal organization. While there have been great advances made in the last few decades, there is still much that is not understood about DNA, RNA, and protein dynamics in the nucleus. Here we provide a review of recent literature of nuclear proteins implicated in mechanosignaling (**Fig. 1.1**). The next two sections review the mechanical regulation of the nucleus by mechanical forces and highlight recent advances in quantifying real-time nuclear mechanics. Finally, we will introduce fluorescent labeling strategies that will make visualizing the DNA, RNA and protein dynamics during mechanical stimulation possible, as well as cutting-edge microscopy techniques useful for quantifying biomolecular dynamics occurring in response to mechanical stimulation. Together these technologies promise to provide invaluable information on the interplay between the nucleoskeleton proteins, gene expression, and functionality of the chromatin.

Nuclear Structure and Mechanical Force

LINC Complex

The Linker of Nucleoskeleton and Cytoskeleton (LINC) complex forms a physical link between the cytoskeleton and nucleus. Located in the nuclear envelope the LINC complex is formed from multiple proteins that connect to actin, microtubules, and intermediate filaments in the cytoskeleton²¹⁻²⁴. LINC complex proteins can be categorized into two main groups: those that are located on the outer nuclear membrane (ONM) forming connections to the cytoskeleton and span into the perinuclear space (PNS); and those that are located in the inner nuclear membrane creating connections between proteins inside the nucleus and LINC complex proteins in the ONM²¹⁻²⁴. LINC

complex proteins that form the first group are nesprin proteins. In mammalian cells there are four main forms of nesprins, nesprins 1-4. While there are a number of smaller analogs of nesprins found elsewhere in the cell such as N-terminal nesprin-2 that binds to cell-cell junctions and actin²⁵, we will focus on the nesprins that facilitate nucleo-cytoskeletal connectivity and mechanosignaling. Nesprins bind to cytoskeletal elements via their N-termini protruding into the cytoplasm. Their C-termini extend into the PNS where a conserved KASH (Klarsicht, ANC-1, and Syne Homology) domain binds to other major LINC complex proteins called SUN proteins²¹⁻²⁴. Other unique ONM proteins such as KASH5 and Jaw1 that are involved in regulation of cell shape by binding to microtubules but their role in mechanosignaling requires further investigation^{26,27}. Nesprins play an important role in mechanosignaling. During mechanical stimulation, the RhoA signaling pathway is activated, forming F-actin stress fibers over the nucleus creating an “actin cap”²⁸⁻³¹. Nesprins bind to these actin fibers and then regulate nuclear morphology, orientation and motility²⁸⁻³¹. Mechanical stimulation through regulation of cell shape increases the number of nesprin associations with the actin cap in both Human HUVAC³²⁻³⁵ and mouse NIH-3T3 cells³²⁻³⁵. Depletion of nesprins negatively impacts mechanical response as actin cap does not form during shear stress³¹ and mesenchymal stem cells (MSCs) are not able to mechanically activate osteogenesis through extracellular matrix (ECM) stiffening³⁶. Furthermore, the loss of nesprins leads to the dysfunctional mechanoregulation of differentiation in MSCs, pushing their differentiation away from osteogenesis and into adipogenesis³⁶. Interestingly, while substrate strain activates the focal adhesion signaling independent of nesprin function^{6,37} strain-induced YAP nuclear entry is inhibited when nesprin-1 is

depleted in stem cells¹⁷. This data indicates that nesprins provide a unique target that will allow for the investigation into nuclear mechanical signaling and mechanoresponse independent of cytoplasmic mechanoresponse events. While future research into the LINC complex via nesprins is needed a considerable amount of research into the LINC complex SUN proteins has been done, which we will discuss next.

There are two main SUN proteins in the LINC complex in somatic mammalian cells, SUN1 and SUN2. The other SUN proteins SUN3-5 are also found in the LINC complex but are found mainly in germline cells^{22,38,39}. SUN proteins are located in the INM and form trimers⁴⁰ that bind to the KASH domain of nesprins in the PNS via their C-terminal SUN domains, anchoring nesprins to the nuclear envelope^{41,42}. Extending into the nucleus the N-terminal of SUN proteins binds to Lamin A/C⁴¹, emerin⁴³ and chromatin⁴⁴. The LINC complex thus provides a physical connection between the cytoskeleton outside the nucleus and intranuclear actin and chromatin inside the nucleus via its interaction with emerin and barrier-to-autointegration factor (BAF)^{23,45}. Depletion of SUN proteins disrupts centrosome orientation, nuclear positioning⁴⁶⁻⁴⁸, and meiosis³⁶. Important in these processes are microtubules. SUN proteins regulate microtubule dependent DNA repair⁴⁹ and spindle formation⁵⁰. Therefore, an important role of SUN proteins is the regulation of cell proliferation and meiosis. While one aspect of SUN protein effects are centered around microtubule regulation of proliferation, SUN proteins also regulate mechanical response. Mechanical stimulation via low intensity vibration (LIV), strain and ECM activates mechanically sensitive biomolecular pathways such as Yes-associated-protein (YAP) and β -catenin/Wnt pathways^{6,13,18,51,52}, that in turn regulate both proliferation and differentiation^{18,37,51,53-57}. SUN proteins regulate mechanical response to strain and atomic

force microscopy-induced cell deformation by restricting YAP⁵⁸ and β -catenin^{16,59} entry into the nucleus by disrupting nuclear pore complex organization^{60,61}. Additionally, SUN proteins are required for mechanoresponse and mechanoregulation of adipogenesis in MSCs^{37,53-56} during low intensity vibration (LIV). Interestingly, de-coupling of nesprins and SUN proteins also inhibits mechanoresponse to LIV^{37,53-56}. Decoupling of the LINC complex also decreases nuclear strain and deformation during microneedle manipulation indicating physical force transmission from the cytoskeleton into the nucleus is lost during loss of function of the LINC complex⁴⁸. Additionally, isolated nuclei lose their ability to stiffen during magnetic bead displacement pulling on nesprin-1 during simultaneous SUN1 and SUN2 depletion⁶². However, strain can overcome the depletion of SUN proteins and decoupling of the LINC complex activating mechanosensitive pathways located at the focal adhesions and cytoskeleton^{37,48,53-56}. It is clear that the LINC complex is of important for cellular functioning and mechanoreponse and is the lynchpin by which mechanical and biomolecular signals enter the nucleus. However, the LINC complex does not account for all regulatory mechanisms of mechanoreponse in the nucleus. Other factors such as chromatin and Lamin A/C affect cellular outcomes due to mechanical signals. These other systems cannot be underestimated in their contribution to cellular mechanics and mechanoreponse and require further investigation in tandem with the LINC complex to determine their interconnected roles in mechanoresponse.

Emerin

Emerin is a LEM-domain (LAP2 β , emerin, MAN1) family protein that is found in the endoplasmic reticulum and in the nuclear envelope. In the nuclear envelope, emerin is found on the ONM and INM. Emerin is a pointed end actin capping protein that is capable

of regulating actin dynamics in both intra and extra nuclear compartments⁶³. SUN2 levels are significantly decreased in mutated emerin cells compared to wild type, playing a role in altered F-actin dynamics and nuclear structure⁶⁴. Other emerin mutation isoforms cause mis-shaped nuclei, disorganized microtubule networks, and irregular cell shape⁶⁵. Emerin's role in mechanical signaling revolves around regulating nuclear stiffness and binding to the actin-cap. During nuclear tension via nesprin-1-coated magnetic tweezers, the tyrosine kinase Src is activated, which in turn Src phosphorylates emerin to increase nuclear stiffness. During emerin knockdown or expression of mutated, non-phosphorylated emerin, isolated nuclei do not experience nuclear stiffening during force application⁶². During mechanical strain, emerin increases its association with F-actin at the ONM and decreases its association with Lamin A/C at the INM⁶⁶. The mutated emerin isoform Δ K37 reduces actin-cap formation and actin organization in response to stiff substrates and cyclic strain⁶⁷. While emerin regulates the physical connection of the nucleus to the cytoskeleton, its role has redundancy with that of the LINC complex. During LIV, depletion of emerin in MSCs does not impede mechanoactivation of the focal adhesions^{37,53-56}. However, emerin has been shown to have a major impact on chromatin organization. As mentioned previously, emerin connects the LINC complex^{43,68} to the chromatin through BAF and to A⁶⁹. As a result of this important connection, depleting emerin results in the dispersion of chromatin from the periphery to the center of the nucleus⁷⁰ potentially switching chromatin from facultative to constitutive states. Additionally, emerin dependent switching of heterochromatin from H3K9me3 to H3K27me3 occurs during strain⁶⁶. In DLD-1 cells co-depletion of emerin and Lamin A/C results in mislocalization of chromosomes⁷¹. Chromosome 19, which is positioned in the center of the nucleus, experiences

relocalization to the periphery of the nucleus while chromosome 18 at the periphery sees no changes in positioning. Fluorescence recovery after photobleaching (FRAP) of H2A shows chromatin mobility increase of chromatin located internally of the nucleus which was aided by increased activity of nuclear myosin-1 (NM1) and nuclear actin during Lamin A/C-emerin co-depletion⁷¹. The effects seen from the loss of emerin function range from loss of nuclear stiffness to chromatin organization, indicating emerin's important role in the nuclear envelope. However, most of the effects from the loss of emerin also requires other nuclear envelope and nucleoskeleton elements like that of Lamin A/C and F-actin. This indicates that emerin's involvement in regulating nuclear structure and mechanoreponse is more intricate than previously believed. Therefore, these interactions with chromatin, LINC complex, and Lamin A/C must be further explored to fully understand emerin's regulatory role in the nucleus during mechanical stimulation. Further insight into emerin's potential role in regulating intra-nuclear actin should also be explored. As emerin associates with the actin-cap, regulates actin dynamics^{63,72,64}, and actin-driven nuclear positioning⁷³ emerin's regulatory role on intranuclear actin could affect DNA repair and chromosome organization.

Spectrin, Intranuclear Actin, and Other Nuclear Proteins

Spectrins are tetramer proteins formed by association of two α - β heterodimers and are encoded in seven genes that are alternatively spliced to form different isoforms. Three types of spectrins are found in the nucleus: α II-spectrin, β IV Σ 5-spectrin, and β II-spectrin of which α II-spectrin is the most common⁷⁴. Spectrin creates a network of nucleoskeleton proteins through crosslinking nuclear actin and protein 4.1, providing elastic properties as nuclei lacking α II-spectrin have decreased recovery of nuclei shape after compression⁷⁵.

Spectrin also plays an important role in DNA homologous recombination repair (HRR), nonhomologous end-joining (NHEJ), and nucleotide excision repair (NER) through recruiting DNA repair proteins to the repair site^{76,77}. In addition to actin and protein 4.1, spectrins also associate with A, B, SUN2, emerin, and MYO1C. Knockdown of protein 4.1, a spectrin-actin stabilizer⁷⁸, results in nuclear blebbing and mislocalization of α II-spectrin, emerin, actin, and Lamin A^{74,79}.

Actin is present in the nucleus as either monomeric G-actin or polymeric F-actin. The F-actin polymers in the nucleus differ from that of the cytoskeleton in that F-actin polymers in the nucleus form short, anti-parallel structures that are bound to Lamin A, Lamin B, and emerin⁸⁰. Intra-nuclear actin binding to emerin causes intra-nuclear actin polymerization and is linked to localizing chromatin remodeling complexes^{63,81}. Binding of F-actin to A has also been associated with regulating actin polymerization as cells lacking A form rod-like structures of F-actin in the nucleus⁸⁰. G-actin monomers are required for proper DNA repair⁸² and chromatin modifications^{83,84}. While nuclei of *Xenopus* oocyte differs from mammalian nuclei, blocking intra-nuclear G-actin export out of the nucleus stabilizes nuclei and prevents nuclear rupture, indicative of increased mechanical competence⁸⁵. Intra-nuclear F-actin also increases during cell spreading which is likely to exert complex loading on nuclei. Intranuclear F-actin formations due to cell spreading are prevented when Lamin A/C, SUN1/2, or emerin are depleted⁸⁶. Myosin motor proteins are also found in the nucleus and are unsurprisingly associated with the nuclear actin. Nuclear Myosin 1 (NM1) was the first nuclear myosin protein found in the nucleus and is an isoform of MYO1C produced by an alternative transcription start site of the *Myo1c* gene. Strain activates nuclear myosins and increases nuclear myosin localization

to the INM, as well as increases of emerin-actin association. NM1 has been shown to be required for proper RNA polymerase I and II transcription through moving chromatin to transcription initiation sites⁸⁷⁻⁸⁹. When myosins I and V are depleted via RNAi, myosin I and V cannot relocalize to repair sites for heterochromatic double strand breaks⁹⁰. While other myosin proteins have been found in the nucleus their impact on nuclear function is still under investigation. Additionally, nuclear actin has a role in regulating chromatin organization and structure during mechanical stimulation, but this avenue of research has yet to be fully explored. Therefore, research into nuclear actin and other nuclear proteins should investigate their roles in regulating nuclear response to mechanical signals.

Nuclear Lamins

One family of nuclear proteins that has been extensively investigated are the Lamins. The Lamin family of proteins are type V intermediate filaments and consist of Lamin A, Lamin B, and Lamin C. Alternative splicing of the *LMNA* gene produces either Lamin A or Lamin C⁹¹ and together are termed Lamin A-types. Another Lamin family protein is Lamin B which has three isoforms: Lamin B1 encoded by *LMNB1* gene, Lamin B2 and B3 which are encoded by *LMNB2* and are formed via alternative splicing⁹². Lamin B-types are found in all cell types, though B3 is only found in spermatogenic cells⁹³⁻⁹⁵. Together Lamin A/C and B proteins form the majority of the nuclear lamina located at the INM. Lamin A/C proteins associate with emerin, the LINC complex via SUN1/2, intranuclear actin, BAF, histones, and DNA^{92,96}. Lamin B binds to emerin⁹⁷, intranuclear actin⁸⁰, DNA which is done through the nuclear envelope protein binding receptor (LBR)^{96,98}, and other nuclear proteins⁹⁹. Each Lamin family protein has a distinct role in nuclear structure and function. During the loss of Lamin A/C the nucleus experiences blebbing, wrinkling, loss of

circularity, increased volume, height, area, and decreased cellular and nuclei stiffening^{100–104}. This loss of structural properties causes increased migration and proliferation^{105–107}. Investigation into Lamin A/C shows that during Lamin A/C depletion fibroblasts are unable to harness apical F-actin fibers that are formed during substrate strain³⁰. This inability to associate with F-actin fibers is also observed in progeria models. In progeria, a devastating early aging disease, a silent mutation in *LMNA* causes permanent farnesylation, preventing proteolytic cleavage causing progerin, a misfolded form of Lamin A, to build up at the nuclear periphery^{108,109}. *LMNA* mutation results in the increased phosphorylation of ERK1/2. *LMNA* dependent phosphorylation of ERK1/2 causes the phosphorylation of FHOD1/3, inhibiting actin bundling at the nuclear envelope¹¹⁰. The regulatory role of Lamin A/C in connecting to F-actin fibers results in the loss of nuclear positioning¹¹⁰, nuclear movement¹¹⁰, and negates jasplakinolide-induced nuclear F-actin formation in fibroblasts leading to reduced transcription¹¹¹. These observations of Lamin A/C loss and nuclear morphology alterations are constant throughout mechanical force stimulation. Fluid shear stress (FSS) is a common *in vitro* mechanical stimulation model to simulate both blood and interstitial fluid flow in tissues. Application of FSS *in vitro* causes remodeling of F-actin cytoskeleton^{112–116}. *LMNA* *-/-* mouse embryonic fibroblasts (MEF) cells fail to form actin-cap associated F-actin fibers³¹, suggesting an active role of Lamin A/C in recruiting F-actin to nuclear surface in response to fluid shear³⁰. Further corroborating with the idea that Lamin A/C may play a role in stabilizing nuclear envelope in response to mechanical force, when cells are elongated via rectangular microstamps, depletion of Lamin A/C causes increased nuclei fluctuations when compared to control cells³⁴.

Unlike Lamin A/C that is largely expressed in committed or multipotential cell types, Lamin B is found in the brain cells of mice at birth and are expressed in early stages of embryonic development^{117,118,98}. Similar to Lamin A/C related laminopathies, *LMNB1* and *LMNB2* are also linked to disease. For example, adult-onset leukodystrophy which causes demyelination of the central nervous system and is linked to duplication of *LMNB1*. Heterozygous mutation of *LMNB2* is linked to acquired partial lipodystrophy which presents as a loss of subcutaneous tissue in the neck, arms, legs, and face¹¹⁹. Depletion of Lamin B results in chromatin instability and increased DNA double strand breaks¹²⁰, chromatin reorganization¹²¹, and increased senescence similar to that of progeria¹²¹. Alterations to nuclear structure occur as well as increasing micronuclei¹²⁰ and nuclear rupture^{122,123}. B has a critical role for the proper development of mice as *LMNB1* *-/-* mice experience die at birth and increased bone ossification¹²². Lamin B therefore has an important role in maintaining normal nuclear functioning. However, the role of Lamin B during mechanical signaling is not as vital and is different from the role of Lamin A/C. The role differences between Lamin A/C and Lamin B are largely seen during mechanical stimulation of the nucleus. Modulation of extracellular matrix (ECM) stiffness causes mechanical force effects on Lamin A/C protein levels, Lamin A/C structure, and nuclear organization. Decreasing ECM stiffness decreases Lamin A/C levels and causes re-localization of Lamin A/C and Lamin B into the interior of the nucleus⁷⁰ and causes the deformation and folding of Lamin A/C^{124,125}. In MSCs ECM stiffness alters LBR: Lamin A/C ratios. Softer extracellular matrices induce LBRs to be highly expressed relative to Lamin A/C¹²⁶ correlating with increased adipogenesis while stiffer ECM induces a lower LBR/ A relationship pushing the MSCs to osteogenesis¹²⁶. While these results show a role

for Lamin A/C, Lamin B, and LBRs in mechanosensing pathways, cells with defective B experience little changes in gene expression during mechanical stimulation¹²⁷ which further supports that Lamin A/C is the main target to regulate mechanical signals and mechanoregulation. Indeed, further research into Lamin A/C through microstamp cell shape regulation shows that cells forced into rectangular shapes increase A association at the nuclear envelope³², decrease nuclear size fluctuations³⁴, and induce osteogenic differentiation¹²⁸. Contrastingly, cells forced into circular shapes have decreased Lamin A association with nuclear envelope³², large nucleus size fluctuations³⁴, increased chromatin and telomere diffusion³⁴, and inducement into adipogenesis¹²⁸. Lamin A/C therefore has a more important role in regulating cellular and nuclear response to mechanical signals. However, we have shown that mechanoregulation of adipogenic differentiation in MSCs is independent of Lamin A/C indicating that Lamin A/C may have a limited or at least overlapping functionality with other nuclear proteins during mechanically induced repression of adipogenesis¹⁰⁰. Further research into the role of the nuclear a, specifically, Lamin A/C, is needed during mechanoregulation of differentiation in combination with other nuclear envelope elements such as emerin or the LINC complex to fully elucidate the full mechanoregulatory effects of nuclear envelope proteins.

Chromatin

As the organized and packaged structure of histones and DNA, chromatin provides the nucleus with a mechanism to regulate not only genomic expression but also genomic organization and nuclear structural properties. Chromatin is known to associate with SUN proteins⁴⁴, emerin, Lamin A/C through DNA binding domains and BAF, to B via LBRs, and other nuclear proteins. Chromatin domains that are in proximity to and associated with

the nuclear pores are called lamina-associated-domains (LAD)^{129,130} (**Fig. 1.1A**). These domains have been shown to be correlated with heterochromatin, producing repression of gene expression of genes located in the LADs¹³¹. However, this model of LAD-mediated repression at the nuclear periphery does not account for the changes in the 3D chromatin organization observed under Lamin depleted cells. Disabling the interaction of chromatin and nuclear pores results in the loss of the inter and intra-interactions between topological-associated domains (TADs) at both the periphery and internal regions of the nucleus¹³². Additionally, loss of Lamin A/C alters chromatin diffusion¹³³. Therefore, disabling the interaction of chromatin with the nuclear pores not only affects the nuclear periphery but alters 3D organization of chromatin. Mechanical forces also regulate chromatin structure. Soft ECM induces increases in euchromatin¹³⁴ and localization of chromosomes 1, 18, and 19 to the nuclear interior, and upon replating on stiffer substrates only chromosome 18 experiences recovered localization⁷⁰. Substrate strain causes an increase of heterochromatin and switching of heterochromatin from H3K9me3 to H3K27me3^{66,135}. Direct magnetic bead shear stress on the nucleus of Chinese hamster ovary (CHO) cells also shows that chromatin is induced into an open state and increases gene expression¹³⁶. Depletion of SUN1/2, Lamin B, Lamin A/C, emerin, and BAF all cause similar chromatin movement and gene expression as magnetic bead shear stress¹³⁶. Ultimately, these alterations of chromatin structure have major regulatory effects on differentiating stem cells. In MSCs, the heterochromatin marker H3K27me3 is decreased in cells differentiating into adipocytes, while the euchromatin markers H3K9ac, H3K4me3, and H4K5ac see an increase^{51,137}. Alterations to chromatin are one of the first steps in cellular responses to mechanical signals. Understanding how stem cells alter their chromatin structure and

organization in response to mechanical forces is required to truly understand and manipulate stem cell fate.

As the main house for DNA, it is a logical conclusion that both alteration to nuclei structure and mechanical force stimulation would alter chromatin. However, chromatin also has an important role in regulating the nuclear response to mechanical forces and regulating nuclear morphology. Disruption of chromatin structure via chromatin digestive MNase protein retards cell stiffening in response to low levels of strain displacement ($<3\mu\text{m}$)¹³⁸. Additionally, increases in heterochromatin induces nuclear stiffening^{138,139} while increases in euchromatin results in decreased stiffness^{138,139}. Reduced H1, a histone protein that stabilizes formation of condensed chromatin, does not alter heterochromatin markers but does result in decreased nuclear rigidity inducing increased nuclei fragility¹⁴⁰. Additionally, decreased levels of heterochromatin also result in blebbing and protrusion of the nuclear envelope independent of Lamin A/C¹³⁹⁻¹⁴¹. Therefore, chromatin is a vital nuclear element that regulates gene expression, nuclear morphology, and nuclear mechanics. In order to fully understand how the nucleus responds to and senses mechanical signals the interaction of chromatin and nuclear proteins must be further explored. Specifically, understanding the connections between chromatin and the nuclear envelope proteins is of great importance. As mechanical signals enter the nucleus through the nuclear envelope proteins, like that of the LINC complex, and are transferred to the chromatin, understanding the chromatin dynamics is of vital importance. A potential tool to investigate these dynamics is fluorescence microscopy, as the advancement of fluorescence microscopy beyond the diffraction limited spot has now provided a way to visualize these dynamics at the single molecule level, providing a launching point for further exploration

and quantification of these changes that have not been achievable before.

Characterization of Nuclear Structure and Mechanics

The nucleus is a mechanosensitive organelle of the cell that allows for gene regulation and adaptation as an active response to biophysical stimuli from the cytoskeleton and surrounding environment. Numerous methodologies have been developed to probe nuclear structure and mechanics, including fluorescence anisotropy¹⁴²⁻¹⁴⁴, micropipette aspiration^{145,146}, nanoindentation^{147,148}, and image-based assessment of aspect ratios^{149,150}, volume^{151,152}, deformable image registration^{153,154}, and deformation microscopy¹⁵⁵. Characterization of bulk or local structure and mechanics is possible for isolated cells or nuclei, and additionally of cells embedded in two- and three-dimensional microenvironments. Like most biological structures, the nucleus is well-known to exhibit complex (e.g., nonlinear, time-dependent) properties, and available methods allow for the characterization of this behavior following a wide range of mechanical perturbations^{62,156}.

Nuclear Structure

Recent research reveals that the nuclear structure, with distinct euchromatin and heterochromatin subdomains, demonstrates a scale-dependent and solid-like behavior under some conditions that provides insight for the physical organization and regulation of the genome¹⁵⁷. While microscopy methods like fluorescence microscopy and fluorescence recovery after photobleaching provide the ability to visualize the nuclear interior, additional methods are required to provide value-added characterization of nuclear structure. The morphology of the nucleus is commonly assessed based on measurement of the aspect ratio, volume, or a characteristic dimension such as major/minor axes^{150,153,158}. Morphological analysis of this type commonly considers geometric changes of the nuclear

periphery using automated or semi-automated algorithms and does not provide any intranuclear spatial information. A major strength of nuclear morphology measurements is the ability to assess large numbers of cells in a high-throughput manner, enabling population-level analysis of treatment responses, often at the cost of detailed intranuclear spatial information.

Intranuclear Strain

Local mechanical deformations, i.e., displacements and strains within the nuclear interior, may be related directly to altered transcriptional activities, possibly through the alteration and regulation of chromatin domains¹⁵⁹. While the measurement of local deformation may reveal fundamental mechanobiological mechanisms, direct imaging of intranuclear mechanics is challenging. Commonly, fluorescent microscopy of viable cells is required to capture and tag the deforming nucleus in multiple (e.g., resting and mechanically loaded or stretched) states to allow for a description of motion of the nucleus in a “current” configuration with respect to an initial “reference” configuration. Widefield and confocal microscopy can be used to visualize living cells before and after deformation¹⁵⁴, and a natural extension of imaging modalities to include modern methods like super-resolution microscopy are possible.

Spatial mapping of deformation within the nucleus is accomplished using fluorescence anisotropy¹⁶⁰, and texture correlation^{153,161}. Recently, deformation microscopy, based on hyperelastic warping and deformable image registration¹⁵⁵, demonstrated the ability to map biophysical and biochemical interactions due to substrate stiffness or hyperosmotic changes, or LINC disruption treatments, and have been used broadly to describe the mechanics of nuclei in cardiomyocytes, chondrocytes, and skeletal

muscle *in vivo*^{155,161,162}. Additionally, detailed strain patterns have been associated with distinct epigenetic modifications that impact development¹⁶³. The use of hyperelasticity enables the measurement of complex nuclear behavior, including nonlinear elasticity in two and three dimensions, that would be expected to sufficiently describe intranuclear deformation for most anticipated applications. Certainly, nuclei have demonstrated extreme deformations, such as in migratory cancer cells in constrained geometries¹⁶⁴, and yet recovery of the nucleus is observed, aligning more with hyperelastic, and not plastic or permanent, deformation behavior.

Intranuclear Stiffness

Emerging methods also enable the description of the mechanical properties of heterochromatin and euchromatin domains. One method is intranuclear rheology^{165,166} which tracks the passive movement of fiduciary markers such as fluorescent beads but may suffer from limitations including the possible invasive nature of bead insertion and the impact of embedded beads on cell viability. Recently confocal Brillouin microscopy, a non-contact, direct readout of the viscoelastic properties of a material¹⁶⁷ has been applied to migrating tumor cells, which allows a real-time live cell metric for measuring stiffness changes in cell nuclei¹⁶⁸. Atomic force microscopy with a needle-tip probe has recently demonstrated the ability to directly map the nuclear envelope and cell membrane stiffness in within native tissue¹⁶⁹, and showed that the nuclear stiffness decreases with disruption of the extracellular matrix in living tissues, further emphasizing the physical links connecting the nucleus to the surrounding microenvironment. Optical microscopy-based¹⁷⁰⁻¹⁷² elastography is a powerful potential method to measure the distribution of mechanical properties noninvasively within the nucleus. Based on techniques like

deformable image registration and inverse finite element methods, image-based elastography of heterochromatin and euchromatin domains in the deforming cell nucleus is now possible^{173,174}.

Linking Nuclear Mechanics and Mechanobiology

While characterization of the nucleus structure and mechanics is possible using numerous methods, still lacking are studies that carefully link biomechanics with cell and nuclear biological activity. Methods are required that allow for the rapid acquisition of biomechanical data coupled simultaneously with techniques that capture activities like rapid gene expression in response to mechanical loading. High spatial resolution imaging is needed to probe the single-cell level, ideally in complex three-dimensional microenvironments like hydrogels or native tissue. New methods explore combinatorial methods, including the use of photobleaching with unique Förster Resonance Energy Transfer (FRET) pairs^{175,176}, or deformable image registration with independent assessments of histone modifications or LINC disruption¹⁶³.

Visualizing Chromatin Dynamics in Living Cells

In the sections leading here we have detailed the mechano-responsive structures that make up nucleus as well as methods to apply mechanical force as well as methods to measure nuclear mechanics. While it is accepted that 3D structure and function of the nucleus and chromatin are inherently connected, “seeing is believing”¹⁷⁷, and therefore visualizing is critical to understanding the structure and function of the genome. There are an increasing number of studies aimed at understanding how mechanical signals regulate nuclear mechanics at higher resolution, while at the same time there are several state-of-the-art optical techniques under-utilized in the field of mechanobiology that are capable of

visualizing nuclear dynamics. In this section we will first discuss possible approaches that can be combined to perform correlative measurements of mechanical stimulation and gene expression at high resolution as these may provide critical information about the relationship between mechanics and spatiotemporal (3D+1D) dynamics of the nucleus. Finally, we will focus on current methods of labeling DNA, RNA, and proteins in living cells and discuss details of different imaging modalities that can be used to discern the motion of these labeled structures.

Fluorescence Imaging Techniques

For the study of living cells and tissues there is no substitute for light microscopy. The limited interaction of photons with biological matter combined with superb contrast provided by fluorescent labelling allows us to study both the prevalence and subcellular organization of selected biomolecules within living cells and tissues. The ever-growing list of highly specific fluorescent labels makes fluorescence microscopy one of the techniques of choice for studying nuclear architecture and function¹⁷⁸. In the last decade the nucleus, which was a proverbial black box has been unmasked as a highly dynamic, ultra-structured entity that is dynamically reforming based on biochemical cues from the microenvironment and mechanical cues from the tissue. This evolution of scientific understanding is in large part due to advances in light microscopy and new creative imaging techniques^{179,180}.

The methods we will discuss here can provide information about nuclear structure and mechanics. One of the main methods is visualizing tracer particles. Depending upon its size, a tracer particle may sample and provide information on either the micro or macro environment of the local nuclear region through the generalized stokes einstein's

equation¹⁸¹. Confinement of a particle within a region of the nucleus may also allow determination of phase separated domains which have been reported to correlate with specific histone modifications and transcriptional activity^{182,183}. Methods such as fluorescence anisotropy can also characterize properties of the local environment of a tracer particle. If mechanical stimulus is applied to the nucleus, particle image velocimetry can be used as a control to quantify the applied stress or strain rate. Microrheology may be applied after mechanical stimulus to determine its effect on the local nuclear environment of a tracer particle¹⁸⁴. Another more novel application in fluorescence microscopy, is to monitor changes in gene expression affected by mechanical stimulus. It may be that in some cases there is a direct relationship between gene activation or repression and the mechanical environment of the nucleus. While this effect is well known in population measurements of stem cell differentiation¹⁸⁵, it has never been directly verified at the single cell or single molecule level.

As with determining the appropriate fluorescent label for the experimental question, there are a variety of labeling techniques with benefits and drawbacks. Some focus on temporal resolution at the expense of spatial resolution. Others are focused on determining molecular interactions and binding events. The below chart provides an overview of techniques that are available and useful in determining the structure and function of nuclear architecture and its role in nuclei's mechanoresponsonse (**Table 1.2**). We will then further highlight several methods that promise to be valuable.

Fluorescence Correlation Spectroscopy (FCS) utilizes fluctuations in fluorescence intensity in small detection volumes in samples of low concentration to investigate molecular dynamics namely, diffusion, molecular conformations, binding events, and

chemical reaction kinetics¹⁸⁶. It was first developed by Elliot, Magde and Webb¹⁸⁶ and later developed by Gratton et al.¹⁸⁷⁻¹⁸⁹, Schwille et al.¹⁹⁰⁻¹⁹⁴ and many others for scanning multiple labels and two photon excitation and was eventually extended to the study of transcription¹⁹⁵, translation¹⁹⁶ and splicing¹⁹⁷, and more recently gene activation^{198,199}. FCS is conducted by measuring fluctuations in fluorescence intensity as fluorescent molecules enter and exit an illuminated space. Large jumps in intensity signify larger molecules or multiplexes as opposed to small jumps in intensity that signify smaller, individual molecules. Similarly, slow changes in intensity indicate slower moving, often larger molecules, while quick fluctuations in intensity indicate faster moving, often smaller molecules. FCS calculations are done using a correlation curve from the fluctuations in intensity. The taller the curve the lower the concentration of molecules within the observation volume. The longer the curve, the slower they are moving¹⁸⁶. FCS was originally conducted on homogenized samples in a cuvette, now this technique has been extended for use in live cell microscopy²⁰⁰. The cell now acts as the confined space like the cuvette. Not only can single biomolecules be analyzed through FCS, but multiple molecules can be studied simultaneously, and their intermolecular interactions can be quantified as well by using fluorescence cross correlation spectroscopy (FCCS)^{189,201}. FCCS has been used extensively to quantify the kinetics of transcription factor binding and elongation as well as many other biomolecular interactions within the nucleus²⁰²⁻²⁰⁴.

Single Particle Tracking (SPT) is a method that requires bright and stable fluorescent labelling, highly sensitive CCD or sCMOS cameras and extremely low fluorescent background. In living cells this can only be achieved using a Total Internal Reflection Fluorescence (TIRF)^{205,206} or Highly inclined illuminated optical sheet

(HILO)²⁰⁷ microscopes. SPT can be useful in determining the trajectories of individual particles with nanometer precision providing dynamic information about biomolecule locations. One of the major challenges with SPT is photobleaching. Even with improved fluorophores photobleaching often occurs within seconds or at most minutes on a widefield microscope, reducing the temporal resolution of correlative measurements. Recent advances have been made in this area with the development of lattice light sheet²⁰⁸ and other microscopy methods^{209,210,211,212}, and has also been addressed by combining SPT with FCS and 3D Orbital Tracking^{195,197–199}. This synergistic approach has been successfully used to visualize transcription factor binding dynamics²¹³.

3D Orbital Tracking, which was developed in 2005 by Levi and Gratton et al.^{214,215}, gets around photobleaching issues by changing the laser scanning pattern from x-y to a circular orbit²¹⁴. Instead of exciting the molecule directly, the laser passing around the bright spot indirectly excites it, resulting in a longer imaging window^{187,214}. This method has been used to acquire quantitative, single-cell, live data on transcription factor binding and elongation^{198,199}, as well as study lysosome active transport and free diffusion^{214,216}. In addition to information on transcription factor binding and transcriptional activity, a laplace transformation of the mean squared displacement (MSD) of the 3D trajectory of a gene locus by orbital tracking may also give information on the complex viscoelastic modulus of the nuclear compartment²¹⁷.

Moving forward it is becoming increasingly necessary to combine these techniques to both validate findings as well as discover new information about nuclear structure and dynamics. By combining techniques, both spatially and temporally relevant data can be gleaned. FRAP and FRET are being used in conjunction to determine the

dynamics of BAF and emerin interactions²¹⁸. Colocalization and FRAP together showed that the crosstalk seen between the cytoskeleton and the nucleus is in large part regulated by Lamin A/C and emerin modulating structural cytoskeletal proteins like actin⁷¹. FCCS and 3D Orbital tracking have been used synergistically to determine the kinetics of transcription factor binding and RNA synthesis¹⁹⁸. It is not enough to solely study RNA, DNA-Protein interactions, or chromatin-chromatin interactions; each must be combined to understand how nuclear structure and gene expression are affected by mechanical and environmental cues. Not only is it powerful to combine two imaging techniques or two sequencing techniques, when both sequencing and imaging are combined unique research questions can be addressed.

Fluorescent Biomolecule Labeling

There are a variety of labeling strategies available for visualizing biomolecules. Each provides varying pros and cons, making them ideal for different experimental questions. Some questions to consider when choosing a label method include: Is the experimental imaging going to be performed in live cells? How bright does my fluorophore need to be? Do I want the flexibility of adding my probe before each experiment or do I want the stability of having a self-labeling cell line? How important is fluorescent background and labeling efficiency? Based on the answers to these questions, the proper labeling method for your experiment can be identified. While well-established methods such as LacR²¹⁹ and MS2/PP7²²⁰ are powerful, readers are referred to **Table 1.3** for an extensive list of methods that are available to researchers. Below we highlight the most promising methods for imaging the nucleus while it undergoes mechanical stimulation.

The newest addition to genome editing, CRISPR, has revolutionized our ability to edit the genome as well as visualize it. Deactivated Cas9 (dCas9) provides the technology necessary to document the dynamic properties of different gene loci simultaneously²²¹⁻²²⁸. dCas9 uses the CRISPR gene editing system for DNA labeling with a fluorescently tagged Cas9 in combination with specifically engineered guide RNAs (gRNA). This method can be used to successfully image multiple gene loci simultaneously within a living cell, which makes it an ideal labeling method for studying chromatin dynamics during mechanical stimulation²²⁶. One of the major challenges with CRISPR/dCas9 systems is sensitivity of detection. Most of the approaches are only successful for repetitive DNA sequences in which a single gRNA can result in labeling with numerous GFP-dCas9 proteins. Similarly, dCas13, a molecule like dCas9, targets complementary sequences of RNA. Together the gRNA and dCas13 protein can locate a specific sequence of RNA and fluorescently label it. While this method of RNA labelling is still in development, it promises a versatile method for labelling RNA's which have not been modified through the insertion of an RNA hairpin or other sequence. In this system either the gRNA²²² or dCas13 molecule²²⁹ may be fluorescently labelled. Like dCas9 it suffers from low affinity but that can be overcome through multimerization of the guide RNAs. Now specific sequences of RNA can be labeled for real-time imaging and tracking²²⁹.

Another newer option for live-cell imaging of RNA are RNA aptamers like RNA Mango²³⁰, RNA Spinach²³¹ and RNA Broccoli²³². RNA aptamers are sequences designed as molecular beacons and selected through SELEX^{233,234}. The resulting aptamer is capable of binding specific fluorophore derivatives with nanomolar affinity. This results in an increased fluorescence of up to 1,000-fold. The main advantage of this method is that it

provides a fluorescence enhancement upon binding, lowering the considerable fluorescence background that is typically present in other methods such as dCas9 and dCas13. This technology for visualization of RNA Mango has been used in conjunction with single-molecule fluorescence microscopy on a wide range of projects including visualizing RNA complexes in live *C. elegans*²³⁵ and protein tyrosine kinase activity²³⁶. While this method is still very new it holds promise for visualizing RNA dynamics as no other label has, providing invaluable information of the inner workings of the nucleus and the results of mechanostimulus on the transcriptome. An additional tool that has been developed recently for advanced protein imaging studies are self-labeling protein tags such as HaloTag and SNAP-tag^{237,238}. These self-labeling organic protein tags can be inserted into cloning vectors²³⁷, allowing for a specific binding site for fluorophores. The SNAP-tag and HaloTag technology can be used with a wide range of fluorophores, allowing for more flexibility than with fluorescent proteins alone. They are often used in conjunction with small, membrane permeable chemically derived dyes like “Janelia Fluor” (JF) dyes that are known to be highly photostable²³⁹. There are many labeling options available (**Table 1.3**), but the ones described above CRISPR/Cas, RNA Aptamers, and HaloTag promise to be the most valuable for characterizing the dynamics of DNA, RNA, and protein while the nucleus is undergoing mechanical perturbations.

Conclusion

Recent advances in the field of nuclear mechanobiology clearly indicates that the nucleus is not a passive element but actively participates in regulating cell phenotype in response to extracellular and cytoskeletal mechanical cues. As highlighted in this review, large numbers of proteins as well as inter-related structural and signaling events propose

a daunting task for researchers who like to study the mechanical basis of nuclear function. While many studies focus on simplifying assumptions, mechanistic understanding of nuclear mechanobiology requires inherently complex live-cell approaches that utilize innovative experimental designs using versatile model systems such as mesenchymal stem cells that rely on reconfigurations chromatin and nucleoskeleton for their differentiation programs. Further, some of the methods highlighted here provide a high level of control on cell geometrical constraints as well as applying precise dynamic mechanical forces. Therefore, uniquely combining powerful models with experimental mechanics such as “deformation microscopy” and with state-of-the-art visualization techniques to track mRNA transcription within a gene loci, should yield currently unstudied correlations between subnuclear mechanics and mRNA transcription and significantly advance the current scientific knowledge in how external mechanical force regulates cell function by altering nuclear interior.

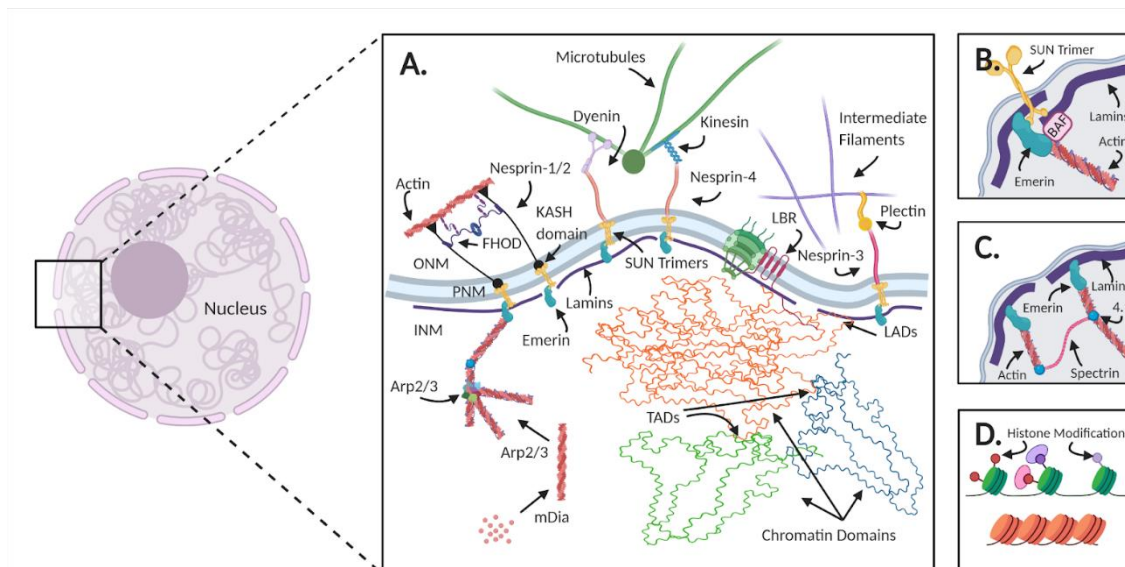
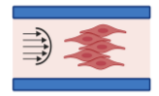


Figure 1.1 Nucleus is a mechanically-integrated mechanosignaling center

Nuclear structural proteins interact with the cytoskeleton, chromatin, and the nuclear membrane to stabilize the nucleus and provides mechanosensing functions (Insert A). LINC complexes composed of Sun 1/2 trimers and Nesprin 1/2 mechanically couple the actin cytoskeleton. The LINC complex also interacts with nuclear pore complexes (NPC) and in-part regulate the access of important mechanical transducers such as β -catenin and YAP/TAZ into the nucleus. Nesprin-3 through interactions with plectin and nesprin-4 are also known to interact with cytoplasmic intermediate filaments and microtubules, respectively. Nesprins can also bind to microtubules via dynein and kinesin. Mechanical coupling of actin and the LINC complex involves cytoplasmic formins such as FHOD1 that attaches nesprins and actin at multiple points for a more robust association. Torsin A may also facilitate the LINC assembly at the nuclear envelope. A nuclear envelope transmembrane protein, Emerin connects the LINC complex, via SUN1/2 and nesprin-1/2 to the chromatin through BAF and Lamin A/C (Insert B). Emerin also associates with and plays a role in regulating extra and intranuclear actin. The intranuclear actin network is formed through the crosslinking of short F-actin fibers via protein 4.1 and spectrin that provides elastic structural properties to the nucleus (Insert C). Inside the nucleus, G-actin is assembled into linear and branched networks through regulatory proteins such as arp2/3 and mDia2 to and influence chromatin dynamics and gene access. Chromatin domains that bind to the nuclear s are called -associated-domains (LAD). These domains have been shown to be correlated with heterochromatin, producing repression of gene expression of genes in the LADs. These chromatin domains conserve epigenetic histone modifications. Changes of histone modifications, topologically associated domains (TADs), and LADs all result in changes in gene expression and cell differentiation (Insert D).

Table 1.1 Common in vitro mechanical force simulation methods and their major studied outcomes

Mechanical Force	Description	Major Outcomes	Benefits	Drawbacks
 <p><i>Extracellular Matrix Stiffness</i></p>	Stiffening or softening of extracellular matrix to induce mechanical responses similar to that of native tissue ^{124,134,240,241}	<ul style="list-style-type: none"> • Focal adhesion activation • Actin cytoskeleton polymerization • Nuclear stiffening • Cell differentiation • Chromatin organization 	<ul style="list-style-type: none"> • Replicates to native tissue mechanics • No additional apparatus required to induce mechanical signals • No additional apparatus required to induce mechanical signals 	<ul style="list-style-type: none"> • Can have uneven stiffness profiles across surfaces • Harder to image live or fixed cells
 <p><i>Micropillars and Microstamps</i></p>	Restricting cell shape through physical impediments or shape of adherent surface ^{32-35,242}	<ul style="list-style-type: none"> • Cytoskeleton & nucleus shape • Cell differentiation • Chromatin organization 	<ul style="list-style-type: none"> • Easy to manufacture and implement • Isolates function of cell shape in cellular functions • Can image live or fixed cells 	<ul style="list-style-type: none"> • Low cell density • Partial homology to tissue environment
 <p><i>Fluid Shear</i></p>	Mimicry of fluid shear stress forces found in vasculature	<ul style="list-style-type: none"> • Cell and nucleus orientation 	<ul style="list-style-type: none"> • High homology to vasculature 	<ul style="list-style-type: none"> • Requires use of specially designed

<p><i>Stress</i></p>	<p>systems^{31,112-115,243,244}</p>	<ul style="list-style-type: none"> • Cytoskeleton remodeling 	<p>forces</p> <ul style="list-style-type: none"> • Easy to mimic human pathologies 	<p>bioreactors</p> <ul style="list-style-type: none"> • Fluid force can be non- uniform between experiment sets
 <p><i>Strain</i></p>	<p>Stretching of adherent substrate to produce dynamic or static strain forces^{6,7,13-17,37,52,56,100,127}</p>	<ul style="list-style-type: none"> • Actin cytoskeleton • Cell differentiation • Cell proliferation • Focal adhesion signaling • Nuclear signaling and structure • Chromatin organization 	<ul style="list-style-type: none"> • Easy to use • Induces strong regulation of differentiation and stimulation of the actin cytoskeleton 	<ul style="list-style-type: none"> • Requires expensive strain application machinery • Limited by size of specialized cell culture plates
 <p><i>Low Intensity Vibration</i></p>	<p>Low magnitude strain induced by low amplitude, high frequency vibration^{19,37,53,55,56,100}</p>	<ul style="list-style-type: none"> • Focal adhesions signaling • Cell differentiation • Cell proliferation • Nuclear signaling and structure 	<ul style="list-style-type: none"> • Similar homology to muscle-induced vibration forces observed in native tissue • Can be utilized in cell culture, tissues, and mammalian models 	<ul style="list-style-type: none"> • Requires custom-made bioreactors • Requires long term exposure to mechanical signals • Less potent mechanical signal compared to strain and fluid shear

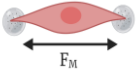
 <p><i>Atomic Force Microscopy</i></p>	<p>Probing of individual cells and nuclei with rounded-tip atomic force microscopy^{100,145,147,169,245}</p>	<ul style="list-style-type: none"> • Measure Cell and nuclear stiffness • Force induced translocation of mechanically sensitive biomolecules 	<ul style="list-style-type: none"> • Provides high resolution stiffness measurement of cells and nuclei • Targeted mechanical activation of mechanosensitive signaling pathways 	<ul style="list-style-type: none"> • Require expensive equipment <p>Challenging to provide population-based measurements</p> <ul style="list-style-type: none"> • Hard to determine if measuring proper target versus non-desired targets
 <p><i>Magnetic Bead Stretching</i></p>	<p>Use of magnetic beads to induce physical strain on individual cells^{136,246–248}</p>	<ul style="list-style-type: none"> • Force induced translocation of mechanically sensitive biomolecules • Nuclei mechanoresponse • Actin cytoskeleton remodeling • Chromatin 	<ul style="list-style-type: none"> • Allows for targeted strain on an individual cell level • Can induce targeted chromatin structure changes 	<ul style="list-style-type: none"> • Does not provide population-based measurements • Requires use of special equipment

Table 1.2 Fluorescence Imaging Techniques

Technique	Description	Benefits	Drawbacks
<i>Colocalization</i>	The observation of spatial overlap between different fluorescent labels, which reveals associations and interactions between two molecules 249,250	<ul style="list-style-type: none"> • Can be conducted on widefield, confocal, and superresolution microscopes • Shows biomolecular associations and co-distributions 	<ul style="list-style-type: none"> • Limited spatial and temporal resolution • Limited by resolution as the colocalization of two probes does not always signify association.
<i>Fluorescence Recovery After Photobleaching (FRAP)</i>	FRAP is used to determine the kinetics and diffusion of various biomolecules by intentionally photobleaching a portion of the sample and then observing how the fluorescence distribution returns to its previous state 71,251–254	<ul style="list-style-type: none"> • Useful for finding ratios of bound and unbound molecules, as well as protein mobility • Turns photobleaching, which is generally avoided, into a desirable 	<ul style="list-style-type: none"> • The photobleaching process can be destructive to the sample because of the high light intensity • Sometimes incomplete fluorescence recovery occurs due to obstruction of diffusion • A local temperature increase at the photobleached site can affect the calculated diffusion rate²⁵⁵
<i>Fluorescence Correlation Spectroscopy (FCS)</i>	FCS utilizes fluctuations in fluorescence intensity in small detection volumes in samples of low concentration to investigate molecular dynamics 186187–189190–194	<ul style="list-style-type: none"> • Kinetics data can be measured in a living cell • Number of molecules of interest and their molecular brightness can be calculated 	<ul style="list-style-type: none"> • Requires high labeling efficiency in order to get accurate kinetics data • Only counts the molecules in the observation volume, not the entire field of view
<i>Single Particle Tracking (SPT)</i>	SPT is a microscopy tool that allows the movement of individual particles to be followed within living cells. It	<ul style="list-style-type: none"> • Monitors the trajectories of individual biomolecules in living cells • Good for studying 	<ul style="list-style-type: none"> • Requires extremely low fluorescent background and very bright labels • Requires highly sensitive cameras

	provides information on molecular dynamics over time ^{256,257} .	localization dynamics	<ul style="list-style-type: none"> • Requires TIRF or HILO microscopes • Photobleaching (due to widefield imaging)
<i>3D Orbital Tracking</i>	3D Orbital Tracking uses an unique scanning pattern. Instead of exciting the molecule directly, the laser passing around the bright spot indirectly excites it, resulting in a longer imaging window ^{187,214} .	<ul style="list-style-type: none"> • Minimal photobleaching • Can collect data for long periods of time 	<ul style="list-style-type: none"> • Can only track one particle at a time • Only collects data on the molecule being tracked, not the rest of the field of view
<i>Förster Resonance Energy Transfer (FRET)</i>	FRET exploits the energy transfer that occurs between two chromophores that are in close proximity. The donor when in an excited state can transfer its energy to the acceptor through dipole-dipole coupling ²⁵⁸ . The excitation is accompanied by light emission and the transfer of energy is characterized by a loss of light emission. The efficiency of this transfer can be used to calculate small changes in distance between the chromophores ²⁵⁹ .	<ul style="list-style-type: none"> • FRET is a nondestructive spectroscopic technique • Characterized molecular interactions with high accuracy (on the 1-10nm scale) 	<ul style="list-style-type: none"> • Low signal-to-noise ratio • Sensitivity of probes to pH, temperature, ionic concentration, etc..

<p><i>Fluorescence Lifetime Imaging (FLIM)</i></p>	<p>FLIM specifically measures how long a fluorophore stays in an excited state before emitting a photon ^{260,261}.</p>	<ul style="list-style-type: none">• Can detect molecular variations of fluorophores that are not apparent with spectral techniques alone• Ideal tool for removing background fluorescence intensity• Collects lifetime measurements for every pixel within the image	<ul style="list-style-type: none">• Difficult to conduct in live cells because there are not enough photons per pixel• Requires in-depth data analysis
--	---	--	---

Table 1.3 Fluorescence Labeling Technologies and their benefits and drawbacks

f	Target Biomolecule	Description	Benefits	Drawbacks
<i>DNA Binding Dyes (DAPI, Hoechst, SiR-DNA, and SPY650)</i>	DNA	These dyes fluoresce when they intercalate into the minor groove of DNA. ²⁶²⁻²⁶⁴	<ul style="list-style-type: none"> • Requires minimal sample preparation • Labels all DNA indiscriminately 	<ul style="list-style-type: none"> • Cannot label specific genes
<i>FiSH</i>	DNA/RNA	Fluorescence in-situ hybridization (FiSH) labels gene loci or RNA specifically with fluorescently labeled single stranded probes. ^{265,266}	<ul style="list-style-type: none"> • Labels DNA gene loci or RNA specifically • Multiple gene loci labeled at one time 	<ul style="list-style-type: none"> • Cannot be used for live cell imaging • Requires specific probe design
<i>LacR & TetR</i>	DNA	LacR and TetR specifically label chromatin locus in living cells with a GFP-fusion protein ^{267,268} .	<ul style="list-style-type: none"> • Results in stable cell line that can be used over and over • Specific gene loci and individual gene loci can be imaged in live cells over multiple generation without the addition of probes 	<ul style="list-style-type: none"> • Requires integration of prokaryotic operon sequences into the DNA • The gene editing may result in abnormal gene expression profiles
<i>dCas9</i>	DNA	dCas9 uses the CRISPR gene editing system for DNA labeling with a fluorescently tagged nuclease dead Cas9 in	<ul style="list-style-type: none"> • Live cell imaging without laborious or disruptive gene editing • Multiple gene loci labeled at one time • Ideal for studying chromatin dynamics 	<ul style="list-style-type: none"> • Requires multiple CRISPR/Cas9 to produce a bright enough signal for imaging • The binding affinity of CRISPR/Cas9 is highly dependent upon the gRNA sequence

		combination with specifically engineered guide RNAs ²²¹⁻²²⁸ .		
<i>MS2/PP7</i>	RNA	Fluorescent molecules bind to repetitive stem loops that have been introduced into the gene of interest. Each stem loop, of which there are often up to 24 copies, binds to a dimer of a chimeric protein composed of the phage protein, a nuclear localization signal and a fluorescent protein ^{269,197} .	<ul style="list-style-type: none"> • Actively transcribing RNA can be imaged in real-time within a cell • Since MS2-RNA and PP7-RNA are sequence specific, both can be used simultaneously within a given cell, allowing for multiple RNAs to be visualized at the same time. 	<ul style="list-style-type: none"> • Can only be used to label two distinct RNAs at a time • The multimerization of the stem loops results in a bulky label that can alter RNA kinetics
<i>dCas13</i>	RNA	dCas13 uses the CRISPR gene editing system for RNA labeling with a nuclease dead Cas13 in combination with specifically engineered guide RNAs ^{222,229} . Either the	<ul style="list-style-type: none"> • Versatile method for labelling RNA's which have not been modified through the insertion of an RNA hairpin or other sequence • Sequence specific • Ideal for studying RNA dynamics 	<ul style="list-style-type: none"> • Requires multiple copies of the RNA of interest and multiple CRISPR/Cas13 to produce a bright enough signal for imaging • The binding affinity of CRISPR/Cas13 is highly dependent upon the gRNA sequence

		gRNA or the Cas13 can be fluorescently tagged.		
<i>RNA Aptamers</i>	RNA	RNA aptamers, like Mango ²³⁰ , are sequences designed as molecular beacons and selected through SELEX ^{233,234} . The resulting aptamer is capable of binding specific fluorophore derivatives with nanomolar affinity.	<ul style="list-style-type: none"> • Provides a fluorescence enhancement upon binding (up to 1000x), lowering the considerable fluorescence background that is typically present 	<ul style="list-style-type: none"> • Requires binding to a target molecule to fluoresce • Requires specific environmental parameters to perform optimally (magnesium concentration, temperature, ect.)
<i>Fluorescent Protein Tags (ex. GFP)</i>	Protein	Fluorescent proteins can be inserted into a cell line so that as a protein is expressed it fluoresces ²⁷⁰ .	<ul style="list-style-type: none"> • Proteins are produced directly by the cell • 100% labeling efficiency 	<ul style="list-style-type: none"> • These protein labels are bulky and can change protein dynamics and function.
<i>HaloTag and SNAP-tag</i>	Protein	Self-labeling protein tags such as HaloTag and SNAP-tag ^{237,238} are organic protein tags that can be inserted into cloning vectors ²³⁷ , allowing for a	<ul style="list-style-type: none"> • Can be used with a wide range of fluorophores • Improved brightness and photostability • Self-labeling 	<ul style="list-style-type: none"> • Does not have 100% labeling efficiency, therefore “dark” or unlabeled proteins sometimes occur • Requires gene editing

		specific binding site for fluorophores.		
<i>Fluorescent Antibody Fragments (Fabs)</i>	Protein	This is a technique that uses monoclonal antibodies which lack the Fc component to specifically tag proteins of interest ²⁷¹ . The fluorophore is conjugated to a single chain antibody specific to the protein of interest ²⁷² .	<ul style="list-style-type: none"> • Ideal method of quantifying the timing of post-translational modifications and their effects in living cells 	<ul style="list-style-type: none"> • Challenging to design probes • Low yield when designing Fabs

Study Objective and Hypotheses

The main objective of this study is to understand the role of the nucleoskeleton during mechanical regulation of adipogenesis. This objective will be address using the following hypothesis.

Hypothesis 1

- a. Mechanical activation of Focal Adhesion Kinase (FAK) is independent of lamin A/C.
- b. Mechanically-induced repression of adipogenesis does not require lamin A/C.

Research Questions

1. Does acute application of low intensity vibration and substrate strain induce activation of focal adhesion kinase at Tyrosine 397 in cells with depleted lamin A/C?
2. Does daily application of low intensity vibration reduce adipogenesis in lamin A/C depleted MSCs?

Hypothesis 2

- a) Sun1/2 regulates the inner nuclear functions of chromatin organization and adipogenic differentiation independent of the LINC complex function.
- b) Loss of the LINC complex function via dnKASH expression accelerate adipogenesis.

Research Questions

1. Does depletion of Sun1/2 alter nuclear morphology similar to Lamin A/C depletion?
2. Does depletion of Sun1/2 inhibit adipogenesis and increase heterochromatin marker H3K9me3?
3. Does loss of the LINC complex function via dnKASH accelerate adipogenesis without increasing heterochromatin marker H3K9me3?

CHAPTER TWO: LAMIN A/C FUNCTIONS INDEPENDENTLY FROM
MECHANICAL SIGNALING DURING ADIPOGENESIS

Abstract

Mesenchymal stem cells (MSC) maintain the musculoskeletal system by differentiating into multiple cell types including osteocytes and adipocytes. Mechanical signals, including strain and low intensity vibration (LIV), are important regulators of MSC differentiation. Lamin A/C is a vital protein for nuclear architecture that supports chromatin organization, as well as mechanical integrity and mechano-sensitivity of the nucleus in MSCs. Here, we investigated whether Lamin A/C and mechano-responsiveness are functionally coupled during adipogenesis. Depletion in MSCs using siRNA increased nuclear area, height and volume and decreased circularity and stiffness, while phosphorylation of focal adhesions and dynamic substrate strain in response to LIV remained intact. Lamin A/C depletion decelerates adipogenesis as reflected by delayed appearance of key biomarkers (e.g., adiponectin/ADIPOQ). Based on RNA-seq data, reduced Lamin A/C levels decrease the activation of the adipocyte transcriptome that is normally observed in response to adipogenic cues mediating differentiation of MSCs. Mechanical stimulation via daily LIV application reduced the expression levels of ADIPOQ in both control and Lamin A/C depleted cells. Yet, treatment with LIV did not induce major transcriptome changes in either control or Lamin A/C depleted MSCs, suggesting that the biological effects of LIV on adipogenesis may not occur at the transcriptional level. We conclude that while Lamin A/C activation is essential for

normal adipogenesis, it is dispensable for activation of focal adhesions by dynamic vibration induced mechanical signals.

Introduction

As one of the family proteins that form the nucleoskeleton, Lamin A/C (gene symbol: LMNA) has a vital role in providing the mechanical and structural integrity of the cell nucleus¹⁻³. Mutations in LMNA lead to premature aging in Hutchinson Gilford progeria syndrome [2-4], also known as progeria¹⁻³. This mutation in LMNA causes alterations at histone methylation sites in heterochromatin. In pluripotent embryonic stem cells (ESCs), Lamin A/C protein is expressed at low basal levels in undifferentiated cells, but expression is elevated after differentiation into ESC derivatives⁴⁻⁶. Because Lamin A/C supports the formation of transcriptionally suppressed chromatin (i.e., heterochromatin), its low levels in ESCs is consistent with absence of heterochromatin in ESC cells⁷. In contrast, the nucleoskeleton protein B (encoded by the LMNB1 and LMNB2 genes) was found to be present both before and after differentiation. These studies collectively indicate that Lamin A/C plays a specific role during the differentiation of ESCs.

Mechanical and structural attributes of the cell and nucleus change during Lamin A/C loss⁸. When Lamin A/C is depleted, cellular elasticity and viscosity of the cytoplasm decreases⁹. Such a change in mechanical properties affects the response to external forces: the nucleus of Lamin A/C deficient cells display higher displacement magnitude than that of wild type cells in response to biaxial strain, indicating a lower nuclear stiffness¹⁰. In contrast, nuclei containing the progeroid farnesylated Lamin A/C (i.e. progerin) show increased stiffness when visualized under strain¹¹. Both loss and

mutation of Lamin A/C are associated with irregular nuclear morphology, including blebbing and loss of circularity^{12,13}. Additionally, because Lamin A/C is located at the inner nuclear membrane, it acts as an anchoring site for chromatin. Depletion of Lamin A/C has been shown to affect both the dynamics and the organization of the chromatin^{14,15}, and may secondarily play a role in chromatin mediated mechanical properties of the cell nuclei¹⁶. Therefore, Lamin A/C plays a vital role in regulating cellular and nuclear mechanical structure and shape.

Mesenchymal Stem/Stromal Cells (MSCs) are tissue resident multipotent cells that can differentiate into musculoskeletal lineages including osteoblasts and adipocytes¹⁷. MSCs replace and rejuvenate skeletal and connective tissues in response to environmental mechanical demand, and their differentiation program is responsive to mechanical stimuli¹⁸⁻²⁰. For example, application of external mechanical challenge in the form of LIV over 14-days increases proliferation and osteogenic differentiation markers and subsequent mineralization of MSC cultures *in vitro*^{21,22}. In contrast to ESCs, MSCs are somatic cells that have the potential to differentiate into distinct mesenchymal lineages and express Lamin A/C in their native state. In this way, depletion of Lamin A/C in MSCs severely impedes osteoblast differentiation. MSCs treated with a siRNA targeting LMNA showed a drastic reduction in osteoblast differentiation transcription factors such as OCN, OSX, and BSP, and an increase in fat droplet formation when induced to differentiate into adipocytes²³. Mutations of Lamin A/C, specifically the lipodystrophy-associated LMNA p.R482W mutation, can also serve to slow adipogenic differentiation in cells²⁴. Additionally, overexpression of Lamin A/C has been shown to induce osteogenesis while inhibiting adipogenesis in human MSCs²⁵. Mouse studies

have shown that *Lmna* ^{-/-} mice have a significant reduction in bone mass compared to WT mice reflecting reduced osteoblast numbers ²⁶. While these findings suggest a role for Lamin A/C in regulating the differentiated state of MSCs, whether Lamin A/C depletion contributes to mechanical regulation of MSC differentiation remains insufficiently explored.

An important signaling node for mechanical control of MSC are focal adhesions, macromolecule protein complexes located on the cellular membrane, that connect the cytoskeleton to the extracellular matrix (ECM) where the cell is anchored to the extracellular environment through integrins ²⁷. During dynamic mechanical stimulus, integrin engagement is regulated by activation of Focal Adhesion Kinase (FAK) at tyrosine 397 residue ²⁸. We have reported both LIV and substrate strain lead to FAK phosphorylation at tyrosine 397²⁹. This activation of FAK at focal adhesions both recruits signaling molecules that lead to cytoskeletal restructuring and activates concomitant mechanosignaling events such as the Akt/ β -Catenin (AKT1-CTNNB1) pathway ³⁰. Application of mechanical stimuli with strain, fluid flow, and LIV generates concomitant activation of β -Catenin and RhoA signaling in MSCs ^{29,31,32}. Within the context of MSC adipogenesis, activation of these parallel signaling pathways results in decelerated adipogenic commitment of MSCs as measured by reduced production of adipogenesis related proteins such as adiponectin (encoded by adiponectin gene ADIPOQ) and peroxisome proliferator-activated receptor gamma (PPARG1) ³³. In addition to cytomechanical signaling events initiated at focal adhesions and cytoskeleton, control of MSC differentiation is also dependent on nuclear connectivity within the cytoskeleton. Inhibiting nucleo-cytoskeletal connectivity by disabling the function of

Linker of Nucleoskeleton and Cytoskeleton (LINC) complexes impedes the nuclear entry of important molecular transducer mechanical information such as Yap/Taz and β -Catenin which act as co-transcriptional factors for regulating MSC adipogenesis and osteogenesis³⁴. As opposed to LINC complex depletion, Lamin A/C depletion has no effect on mechanically induced nuclear β -Catenin entry³⁵, suggesting that Lamin A/C may be dispensable for the mechanically-induced activation of focal adhesions that lead to de-phosphorylation and subsequent nuclear entry of β -Catenin.

These previous studies show that Lamin A/C plays a central role in nuclear organization and structure, as well as contributing to the cell's ability to sense structural qualities of the extracellular matrix to guide differentiation of MSCs. However, the role of Lamin A/C in focal adhesion signaling and mechanically-induced control of MSC fate in response to dynamic mechanical challenges remains incompletely understood. Therefore, we tested the requirement of Lamin A/C for the mechanical response of MSCs. Using LIV, we have investigated the role of Lamin A/C depletion on the mechanical control of MSC adipogenesis.

Results

siRNA Depletion of Lamin A/C Weakens the Nuclear Elastic Modulus in MSCs

We investigated the effects of Lamin A/C loss on cellular and nuclear morphology as well as mechanical properties. MSCs treated with either a control siRNA (siCntl) or a Lamin A/C specific siRNA (siLMNA) were stained against F-actin and DNA. Compared to the siCntl group, siLMNA treated MSCs showed a more elongated nuclear morphology but no apparent changes in the F-actin cytoskeleton (**Fig. 2.1A**). Shown in **Fig. 2.1B**, morphology quantification indicated a 9% decrease of nuclear

sphericity in siLMNA treated MSCs when compared to MSCs treated with a control siRNA ($p < 0.001$). The nuclear area, volume, and height were increased 32%, 31%, and 11% in siLMNA treated MSCs, respectively, compared to control siRNA treated cells (**Fig. 2.1B**, $p < 0.001$). The Young's modulus was measured for both whole cells and extracted nuclei treated with either siLMNA or siCntl. The Young's modulus was measured using a rounded AFM probe tip which was pressed onto the surface of the whole cell directly above the nucleus or on an isolated nucleus (**Fig. 2.1C** and **2.1D**). Confocal imaging with DNA and Lamin A/C labeling of a representative isolated nucleus (**Fig. 2.1E**), indicates that nuclear structure remains intact following isolation. Treatment with siLMNA caused a 45% reduction in whole cell stiffness when compared to siCntl treated MSCs (**Fig. 2.1F**, $p < 0.001$), while extracted nuclei exhibit a 55% reduction in stiffness in Lamin A/C depleted cells compared to siCntl ($p < 0.01$) (**Fig. 2.1G**).

siRNA Depletion of Lamin A/C (LMNA) Increases Sun2 (SUN2) Nuclear Levels and Focal Adhesion Proteins

To further characterize the effects of Lamin A/C loss on nuclear envelope and focal adhesions, the LINC complex and focal adhesion proteins were investigated. Confocal images of the siCntl and siLMNA groups indicated that there were no visible changes in the LINC proteins Sun1 (SUN1) and Sun2 (SUN2) when Lamin A/C was depleted (**Fig. 2.2A**). Quantitative analysis of the confocal images did not detect any differences in Sun1 or Sun2 nuclear envelope localization. We examined the same proteins using cellular fractionation followed by western blotting and densitometry analysis (**Fig 2.2B**). All the measurements were normalized to whole cell siCntl protein amounts which was set to 1. Comparing siLMNA treatment with siCntl, Lamin A/C

significantly decreased in whole cell Lamin A/C (-35%, $p < 0.05$). The relative Lamin A/C concentration was greater in the nuclear fraction and led to larger values, while band intensities of the siLMNA group remained significantly lower compared to siCtrl (-11%, $p < 0.05$). Except for a small amount of Sun1 detection in the cytoplasm, both Sun1 and Sun2 were largely restricted to the nucleus. Knocking down Lamin A/C was associated with an increase in nuclear Sun2 (+44%, $p < 0.05$). Focal adhesion proteins also were altered under siLMNA treatment. Total focal adhesion kinase (FAK) adhered to the cell culture plate experienced an increase of 39% compared to control treated cells ($p < 0.05$) (Shown in **Fig. 2.2D** and **Fig. 2.2E**). The amount of Akt adhering to cell culture plates also increased by 50% ($p < 0.05$). No changes in vinculin were detected.

Focal Adhesions Maintain Response to Mechanical Stimulus in Lamin A/C Depleted MSCs

Basal levels of FAK were increased in Lamin A/C depleted cells. We next asked if mechanical activation of FAK was altered by further quantifying the mechanical activation of FAK via its phosphorylation at Tyrosine 397 residue (pFAK) which is indicative of integrin engagement²⁸. MSCs were treated with either strain or LIV and compared to non-mechanically stimulated controls. Basal pFAK levels normalized to total FAK (TFAK) were 85% elevated in the siLMNA groups when compared to the siCtrl groups ($p < 0.05$) (**Fig. 2.3A** and **Fig. 2.3B**). Phosphorylated FAK levels from both siCtrl and siLMNA treated groups increased by 101% ($p < 0.05$) and 87% ($p < 0.001$) in response to 20 min strain (2%, 0.1Hz) when compared to non-strained counterparts. LIV also activated FAK: pFAK increased by 331% ($p < 0.001$) in siCtrl and 83% ($p < 0.001$) in siLMNA treated MSCs in response to LIV (0.7g, 90Hz).

Application of Daily LIV Treatment Decreases Adipogenic Differentiation in MSCs

As focal adhesion signaling was intact in siLMNA treated MSCs, we next probed downstream processes to ask whether the LIV application known to slow adipogenesis³⁶ was effective when Lamin A/C was depleted. In our experiment timeline, cells were first treated with siRNA on day 1 and then cultured in adipogenic media concomitant with LIV treatment (**Fig. 2.4A**). On day 2, adipogenic media was placed on cells and LIV treatment started. LIV treatment occurred twice a day for 20 minutes with two-hour rests in between treatments. On day 7, cell protein or RNA samples were collected for either western blotting or RNA-seq analysis. Probing adipogenesis marker adiponectin between non-LIV controls, Lamin A/C depleted cells showed a 39% decrease in adiponectin protein at 7 days (**Fig. 2.4B** and **Fig. 2.4C**). Similarly, compared within LIV treated groups, adiponectin levels in the siLMNA group was 51% lower than siCtrl treated cells with LIV ($p < 0.01$). Compared to non-LIV controls, daily LIV application decreased adiponectin protein levels by 30% in the siCtrl ($p < 0.01$) and 44% in the siLMNA groups ($p < 0.001$). RNA-Seq analysis indicates that siRNA inhibition of LMNA was successful as LMNA gene expression was reduced by 77% in siLMNA cells compared to siCtrl cells ($p < 0.001$) (**Fig. 2.4D**).

Differential Effect of Lamin A/C Depletion and LIV on mRNA Transcription during Adipogenic Differentiation

RNA-seq was performed to determine the effects of LIV and siLMNA treatment on differential mRNA in MSCs during adipogenesis. Read values were filtered for robust expression by selecting genes with average levels of 0.3 FPKM (Fragments per kilobase of transcript per million mapped reads), t-test $p < 0.05$, and Log₂ fold change greater than

1.4). Hierarchical clustering of these genes generated a heatmap (**Fig. 2.5A**) in which siCntl treated samples clustered together in one clade, while undifferentiated and siLMNA treated samples were clustered together in another clade that is visually separated from siCntl treated samples. Principal component analysis (**Fig. 2.5B**) shows further grouping of siCntl samples and siLMNA samples. Principal component 1 and component 2 explain 40.4% and 15.9% total variance, respectively with prediction ellipses indicating the probability of 0.95 that a new observation of the same group will fall inside the ellipse. Representative RNA-seq data for individual genes shows FPKM levels for a panel of 13 genes associated with the adipogenic pathway, including adiponectin (ADIPOQ), CCAAT/enhancer-binding protein alpha (CEBPA), and peroxisome proliferator-activated receptor gamma (PPARG) and others (**Fig. 2.5C**).

Lamin A/C Depletion Impedes Adipogenic Transcription in MSCs

Cells treated with siLMNA and siCntl with adipogenesis were compared statistically to determine differential gene expression between siRNA treatments. A volcano plot for the comparison between siLMNA and siCntl treated samples under adipogenic constraints (**Fig. 2.6A**) revealed there are 52,607 statistically unchanged transcripts between Lamin A/C depleted and control MSCs with Wald values of $p > 0.05$ (grey and green data points). Shown in green data points, 2,000 of them showed at least a 2-fold difference (i.e. Log_2 fold change ≥ 1). While 749 genes showed statistically significant change between Lamin A/C depleted and control MSCs with Wald values of $p < 0.05$ (shown in blue) and 427 of them had a less than 2-fold difference (i.e. Log_2 fold change ≤ 1). The remaining 322 genes showed at least a 2-fold difference (i.e. Log_2 fold change ≥ 1), which represents significant and differentially expressed genes. Up-regulated

(red genes on the right side, n = 173) and down-regulated genes (red genes on the left side, n = 149) upon LMNA depletion were then assessed by a clustering analysis using ClustVis³⁷. Upregulated genes upon Lamin A/C depletion are associated with cellular processes such as (i) Tissue Repair (e.g., genes generally involved in angiogenesis, hematopoiesis, and mechanical stress shielding), (ii) ECM remodeling (e.g. genes generally involved in take-up and intra-cellular transport of ECM debris as well as suppression of apoptosis), (iii) cell surface transporters (e.g., genes that mediate the trafficking of compounds across membranes) (**Fig. 2.6B**). Collectively, the biological function of these genes appears to be related to tissue repair, inflammation and extracellular matrix homeostasis. Downregulated gene groups upon LMNA knock-down included (i) Cell adhesion and cytoskeletal organization, (ii) interferon signaling and regulation of gene expression (e.g., DNA and RNA binding, and protein degradation), (iii) G protein coupled receptor signaling (e.g., diverse range of cell surface receptors and components of the angiotension system), (iv) lipid metabolism and paracrine inflammatory signaling, and (v) adipogenic phenotype (**Fig. 2.6C**). These down regulated genes together are generally involved in cell migration, energy metabolism and adipogenic differentiation. The results from gene ontology and gene network analysis revealed that Lamin A/C depletion has pleiotropic effects on gene expression, yet many gene pathways converge on cell surface related biochemical events, interactions with the extracellular matrix and internal metabolic pathways.

LIV Decreases Interferon Signaling Pathway in siLMNA and siCntl Treated Cells

To determine the effects of LIV with siCntl and siLMNA controls under adipogenic constraints were compared against their LIV treated counterparts. The

volcano plot comparing the siCntl adipogenesis with or without LIV treatment (siCntl \pm LIV) is shown in **Fig. 2.7A**. There were 53,326 statistically unchanged genes between with Wald values of $p > 0.05$ (grey and green data points) with, 1,939 of them showed at least 2-fold difference (green). While 76 genes showed statistically significant change between LIV treated and control MSCs with Wald values of $p < 0.05$, shown in blue, 26 of them had a less than 2-fold difference. Remaining 53 genes showed at least 2-fold difference (red). Assessing down-regulated genes via clustering revealed an interferon-related cluster in the LIV treatment group (**Fig. 2.7B**). Similarly, LIV treatment upon LMNA depletion also revealed an interferon-related cluster when assessing gene clustering by ClustVis in the significant and highly down-regulated genes (**Fig. 2.7D**). Together, cells treated with siCntl had 11 genes that are part of interferon pathway while cells treated with siLMNA had 16 genes associated with interferon pathway signaling (**Fig. 2.7E**). The physiological relevance of the interferon pathway is uncertain, because this pathway may be linked to cellular responses to events precipitated by siRNA transfection. Excluding this latter finding, it appears that while LMNA loss has a dramatic impact on gene expression programs, LIV has very minimal effects on the transcriptome of differentiating MSCs.

Materials and Methods

MSC Isolation

Bone marrow derived MSC (mdMSC) from 8-10 wk male C57BL/6 mice were isolated as described³⁸. Briefly, tibial and femoral marrow were collected in RPMI-1640, 9% FBS, 9% HS, 100 μ g/ml pen/strep and 12 μ M L-glutamine. After 24 hours, non-adherent cells were removed by washing with phosphate-buffered saline and adherent

cells cultured for 4 weeks. Passage 1 cells were collected after incubation with 0.25% trypsin/1 mM EDTA \times 2 minutes, and re-plated in a single 175-cm² flask. After 1-2 weeks, passage 2 cells were re-plated at 50 cells/cm² in expansion medium (Iscove modified Dulbecco's, 9% FBS, 9% HS, antibiotics, L-glutamine). mdMSC were re-plated every 1-2 weeks for two consecutive passages up to passage 5 and tested for osteogenic and adipogenic potential, and subsequently frozen.

Cell Culture, Pharmacological Reagents, and Antibodies

Fetal calf serum (FCS) was obtained from Atlanta Biologicals (Atlanta, GA). Culture media, trypsin-EDTA, antibiotics, and Phalloidin-Alexa-488 were from Invitrogen (Carlsbad, CA). MSCs were maintained in IMDM with FBS (10%, v/v) and penicillin/streptomycin (100 μ g/ml). For phosphorylation measurements, seeding cell density was 10,000 cells per square centimeter. For immunostaining experiments, seeding cell density was 3,000 cells per square centimeter. For phosphorylation measurements and immunostaining experiments, all groups were cultured for 48h before beginning experiments and were serum starved overnight in serum free medium.

For adipogenic differentiation experiments, the seeding cell density was 21,000 cells per square centimeter. Cells were transfected 24 hours after cell seeding with siRNA targeting Lamin A/C (siLMNA) or a control sequence (siCnt1) using RNAiMax from Invitrogen. Adipogenic media and LIV treatment followed previously published protocol, where twenty four hours after the transfection, the adipogenic media was added which contained dexamethasone (0.1 μ M) and insulin (5 μ g/ml)¹⁸. Cell cultures were incubated with the combined transfection media and adipogenic differentiation media for 7 days

after adipogenic media was added with or without LIV treatment (2 X 20 minutes per day separated by 2 hours).

The following antibodies were purchased: Cell Signaling (Danvers, MA): Akt (#4685), p-Akt Ser473 (#4058L), β -Tubulin (D3U1W), and p-FAK Tyr397 (#3283). ThermoFischer Scientific (Rockford, IL): Adiponectin (PA1-054). Santa Cruz Biotechnology (Dallas, TX): FAK (sc-558), Lamin A/C (sc-7292).

LIV and Strain

Vibrations were applied at peak magnitudes of 0.7g at 90Hz twice for 20min separated by 2h rest period at room temperature. Uniform 2% biaxial strain was delivered at 10 cycles per minute for 20 min using the Flexcell FX-5000 system (Flexcell International, Hillsborough, NC). Controls were sham handled. During adipogenesis experiments, LIV was applied 24 hours after initial transfection, a regimen we previously shown be effective²⁹.

Isolation of Focal Adhesions

Cells were incubated with triethanolamine (TEA)-containing low ionic-strength buffer (2.5 mM TEA, pH 7.0) for 3 minutes at RT, 1 \times PBS containing protease/phosphatase inhibitors. A Waterpik (Fort Collins, CO, www.waterpik.com) nozzle held 0.5 cm from the plate surface at approximately 90 $^\circ$ supplied the hydrodynamic force to flush away cell bodies, membrane-bound organelles, nuclei, cytoskeleton, and soluble cytoplasmic materials so that residual focal adhesions could be isolated as we have reported previously²⁹.

siRNA Silencing Sequences

For transient silencing of MSCs, cells were transfected with gene-specific small interfering RNA (siRNA) or control siRNA (20 nM) using RNAiMax (ThermoFischer) according to manufacturer's instructions. The following Stealth Select siRNAs (Invitrogen) were used in this study: Lamin A/C 5'-UGGGAGAGGCUAAGAAGCAGCUUCA-3' and negative control for Lamin A/C 5'-UGGGAGUCGGAAGAAGACUCGAUCA-3'.

Isolation of Nuclei for Young's Modulus

MSCs were plated at 10,000 cell/cm² cell density. For mechanical and structural testing, nuclei were isolated by scraping cells in PBS and then suspending cells in hypotonic solution followed by centrifugation at 3000xg. Nuclei were then extracted by using percol (81% percol, 19% hypotonic buffer) and centrifugation at 10,000xg. Nuclei were then diluted in PBS and plated. Nuclei Young's modulus was determined using Atomic Force Microscopy (AFM). For strain experiments, cells were plated on Bioflex Collagen-I coated silicone plates.

RNA-Seq

RNA extraction and sequencing were done by Novogene. Quality control of raw data was done using FASTQC. Read Alignment of the genome to the raw reads was done using STAR³⁹. Read count generation was generated using feature Counts and Differential gene expression analysis was done using DESEQ2⁴⁰. For analysis using fragments per kilobase of transcript per million mapped reads (FPKM), data were assessed as previously described⁴¹⁻⁴⁴. Briefly, RNA-Seq data were analyzed by a Mayo Bioinformatics Core called MAPRSeq v.1.2.1⁴⁵, which includes TopHat 2.0.6 alignment

⁴⁶ with and gene expression quantification using HTSeq software ⁴⁷. Normalized gene counts were obtained from MAPRSeq as FPKM. Hierarchical clustering and principal component analysis were assessed and visualized using ClustVis ³⁷. RNA-Seq data were deposited in the Gene Expression Omnibus of the National Institute for Biotechnology Information (GSE157056).

Immunofluorescence

Twenty-four hours after the siRNA treatment against Lamin A/C protein, cells were fixed with 4% paraformaldehyde. Cells were permeabilized by incubation with 0.3% Triton X-100. Cells were incubated in a blocking serum in PBS with 5% Donkey Serum (017-000-121, Jackson Immuno Research Laboratories). Primary antibody solution were incubated on the cells for 1h at 37°C, followed by secondary antibody incubation of either Alexa Fluor 594 goat anti-rabbit (Invitrogen) or Alexa Fluor 647 donkey anti-mouse. For nuclear staining cells were incubated with NucBlue Hoeschst stain (Fischer Scientific). For actin staining, cells were incubated in Alexa Fluor 488 Phalloidin (Life Technologies). Primary and secondary concentrations were both 1:300.

Nuclear Morphology

To test the nuclear morphology that will show the level of mechanical constraint on nucleus, MSCs seeded at 3000cell/cm² on plastic slide chambers (iBIDI μ slide # 80421). 72h after the siRNA treatment against Lamin A/C protein, DNA (Hoechst 33342, Life Technologies), and or immunostained against actin (Alexa Fluor 488 Phalloidin, Life Technologies). Z-stack confocal 3D images were obtained with a Zeiss LSM 710 with a separation interval of 0.15 μ m. Z-stack images were analyzed using IMARIS software.

Western Blotting

Whole cell lysates were prepared using an radio immunoprecipitation assay (RIPA) lysis buffer (150mM NaCl, 50mM Tris HCl, 1mM EDTA, 0.24% sodium deoxycholate, 1% Igepal, pH 7.5) to protect the samples from protein degradation NaF (25mM), Na₃VO₄ (2mM), aprotinin, leupeptin, pepstatin, and phenylmethylsulfonylfluoride (PMSF) were added to the lysis buffer. Whole cell lysates (15µg) were separated on 10% polyacrylamide gels and transferred to polyvinylidene difluoride (PVDF) membranes. Membranes were blocked with milk (5%, w/v) diluted in Tris-buffered saline containing Tween20 (TBS-T, 0.05%). Blots were then incubated overnight at 4°C with appropriate primary antibodies. Following primary antibody incubation, blots were washed and incubated with horseradish peroxidase-conjugated secondary antibody diluted at 1: 5,000 (Cell Signaling) at RT for 1h in 5% milk in TBST-T. Chemiluminescence was detected with ECL plus (Amersham Biosciences, Piscataway, NJ). At least three separate experiments were used for densitometry analyses of western blots and densitometry was performed via NIH ImageJ software.

Statistical Analysis

Results for densitometry were presented as mean \pm SEM. Densitometry and other analyses were performed on at least three separate experiments. Differences between groups were identified by two-tailed Student's T-test. Analysis of nuclear morphology and Young's modulus were done using Whitney-Mann test and results were presented as mean \pm STD. Differential gene expression analysis was done using Wald test. P-values of less than 0.05 were considered significant.

Discussion

In this study, we have found that Lamin A/C depleted MSCs were able to activate focal adhesion signaling and decrease the output of adipogenic biomarkers (e.g., adiponectin) as efficiently as MSCs with intact Lamin A/C in response to LIV. Our findings indicate that the global adipogenic mRNA repression in Lamin A/C depleted MSCs occurred independent of LIV. RNA-seq analysis showed that LIV had negligible effects on mRNA levels compared to Lamin A/C depletion, suggesting that LIV effects on adipogenesis is likely caused by post-translational mechanisms or other downstream effects.

Lamin A/C depletion interfered with adipogenic differentiation but not with biomechanical responses. Not only was Lamin A/C dispensable for the LIV and strain mediated activation of focal adhesions, but LIV decreased levels of adiponectin protein. Consistent with repression of adipogenesis, in a Lamin A/C independent fashion. Adipogenic mRNA levels determined by RNA-seq were unaffected by LIV suggesting that LIV-induced repression of adipogenesis was post-transcriptional or post-translational.

In Lamin A/C depleted cells, microscopic observations of increased blebbing, elongated nuclear shape, and ruffled nuclear membrane^{8,12,48} indicates a compromised nuclear structure. Quantification of 3D nuclear structure of Lamin A/C depleted cells were supportive of these previous observations and showed reduced sphericity and increased planar nuclear area while nuclear height and volume were increased compared to controls. It has been reported that Lamin A/C depletion increases nuclear height and volume in-part due to reduced recruitment of perinuclear and apical F-actin cables⁴⁹.

While reduction of apical F-actin may contribute to a decrease in elastic modulus in Lamin A/C depleted intact MSCs, a similar decrease was observed in Lamin A/C depleted isolated live nuclei. The similarities in decreased stiffness in both intact cells and isolated nuclei suggests that nuclear softening is the primary driver of decreased cell stiffness upon Lamin A/C loss of function.

Our data suggest that MSCs compensate for Lamin A/C mediated nuclear softening by increasing their focal adhesions. Not only was total FAK (PTK2) and Akt (AKT1) accumulation at the focal adhesions more robust in Lamin A/C depleted MSCs, Tyrosine 397 phosphorylated FAK was also higher which suggests increased integrin engagement²⁸. These findings are not surprising as both depletion of Lamin A/C⁵⁰ and nucleo-cytoskeletal connector Nesprin-1⁵¹ were shown to increase substrate traction in cells. Tracking with increased basal pFAK levels, application of either LIV or strain pushed acute FAK phosphorylation of Lamin A/C depleted cells higher than control cells. These results indicate that the focal adhesion signaling remains intact in Lamin A/C depleted MSCs.

Similar to focal adhesions, nucleo-cytoskeletal connectivity provided by LINC complex remained intact under Lamin A/C depletion. Previous studies have shown that LINC proteins Sun1 and Sun2 bind to the Lamin A/C in order to mediate a connection from the inner nucleus to the cytoskeleton and ultimately to the focal adhesions that make a physical connection to the extra cellular matrix^{52,53}. Quantification of confocal images of Sun1 and Sun2 revealed no changes compared to controls while Sun2 had an increase in proteins levels in both the whole cell and nuclear fractions. These observed protein changes under loss of the Lamin A/C could be in parallel to increased focal adhesion

presence. Therefore, the cell may be increasing the levels of Sun2 that is connected to actin, which in turn are connected to a higher number of focal adhesions. Localization of Sun1 and Sun2 proteins to the nuclear envelope are not entirely dependent upon Lamin A/C, but loss of Lamin A/C still results in some alteration of Sun1 localization and no alteration for Sun2 supporting previous literature as seen in **Fig. 2.2C** in the whole cell and nuclear fractions^{53,54}. While noted changes in the Sun proteins under Lamin A/C depletion suggests a putative relationship, loss of Lamin A/C did not negatively impact the structural Sunmediated integrity of the LINC complex.

Adipogenesis has recently been shown to decrease with mutated Lamin A/C, specifically in cells expressing the lipodystrophy-associated LMNA p.R482W mutation²⁴. Our data supports this previous observation as MSCs treated with siLMNA experienced slower adipogenic differentiation compared to siCntl treated cells (**Fig. 2.4C**). This observation is in contrast to studies that showed increased adipogenesis in depleted MSCs^{23,25,55}. While cell culture conditions vary from experiment to experiment, this study did not utilize strong adipogenic inducers such as indomethacin and IBMX^{25,55}. Instead, we used a milder adipogenic media incorporating insulin and dexamethasone. This selection was based on previous work where LIV was unable overcome the adipogenesis induced by indomethacin and IBMX¹⁸. RNA-seq data indicate that upon MSCs display an undifferentiated phenotype upon Lamin A/C depletion, as reflected by reduced expression of genes associated with adipogenic and lipid related metabolic pathways. In contrast, LIV treatment did not have a significant impact on adipogenic gene expression indicating that Lamin A/C and not low intensity vibration is critical for adipogenic differentiation.

In contrast to large shifts in transcription under Lamin A/C depletion, RNA-seq data indicates that only 21 genes for siCnt1 and 74 genes for siLMNA treated cells were differentially expressed as a result of LIV treatment. Despite the lack of changes at mRNA level, Lamin A/C depleted MSCs retain their ability to respond to mechanical signals and exhibit decelerated adipogenesis reflected by reduced adiponectin protein in LIV treated cells. Although mechanical stimulation using LIV is not causing widespread alteration in mRNA expression, we did observe a distinct LIV-dependent signature characteristic of interferon responsive genes. Changes in interferon responses could be expected, because siRNA transfection affects single and double-stranded RNA accumulation within cells that may provoke interferon responses by mimicking viral RNA transfection. As such, this finding could perhaps be dismissed as technical artefact. However, this interferon related differentially expressed gene changes were compared to non-LIV siRNAs. Hence, a biological cause may also be entertained. A possible relationship between type 1 interferon signaling pathway and the known mechanosensitive Wnt/ β -catenin signaling pathway has been proposed ⁵⁶. GSK-3 β is known to activate type 1 interferon signaling pathway ⁵⁷ and inhibit the Wnt/ β -catenin pathway by causing the degradation of β -catenin ³⁵. Activation of the Wnt/ β -catenin signaling pathway via mechanical stimulus causes GSK-3 β to be inhibited, promoting β -catenin translocation to the nucleus to inhibit adipogenesis ³⁵, and potentially inhibit the type 1 interferon signaling pathway. Additionally, mechanical forces, specifically low intensity forces such as shear strain and vibration, have been shown to inactivate interferons ⁵⁸. Thus, there may be secondary mechanisms by which interferons respond to mechanical forces. The more important finding is the absence of major transcriptome

changes during adipogenesis in response to LIV which points to post-transcriptional or post-translational regulatory events. While the mechanism of the observed mechanoregulation of adipogenesis is beyond of scope of this paper, further research will be needed to fully understand the potential mechanoregulation of adipogenesis during or after transcription.

Conclusion

Lamin A/C depletion resulted in decreased nuclear integrity, more robust focal adhesions, and reduced adiponectin protein levels. Neither Sunmediated LINC connectivity nor focal adhesion signaling in response to acute mechanical challenge were negatively impacted by Lamin A/C depletion. This independence of mechanical signaling from Lamin A/C was further highlighted by the significant reduction in adiponectin protein levels in response to LIV. The small transcriptional response under LIV was dwarfed by large transcriptional changes and blunted adipogenesis under Lamin A/C depletion. Findings of this study indicate that Lamin A/C is required for proper adipogenic commitment of MSCs into the adipogenic lineage and that the mechanical regulation of adipogenesis may not utilize similar pathways to elicit a response in MSCs.

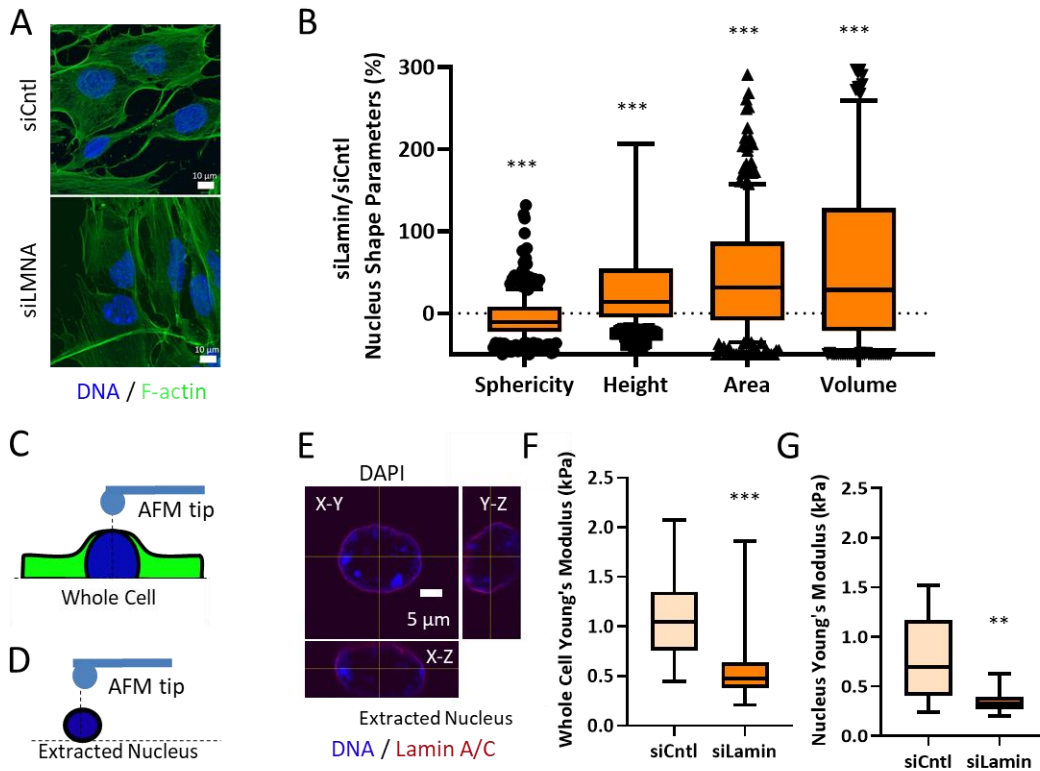


Figure 2.1 siRNA depletion of Lamin A/C weakens the nuclear elastic modulus in MSCs

A Confocal Image of F-actin (phalloidin, green) and nucleus (Hoechst, blue). Scale bar: 10 μ m . B Nuclear sphericity decreased by 8% in MSCs treated with Lamin A/C specific siRNA (siLmna) compared to MSCs treated with a non-specific control siRNA (siCntl) ($p < 0.05$, $n = 342$). Nuclear area of siLmna treated cells showed a 32% increase when compared to siCntl ($p < 0.05$, $n = 342$). Nuclear volume siLmna treated cells increased by 31% compared to siCntl ($p < 0.05$, $n = 342$). Nuclear height of siCntl and siLmna treated cells. When compared to the nuclear height of siCntl MSCs, siLmna treated cells had increased nuclear height of 12% ($p < 0.05$, $n = 342$). C Schematic of AFM probe tip testing whole cell Young's modulus in live MSCs. D Depiction of AFM probe tip testing live extracted nucleus. E Confocal image of extracted nucleus depicting its orthogonal views from X-Y, X-Z, Y-Z planes (Hoechst, blue; Lamin A/C, Red) Scale bar: 5 μ m . F Whole cell Young's modulus of the siLmna group was 45% lower when compared to the siCntl group. G Young's modulus of extracted live nucleus in siLmna MSCs remained 55% lower when compared to siCntl MSCs ($p < 0.01$, $n = 13$). Results are presented as mean \pm STD. Group comparisons were made via non-parametric Mann Whitney tests. $p < 0.05$, ** $p < 0.01$, *** $p < 0.001$, **** $p < 0.0001$ against control.

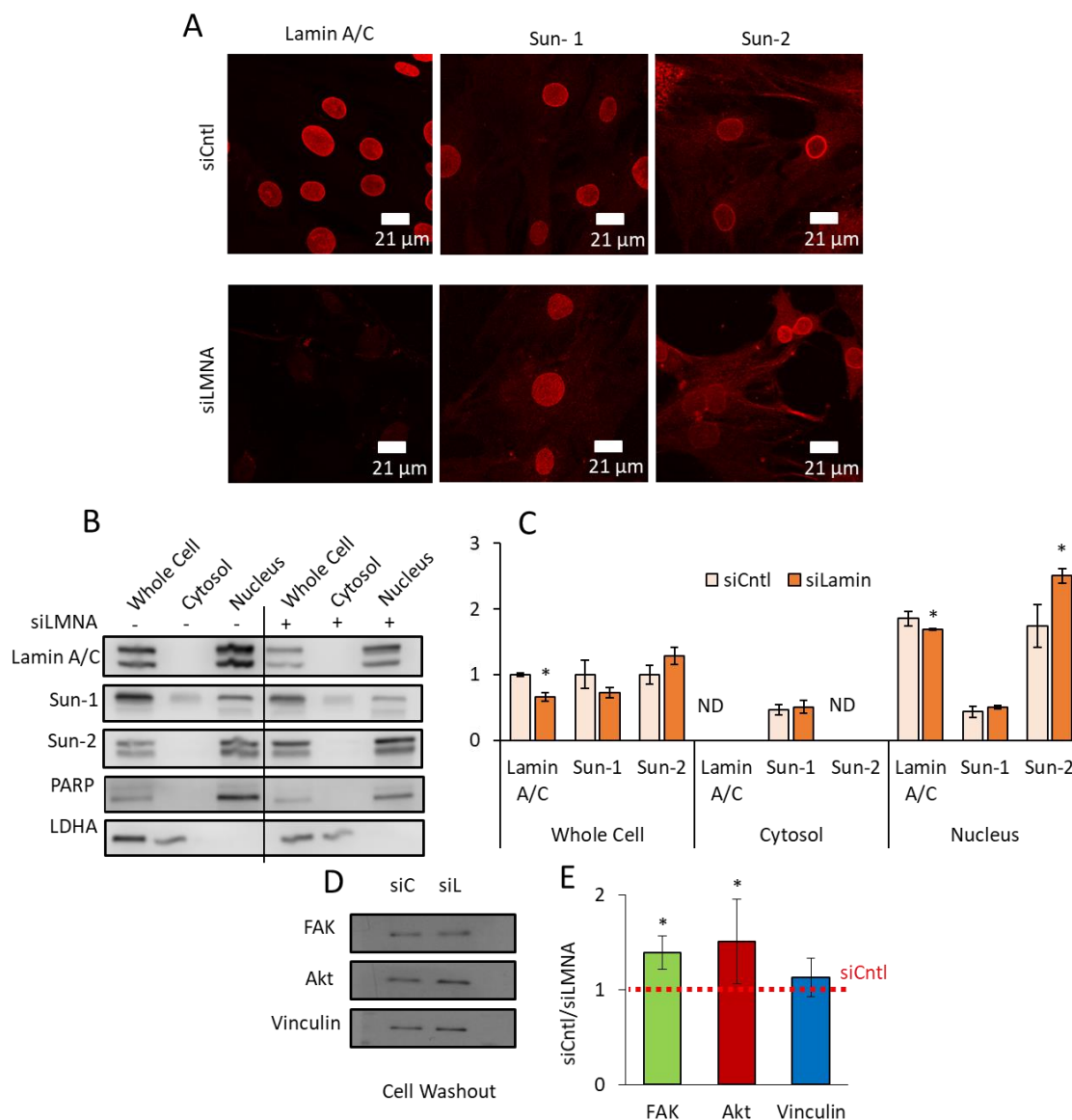


Figure 2.2 siRNA depletion of Lamin A/C (LMNA) Increases Sun2 (SUN2) Nuclear Levels and Focal Adhesion Proteins

A Confocal images of cells treated with the siCntl and siLMNA siRNA groups. Primary antibodies targeted lamin A/C, SUN1, and SUN2. Hoechst stained images can be found in Fig. S2. B Representative western blots of cell fractionations (whole cell, cytosol and nucleus) with cells treated with either siCntl or siLmna. Primary antibodies targeted lamin A/C, SUN1, SUN2, PARP, and LDHA. Line represents removal of protein ladder marker lane, uncropped blots are provided in Fig.S1. C Analysis of western of cell fractionation western blots (n=3/grp). siLmna treated cells had a 44% increase of SUN2 in the nucleus fraction ($p < 0.05$) compared to siCntl samples. SUN1 had no detectable changes. ND represents non-detectable levels. D Representative western blot of focal adhesion proteins following a cell washout. Primary antibodies targeted of FAK, Akt, and Vinculin in siCntl and siLmna siRNA treated cells. E Densitometry analysis showed that, when compared to

siCntl levels siLMNA treated MSCs showed increased levels of total FAK (39%, $p < 0.05$) and total Akt (50%, $p < 0.05$), no change in Vinculin was detected ($n = 3/\text{grp}$). Results are presented as mean \pm STE. Scale bar: $21\mu\text{m}$. Group comparisons were made via parametric two-tailed Student T-test (C) or one-way ANOVA followed by a Newman-Keuls post-hoc test. * $p < 0.05$ against control.

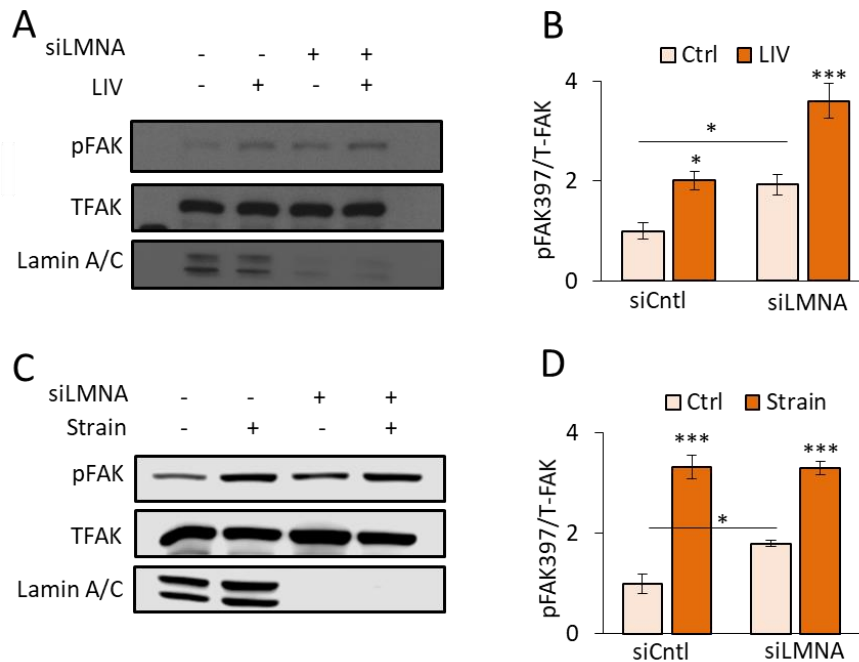


Figure 2.3 Focal adhesions maintain response to mechanical stimulus in Lamin A/C depleted MSCs

A Representative western blots for pFAK (Tyr 397), TFAK, and lamin A/C in siCntl and siLMNA treated cells groups treated with 2 bouts of LIV (20min, 90Hz, 0.7g) separated by 2 hour rest period. LIV treated samples had a 2-fold increase of pFAK compared to non-LIV. B Analysis of western image of pFAK, TFAK, and Lamin A/C during LIV ($n = 4/\text{grp}$). The non-LIV siLMNA group had a 92% ($p < 0.05$) increased basal pFAK compared to the non-LIV siCntl group. In response to LIV, both siCntl and siLmn treated MSCs elicited 101% ($p < 0.05$) and 87% (by a Newman-Keuls post-hoc test. $p < 0.05$, ** $p < 0.01$, *** $p < 0.001$, against control or against each other. $p < 0.001$) increases in pFAK, respectively. C Representative western blots for pFAK (Tyr 397), TFAK, and Lamin A/C of the siCntl and siLMNA groups treated with a single bout strain (20 min, 0.1 Hz, 2% strain). D Analysis of pFAK, TFAK, and Lamin A/C immediately after strain application ($n = 4/\text{grp}$). The non-strain siLMNA group had a 79% ($p < 0.05$) increased basal pFAK compared to the non-strain siCntl group. In response to strain, pFAK levels were elevated by 331% ($p < 0.001$) and 83% ($p < 0.001$) in siCntl and siLmn treated MSCs respectively. Results are presented as mean \pm STE. Group comparisons were made via one-way ANOVA followed by a Newman-Keuls post-hoc test. * $p < 0.05$, ** $p < 0.01$, *** $p < 0.001$, against control or against each other.

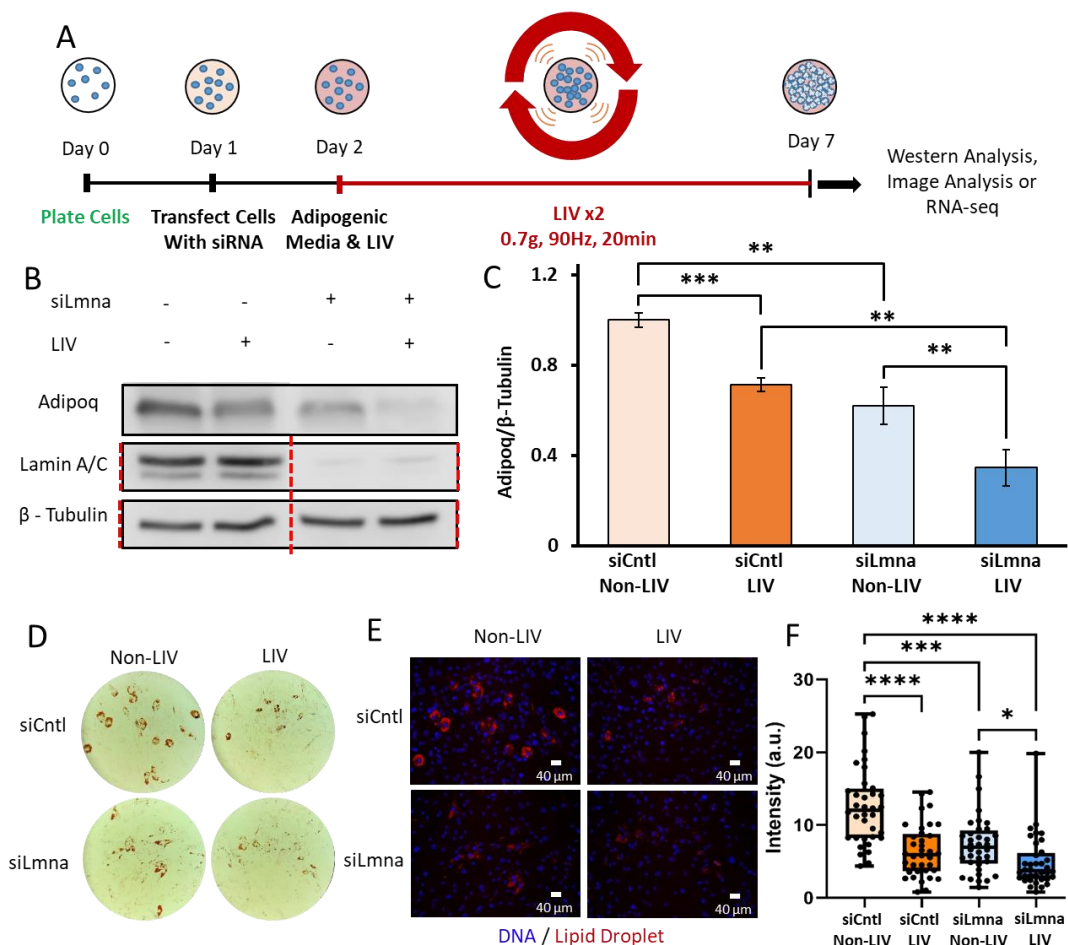


Figure 2.4 Application of daily LIV treatment decreases adipogenic differentiation in MSCs

A On day 0 cells were plated. Then, on day 1 cells were transfected with siRNA. On day 2 adipogenic media was placed on cells and cells were treated with LIV for 20 minutes, twice daily. Once cells differentiated, cells were pulled off for western analysis, image analysis, and RNA-seq. B Representative western blots of cells treated with siCntl and siLmna after 7 days of adipogenic induction with and without LIV treatment. Adiponectin (Adipoq), lamin A/C, and β -Tubulin were targeted. Lamin A/C and β -Tubulin were imaged on the same plot. Red line represents western blot cropped for alignment; uncropped blots were provided in Fig.S4. C Relative levels of adiponectin of the siCntl and the siLmna groups. Adipoq levels in siLmna treated MSCs with no LIV were decreased by 39% ($p < 0.01$, $n=4$) compared to siCntl MSCs with no LIV. LIV treated samples had 30% reduction in Adipoq levels compared to non-LIV controls for siCntl treated cells ($p < 0.001$, $n=3$ /grp). siLmna treated cells treated with LIV had a reduction of Adipoq levels of 44% compared to non-LIV samples ($p < 0.01$, $n=3$ /grp). siLmna cells treated with LIV compared to siCntl cells with LIV treatment had a 51% reduction in Adipoq ($p < 0.01$, $n=3$ /grp). D Representative Oil-Red-O images. E Representative images of lipid droplet staining corresponding to Oil-Red-O images Scale bars: 40 μ m. F Analysis of the mean lipid droplet intensity per cell. LIV treated siCntl cells experienced a decrease of lipid droplet mean intensity by 49% (n

= 36, $p < 0.0001$). siLmna cells treated with LIV had a decrease of 44% compared to non-LIV siLmna samples. ($n = 36$, $p < 0.05$). siLmna non-LIV samples had 42% less mean intensity compared to siCntl non-LIV samples ($n = 36$, $p < 0.001$). Western results are presented as mean \pm STE. Western group comparisons were made via parametric two-tailed Student T-test. Lipid droplet group comparisons were made with Kruskal-Wallis Test. * $p < 0.05$, ** $p < 0.01$, *** $p < 0.001$, **** $p < 0.0001$, against control.

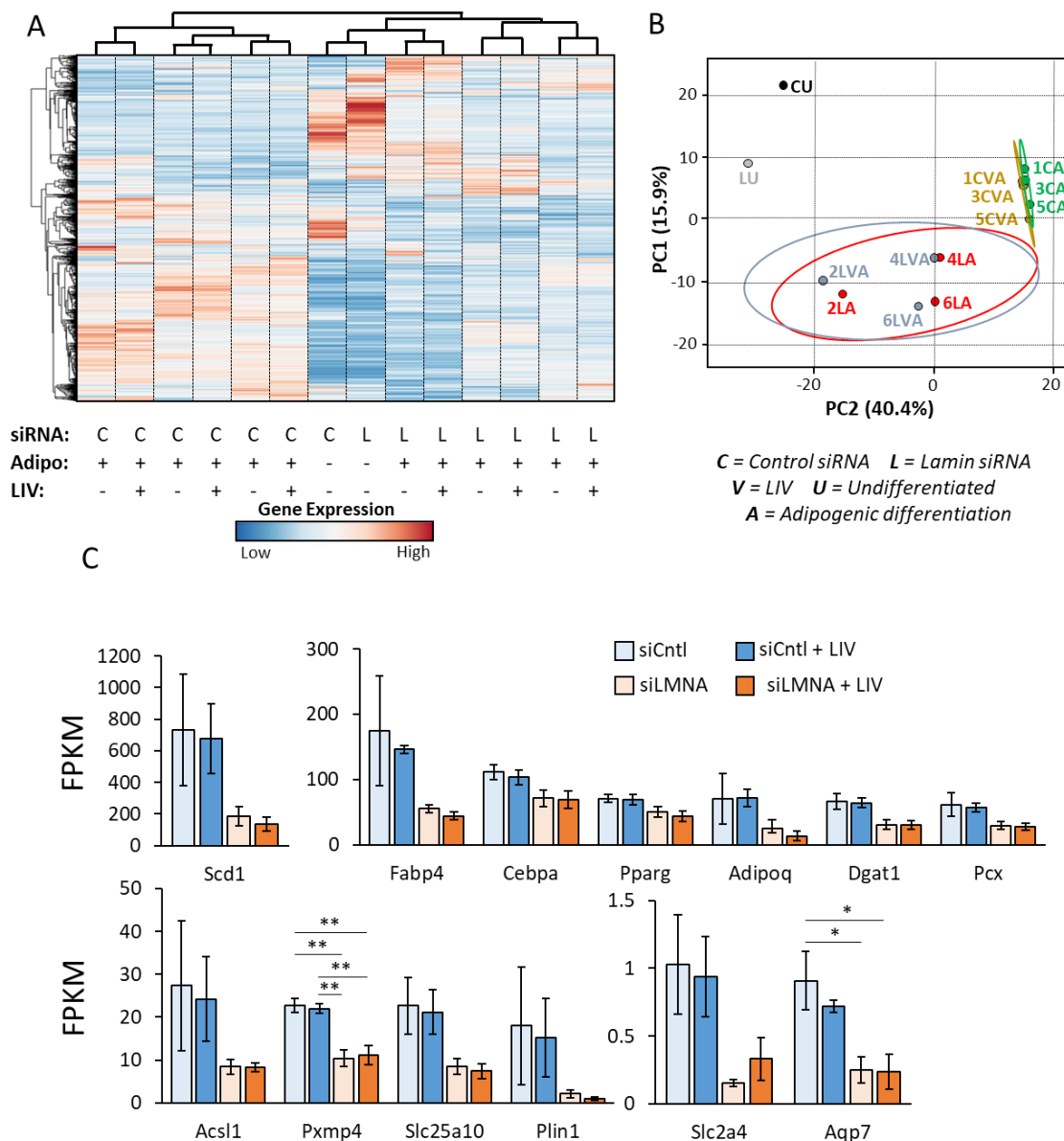


Figure 2.5 Differential effect of Lamin A/C depletion and LIV on mRNA transcription during adipogenic differentiation

A Heat map of genes with average expression of 0.3 FPKM, t-test $p < 0.05$, and fold change greater than 1.4. Unit variance scaling is applied to rows. B Principle component plot where principal component 1 and principal component 2 that explain 40.4% and 15.9% of the total variance, respectively. Prediction ellipses are such that with probability 0.95, a new observation from the same group will fall inside the ellipse. $N = 14$ data points. C Average FPKM values of DESEQ2 analysis for differentially expressed genes related to adipogenic phenotype. Results are presented as mean \pm STE. * $p < 0.05$ and fold change > 1.0 compared to siCntl.

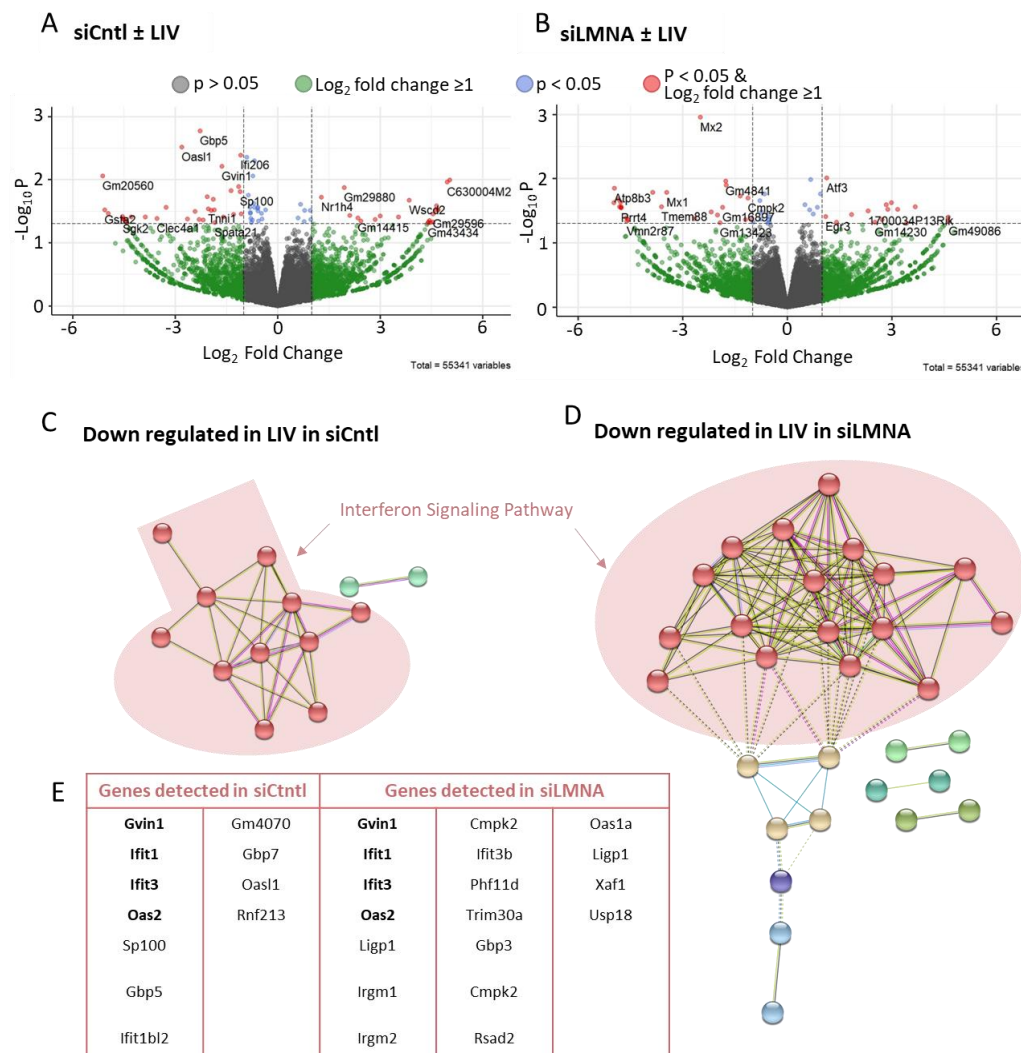


Figure 2.7 LIV Decrease Interferon Signaling Pathway in siLMNA and siCtrl Cells

A Volcano plot comparing the siCtrl adipogenesis with or without LIV treatment (siCtrl \pm LIV). B Volcano plot comparing the siLmna adipogenesis with or without LIV treatment (siLmna \pm LIV). Genes with Wald values greater than p value of 0.05 are colored in grey. Genes with differential gene expression equal to or larger than 2-fold ($\log_2=1$) but have Wald values greater than p value of 0.05 are colored in green. Genes colored with blue have Wald values smaller than p value of 0.05, but differential gene expression less than 2-fold ($\log_2=1$). Genes with Wald values smaller than p value of 0.05 and differential gene expression equal to or larger than 2-fold ($\log_2=1$) are colored in red. Both siCtrl C and siLmna D showed downregulation of genes closely associated with interferon signaling pathway. E Cells treated with siCtrl had 11 genes associated with interferon signaling pathway while siLmna treated cells had 16 genes associated with Interferon signaling pathway. **Bolded** gene names (Gvin, Ifit1, Ifit3, and Oas2) names were found in both siCtrl and siLmna treated samples.

CHAPTER THREE: DEPLETION OF SUN1/2 INDUCES HETEROCHROMATIN
ACCRUAL IN MSCS

Abstract

Mesenchymal Stem Cells (MSCs) differentiation into multiple lineages, such as osteocytes and adipocytes, has been shown to be regulated by mechanical signals. The Linker of the Nucleoskeleton and Cytoskeleton (LINC) complex has been shown to be required for mechanical signal transduction, regulation of MSCs differentiation, and nuclear integrity. The LINC complex is made of Nesprins and Sun proteins. Nesprin proteins associate with the cytoskeleton on the outer nuclear membrane and Sun proteins are bound to the inner nuclear membrane where they bind to inner nuclear proteins and chromatin. We investigated the role of the Sun1/2 in regulating the inner nuclear functions of chromatin organization and adipogenic differentiation independently of the LINC complex function. We show that depletion of Sun1/2 increased nuclear area and perimeter, and decreased circularity. Expression of a dominant-negative KASH (dnKASH) domain targeting the SUN domain on Sun proteins inhibiting Nesprin-SUN association resulting a loss of Nesprin localization to the nuclear envelope decreased nuclear area and circularity. Adipogenesis was inhibited during Sun1/2 depletion while dnKASH expression accelerated adipogenesis. RNA-seq data showed decreased adipogenesis and increased immune response during Sun1/2 depletion. dnKASH responded oppositely with increased adipogenic gene expression and decreased immune response. We also observed increased H3K9me3 levels, increased H3K9me3 foci count,

and enrichment on *Adipoq* during Sun1/2 depletion. No increase of H3K9me3 levels, foci count, or increased H3K9me3 enrichment on *Adipoq* was found during dnKASH expression. We conclude that physically decoupling of the LINC complex via dnKASH accelerates adipogenesis and that Sun1/2 regulates chromatin organization and adipogenesis independently of the LINC complex function.

Introduction

Linker of the Cytoskeleton and Nucleoskeleton (LINC) complex is a regulator for mechanical and biochemical signal transduction to the cell nucleus^{59,60}. The LINC complex achieves this role in-part by connecting the nucleus to cytoskeletal proteins of actin, microtubules, and intermediate filaments. A number of proteins help compose the LINC complex, such as Sun1/2 and Nesprins^{59,61}. Nesprin proteins are found on the outer nuclear membrane where their C-termini are located in the perinuclear space (PNS) and N-termini are bound to cytoskeletal proteins in the cytoplasm^{60,62,63}. Sun proteins are located in the inner nuclear membrane, having a C-termini SUN domain that binds to the KASH domain on the C-termini of Nesprins in the PNS. Sun protein N-termini spans into the nucleoplasm where it binds to multiple proteins such as Lamin A/C^{59,64}, Lamin B^{59,64}, emerin^{59,64}, and chromatin⁶⁵. Additionally, through the association of Sun proteins with LEM proteins, the LINC complex has direct links to the chromatin and ultimately regulation of the genome^{66,67}. Mutations in LINC complex proteins have far reaching effects on human health in the form of nuclear envelopathies⁶⁸. Mutations in Nesprin1 (Syne1) and Nesprin2 (Syne2) have been associated with Emery-Dreifuss Muscular Dystrophy that is characterized by contractures of tendons, muscle wasting and weakness, and cardiac disease⁶⁹. Depletion of Nesprin1 in endothelial cells increases

nuclear height, and increases the number of focal adhesions, indicating a compensatory mechanism due to the loss of the LINC complex⁵¹. Loss of the LINC complex also affects nuclear structure during mechanical stimulation. Loss of Nesprins 1-3 leads to increased nuclear deformation⁷⁰ and loss of increased actin cap formation⁷¹.

Mesenchymal Stem Cells (MSCs) are multipotent cells that differentiate into musculoskeletal lineages such as adipocytes, osteoblasts, and chondrocytes. Regulation of MSCs fate is highly dependent upon the ability to sense extracellular mechanical cues. Inhibition of the LINC complex via expression of the dominant-negative KASH (dnKASH) domain inhibiting binding of Nesprins to Sun1/2, prohibits the initiation of osteogenesis during increased extracellular stiffness in MSCs⁷². Inhibition of Sun1/2 via siRNA inhibits mechanoregulation of adipogenesis and activation of focal adhesion proteins FAK and Akt⁷³. Expression of dnKASH also inhibits activation of FAK and Akt in response to mechanical stimulation, showing the importance for the proper functioning of the LINC complex for cellular functioning and mechanoreponse in MSCs⁷³. Biochemical pathways are also affected by the loss of the LINC complex. Sun1/2 depletion in MSCs causes an inhibition of nuclear import of β -Catenin, a well-known regulator of proliferation and differentiation⁷⁴. Yap, another proliferation⁷⁵⁻⁷⁷ and anti-adipogenesis^{77,78} protein also experiences inhibition of translocation into the nucleus during depletion of Nesprin1⁷⁹.

More recently, research has shown the internal nuclear functions of meiosis and chromatin organization are regulated through Sun1/2 elements of the LINC complex. Through direct connections to Emerin and chromatin, Sun1/2 proteins^{80,81} tether chromatin to the nuclear envelope^{80,81}. During meiosis Sun1^{-/-} mouse cells have impaired

homologous synapsis during oogenesis and disrupted telomere association⁶⁵. For example, we have recently reported that depletion of Sun1/2 both decreases nuclear stiffness and increase heterochromatic spot area on isolated nuclei⁸². Indeed, proper chromatin organization is needed for proliferation and differentiation programs in MSCs. During adipogenesis, inhibition of heterochromatin H3K27me3 via methyltransferase Ezh2 inhibition resulted in increased protein levels of Adipoq and Fabp4 and decreased expression of osteogenic gene expression⁸³. This suggest that Sun1/2 , directly play a role in MSC fate selections through regulating chromatin dynamics. In addition to structural function loss of Sun1/2 proteins i also cause the loss of environmental mechanical information being transduced into the chromatin. For example, stress-induced chromatin stretching was abolished upon depletion of Sun1/2 proteins⁸⁴, inhibiting mechanically induced gene expression in CHO cells. Thus, mechanical information through Sun1/2-mediated connectivity may act on chromatin function. Notably, upon disruption of the LINC complex nucleo-cytoskeletal connectivity via an alternative approach where dnKASH overexpression interferes with Sun-Nesprin binding, increases histone deacetylase (HDAC) activity in human MSCs, leading to decreased expression of osteogenesis marker Runx2 and increased expression of the adipogenesis marker Pparg⁷².

Together these works suggests Sun1/2 proteins may overlapping roles in both in structural and mechanical regulation of chromatin organization and thus on MSC adipogenesis independent of LINC complex mediated mechanical information. However, it is not clear whether Sun protein may regulate MSC differentiation through their structural role, independent of LINC complex mediated mechanical information. Therefore, to investigate the role of Sun1/2 in regulating the intranuclear functions of

chromatin organization and adipogenic differentiation we used siRNA targeting Sun1/2. siRNA targeting Sun1/2 directly depletes Sun1/2 mRNA and protein levels disconnecting the cytoskeleton to the nucleoskeleton and other internuclear components. To inhibit LINC complex function independent of Sun1/2 depletion, we expressed a dominant-negative KASH domain that binds to the SUN domain, blocking Sun-Nesprin association, and displaces Nesprins^{73,85} (Fig. S1) from the nuclear envelope decoupling the LINC complex which disconnects the cytoskeleton to the nucleus. Therefore, utilizing these two different technologies we investigated the role of the Sun1/2 in regulating intranuclear functions of chromatin organization and adipogenic differentiation independent of the LINC complex in MSCs.

Materials and Methods

MSCs Isolation

Bone marrow derived MSCs (mdMSC) from 8-10 wk male C57BL/6 mice were isolated as described^{38,86} from multiple mouse donors and MSCs pooled, providing a heterogenous MSCs cell line. Briefly, tibial and femoral marrow were collected in RPMI-1640, 9% FBS, 9% HS, 100 µg/ml pen/strep and 12µM L-glutamine. After 24 hours, non-adherent cells were removed by washing with phosphate-buffered saline and adherent cells cultured for 4 weeks. Passage 1 cells were collected after incubation with 0.25% trypsin/1 mM EDTA × 2 minutes, and re-plated in a single 175-cm² flask. After 1-2 weeks, passage 2 cells were re-plated at 50 cells/cm² in expansion medium (Iscove modified Dulbecco's, 9% FBS, 9% HS, antibiotics, L-glutamine). mdMSC were re-plated every 1-2 weeks for two consecutive passages up to passage 5 and tested for osteogenic and adipogenic potential, and subsequently frozen.

dnKASH Cell Stable Cell Line

MSCs were stably transduced with a doxycycline inducible plasmid expressing an mCherry tagged dominant-negative KASH domain. dnKASH plasmid was lentiviral packaged as a generous gift from Dr. Daniel Conway. Vector map found here: <https://www.addgene.org/125554/>. Lentivirus supernatant was added to growth media with polybrene (5 µg/ml). Lentivirus growth media mixture was added to 50-70% confluent MSCs. Lentivirus media was replaced 48 hours later with selection media containing G418 (1 mg/ml) for 5 days to select stably infected dnKASH-MSCs.

Cell Culture, Pharmacological Reagents, and Antibodies

Fetal calf serum (FCS) was obtained from Atlanta Biologicals (Atlanta, GA). MSCs were maintained in IMDM with FBS (10%, v/v) and penicillin/streptomycin (100 µg/ml). For immunostaining experiments, seeding cell density was 3,000 cells per square centimeter. For adipogenic differentiation experiments, the seeding cell density was 10,000 cells per square centimeter. Cells were either grown in growth media (GM) or adipogenic media (AM) Cells were transfected 24 hours after cell seeding with siRNA targeting Sun1 and Sun2 (siSun) or a control sequence (siCntl) using RNAiMax from Invitrogen. Adipogenic media was placed on siRNA treated cells twenty-four hours after the transfection, the adipogenic media was added which contained dexamethasone (0.1 µM), insulin (5 µg/ml), and indomethacin (1 µg/ml) for 5 days. For dnKASH cells, cells were seeded at 10,000 cells per square centimeter. Twenty four hours after seeding, dnKASH cells were given growth media containing doxycycline (1 µg/ml). Adipogenic media containing dexamethasone (0.1 µM), insulin (5 µg/ml), indomethacin (1 µg/ml), and doxycycline (1 µg/ml) (AM+Dox) or growth media (GM+Dox) was placed on

dnKASH cells twenty-four hours after adding initial doxycycline. Control cells were grown in growth media (GM) or adipogenic media (AM) without doxycycline. Growth media or adipogenic media with or without fresh doxycycline were changed every 48 hours.

siRNA Silencing Sequences

For transient silencing of MSCs, cells were transfected with gene-specific small interfering RNA (siRNA) or control siRNA (20 nM) using RNAiMax (ThermoFisher) according to manufacturer's instructions. The following Stealth Select siRNAs (Invitrogen) were used in this study: SUN1 (ThermoFischer Scientific, Assay ID #s94913), SUN2 (ThermoFischer Scientific, Assay ID s104591).

qPCR

2ul of each CUT&RUN sample was run in 20ul reaction following Bio-Rad protocols targeting Adipoq (Bio-Rad, 10025636). Briefly, 20ul reactions were made using SsoAdvanced Master Mix (Bio-Rad, 1725270). Reactions were then run at 95°C for two minutes. Then samples were heated at 95°C for 15 seconds then cooled to 60°C for 30 seconds which both steps were repeated for 40 cycles. Finally, samples were run at 60°C for two minutes. Samples were then analyzed for percent of input sample for CUT&RUN-qPCR.

RNA-Seq Analysis

Five days after adipogenic treatment, following the above protocols, total RNA was extracted using RNAeasy (Qiagen) for three samples per group. Total RNA samples were sent to Novogene for mRNA sequencing and analysis. Briefly, index of the reference genome was built using Hisat2 v2.0.5 and paired-end clean 2 reads were

aligned to the reference genome using Hisat2 v2.0.5. featureCounts v1.5.0-p3 was used to count the reads numbers mapped to each gene. And then FPKM of each gene was calculated based on the length of the gene and reads count mapped to this gene. FPKM, expected number of Fragments Per Kilobase of transcript sequence per Millions base pairs sequenced. Differential expression analysis was performed using the DESeq2 R package (1.20.0). DESeq2 provides statistical routines for determining differential expression in digital gene expression data using a model based on the negative binomial distribution. The resulting P-values were adjusted using the Benjamini and Hochberg's approach for controlling the false discovery rate. Genes with an adjusted P-value ≤ 0.05 found by DESeq2 were assigned as differentially expressed. Genes with significant differential gene expression were further analyzed with DAVID⁸⁷ for pathway analysis. Pathways with a FDR ≤ 0.05 were selected.

Immunofluorescence

Twenty-four hours after the siRNA treatment against Sun1/Sun2 or dnKASH expression, cells were fixed with 4% paraformaldehyde. Cells were permeabilized by incubation with 0.3% Triton X-100. Cells were incubated in a blocking serum in PBS with 5% Donkey Serum (017-000-121, Jackson Immuno Research Laboratories). Primary antibody solution was incubated on the cells for 1h at 37oC, followed by secondary antibody incubation of either Alexa Flour 594 goat anti-rabbit (Invitrogen), Alexa Fluor 488 goat anti-mouse (Invitrogen), Alexa Fluor 488 chicken anti-rabbit (Invitrogen), or Alexa fluor 594 Donkey anti-mouse (Invitrogen). For nuclear staining cells were incubated with NucBlue Hoechst stain (Fisher Scientific). Primary and secondary concentrations were both 1:300 by volume.

Image Analysis

Five days after adipogenic media cells were fixed and were stained with Lipid Spot 488 (Biotium, #70069), and NucBlue Hoechst stain. Images were taken using 20x objective and were exported to quantify lipid droplet formation via a custom-made MATLAB program (The MathWorks, Natick, MA) previously published^{86,88}. The minimum pixel intensity of 80 was used to isolate lipid droplet staining. The mean lipid droplet intensity per cell was calculated by dividing the sum of lipid droplet stain intensity by the nuclei count per image. Exported images were used to quantify lipid droplet formation, Sun1, Sun2, mCherry, nuclear area, nuclear perimeter, and nuclear circularity via the custom-made MATLAB program previously published⁸⁶. Cell Profiler (<https://cellprofiler.org/>) was used to count the number of H3K9me3 foci per cell and foci area.

Western Blotting

Whole cell lysates were prepared using an radio immunoprecipitation assay (RIPA) lysis buffer (150mM NaCl, 50mM Tris HCl, 1mM EDTA, 0.24% sodium deoxycholate, 1% Igepal, pH 7.5) to protect the samples from protein degradation NaF (25mM), Na3VO4 (2mM), aprotinin, leupeptin, pepstatin, and phenylmethylsulfonylfluoride (PMSF) were added to the lysis buffer. Western protein amounts were normalized to 15µg through BCA Protein Assay (Thermo Scientific, #23225). Whole cell lysates (20µg) were separated on 10% poly-acrylamide gels and transferred to polyvinylidene difluoride (PVDF) membranes. Membranes were blocked with milk (5%, w/v) diluted in Tris-buffered saline containing Tween20 (TBS-T, 0.05%). Blots were then incubated overnight at 4°C with appropriate primary antibodies.

Following primary antibody incubation, blots were washed and incubated with horseradish peroxidase-conjugated secondary antibody diluted at 1: 5,000 (Cell Signaling) at RT for 1h in 5% milk in TBST-T. Chemiluminescence was detected with ECL plus (Amersham Biosciences, Piscataway, NJ). At least three separate experiments were used for densitometry analyses of western blots and densitometry was performed via NIH ImageJ software.

CUT&RUN

CUT&RUN was performed using the CUT&RUN Assay Kit (Cell Signaling #86652). Briefly, cells were harvested and centrifuged, washed, and bound to Concanavalin A-coated magnetic beads. Cells were then permeabilized with digitonin and incubated with primary antibody at 4°C for two hours. Cells were then washed and resuspended with pAG-MNase enzyme and incubated at 4°C for one hour. Cells were then incubated at 37°C for 10 minutes to elute DNA into solution. Solution was then extracted and purified using DNA Purification Buffers and Spin Columns (ChIP, CUT&RUN, Cell Signaling #14209). DNA samples were then used for qPCR or sequencing.

Statistical analysis and Reproducibility

Results for densitometry were presented as mean \pm SEM. Densitometry and other analyses were performed on at least three separate experiments. Differences between groups were identified by One-Way Anova. Analysis of nuclear morphology histone modifications were done using Whitney-Mann test and results were presented as mean \pm STD. Differential gene expression analysis via DESEQ2 was done using Wald test. P-values of less than 0.05 were considered significant. Lipid image analysis groups were

analyzed via the Kruskal-Wallis test. CUT&RUN-qPCR was analyzed via One-Tailed Students T-Test. All experiments were conducted in triplicate to assure reproducibility.

Results

siSun and dnKASH Expression Alter Nuclear Morphology

We investigated the effects of the depletion of Sun1/2 on the nuclear morphology. Shown in Fig. 1a MSCs treated with siRNA targeting Sun1/2 (siSun) were stained for Sun1 (green), Sun2 (red), and DNA (blue). siSun treated MSCs grown in growth media experienced an increase in nuclear area by 7% ($p < 0.01$), perimeter by 8% ($p < 0.0001$) shown in Fig. 1d and 1e respectively, when compared to siScntl treated MSCs. The nuclear circularity decreased by 9% in siSun treated cells compared to siCntl treated cells shown in Fig. 1f ($p < 0.001$).

To understand the effects of dominant-negative KASH domain (dnKASH) expression on the nuclear morphology of the nucleus dnKASH was expressed via doxycycline inducible stably infected dnKASH plasmid in MSCs. dnKASH nuclei were imaged through Hoechst staining (blue) to reveal nuclear morphology changes, shown in Fig. 2a. Upon treatment of doxycycline MSCs during growth in growth media (GM+Dox) treated samples experienced a 14% decrease of nuclear area ($p < 0.001$) compared to no treatment of doxycycline control MSCs grown in only growth media (GM). Nuclear perimeter had a slight decrease of 1% in GM+Dox treatment group compared to control group GM ($p < 0.05$). The circularity also experienced a decrease of 6% in GM+Dox treatment samples compared to GM samples ($p < 0.0001$).

Depletion of Sun1/2 Inhibits Adipogenesis

To further understand the effects of Sun1/2 depletion on MSCs we next investigated the adipogenesis in Sun1/2 depleted MSCs. Comparing the siCntl treated MSCs cultured in growth media (GM) to MSCs cultured in adipogenic media (AM) via western blot analysis of adipogenesis markers Adipoq (600%, $p < 0.01$), Cebpa (400%, $p < 0.01$), and Pparg (200%, $p < 0.01$), showed a robust increase in siCntl AM treated MSCs compared to siCntl MSCs culture in growth media while no increase was observed in Adipoq and Pparg in siSun treated adipogenic media cultured MSCs (Fig. 3a-c). Shown in Figs 3b-c, comparing adipogenic siCntl samples to adipogenic siSun treated samples showed significant protein level reduction for Adipoq (92% , $p < 0.01$) and Pparg (58% , $p < 0.001$) . Cebpa also experienced reduction but was not statistically significant (38% , $p = 0.22$). To further investigate the adipogenic phenotype lipid droplets were imaged via lipid droplet staining (LipidSpot 488, Biotium, CA, Fig. 3e). Shown in Fig. 3f the quantification of the mean florescent lipid droplet intensity per cell from individual imaging fields also showed a 2000% increase of lipid droplet formation between siCntl GM treated cells and siCntl AM treated cells ($p < 0.0001$). Lipid droplet image analysis also revealed 83% reduction of lipid droplets in adipogenic siSun treatment compared to siCntl ($p < 0.0001$). Comparison of siSun treated MSCs grown in GM and AM media showed a slight increase of lipid droplet formation by 20% ($p < 0.0001$).

dnKASH Expression Induces Accelerated Adipogenesis in MSCs

As depletion of Sun1/2 induced decreased adipogenesis, the effects of dnKASH expression during adipogenesis was next investigated. During adipogenesis doxycycline treated samples (AM+Dox) experienced increased levels of adipogenesis markers

Adipoq, Cebpa, and Pparg compared to samples grown in adipogenic media without doxycycline treatment (AM) (Fig. 4a). Analysis of western blots revealed significant increases of Adipoq by 98% ($p < 0.01$, Fig. 4b) and Pparg by 90% ($p < 0.05$, Fig. 4d) during adipogenesis in doxycycline treated cells compared to control cells. Cebpa experienced an increase of 27% in AM+Dox samples compared to AM samples but was not significant ($p = 0.38$). Comparing doxycycline treated samples grown in growth media (GM+Dox) to adipogenic samples treated with doxycycline (AM+Dox), Adipoq ($p < 0.0001$), Cebpa ($p < 0.01$), and Pparg ($p < 0.05$) had increased protein levels of 1000%, 300%, and 250%, respectively, during adipogenesis. AM sample group had a 500% increase in Adipoq protein levels compared to growth media cultured MSCs (GM) ($p < 0.01$). Cebpa and Pparg also experience increases of 42% ($p = 0.28$) and 40% ($p = 0.56$), respectively, in AM samples compared to GM samples but were not statistically significant. Additionally, doxycycline did to alter adipogenesis differentiation rate (Fig. S2). Lipid droplets (green) were stained and imaged for analysis (Fig. 4e). Quantification of mean lipid droplet intensity per cell in each field of view showed an increase of lipid droplet amounts in AM+Dox treated cells by 258% ($p < 0.05$, Fig. 4f) compared to AM samples. Lipid droplet amounts also had significant increases in AM compared to GM (2,400% $p < 0.0001$) and AM+Dox compared to GM+Dox (6,000%, $p < 0.0001$).

Sun1/2 Depletion Decreases Adipogenesis and Lipid Metabolism Related Genes

RNA-seq was performed on samples treated with siRNA targeting Sun1/2 and control siRNA during culture in growth media (GM) and adipogenic media (AM) to determine effects from the loss of the internuclear LINC complex connection. Genes were filtered by having significant gene expression compared to controls (fold change \geq

1, $p < 0.05$). Hierarchical clustering of these genes generated the heatmap in Figure 5a which shows clustering separating siSun and siCntl treated cells in relatedness. Both siSun and siCntl sample clades have additional clustering separating adipogenic and growth media cultured cells, indicating different gene expression profiles during growth in either adipogenic or growth media. Principle component further shows separation of siCntl and siSun AM and GM transcriptome profiles as variance of principle components 1 and 2 are 16.2% and 19.9% respectively (Fig. 5b). Clustering differences between siCntl and siSun AM samples show Sun1/2 has a transcriptome regulatory role during adipogenesis. Ellipses indicate prediction with 0.95 probability of next sample falling within the given ellipses. DAVID analysis results highlighting pathways that have an of $FDR < 0.05$ that are significantly up regulated (Fig. 5c) and down regulated (Fig. 5d) in siSun AM samples compared to siCntl AM samples. Blue bars indicate pathways related to adipogenesis or lipid metabolism which are found in down regulated pathways in siSun AM vs siCntl AM sample comparison revealing significant inhibition of adipogenic transcriptome (Fig. 5d) and shown in STRING analysis (Fig. S3). Inflammatory response was upregulated during siSun AM treatment group as shown in Fig. 5c and in STRING analysis of up regulated genes (Fig. S4), potentially highlighting a regulatory role of Sun1/2 for inflammation pathways. Tables of DAVID analysis pathways can be found in Table S1-2. Figure 5e shows FPKM values of adipogenic or lipid metabolism genes that were both significantly expressed (fold change ≥ 1 , $p < 0.05$) and were highlighted in DAVID analysis pathways ($FDR < 0.05$).

Dominant-Negative KASH Expression Upregulates Adipogenesis Related Pathways

To understand the observed accelerated adipogenesis during dnKASH expression RNA-seq was performed on samples treated with doxycycline (+Dox) and without doxycycline during culture in growth media and adipogenic media to induce LINC complex loss of function without losing intranuclear connection via Sun1/2. Like the earlier RNA-seq analysis, genes were filtered by having significant gene expression compared to controls (fold change ≥ 1 , $p < 0.05$). Hierarchical clustering of these genes generated the heatmap in Figure 6a showing clustering separating dnKASH expressing and control cells regardless of media type. Adipogenic and growth media cultured cells also further separated inside both dnKASH and control samples clades. Further analysis of transcriptome differences utilizing principle component plot showed variance of principle components 1 and 2 were 25.2% and 16.9% respectively (Fig. 6b). Separation of treatment groups in principle component plot and heatmap clades indicate loss of LINC complex function independent of internuclear connection causes alteration to transcriptome regulation during adipogenesis. Ellipses indicate prediction with 0.95 probability of next sample falling within the given ellipses. DAVID showed adipogenic and lipid metabolism pathways of fatty acid metabolism and PPAR signaling were upregulated (Fig. 6c, FDR < 0.05). Opposite that of siSun treatment, AM+Dox treatment group had downregulated inflammatory and immune pathways, such as immune system response and response to cytokines (Fig. 6d), compared to AM samples as found in DAVID analysis and STRING (Fig. S5). Tables of DAVID analysis pathways can be found in Table S3-4. Blue bars indicate the pathways related to adipogenesis or lipid metabolism. Figure 6e shows FPKM values of adipogenic or lipid metabolism genes that

were both significantly expressed (fold change ≥ 1 , $p < 0.05$) and were highlighted in DAVID analysis pathways (FDR < 0.05) and in STRING analysis (Fig. S6). Expression of dnKASH domain via a secondary plasmid vector that does not utilize doxycycline inducement also showed increased adipogenic marker gene expression during dnKASH expression (Fig. S7), further highlighting the acceleration of adipogenesis during dnKASH expression inhibition of the LINC complex function independent of internal nuclear connectivity.

H3K9me3 Levels and Enrichment at Adipogenic Gene Adipoq Increases during Sun1/2 Depletion

As mentioned earlier, differentiation is regulated by the chromatin organization and dynamic alterations to its structure. Therefore, we next investigated alterations to heterochromatin and euchromatin in siSun treated MSCs and dnKASH expressing cells during adipogenesis. To understand mechanisms regulating the decreased adipogenesis of Sun1/2 depleted MSCs, heterochromatin and euchromatin marker levels were measured via western blots under both GM and AM conditions (Fig. 7a). H3K9me3 levels were increased by 56% in the siSun AM group compared to the siCntl AM group ($p < 0.05$, Fig. 7b). H3K9me3 levels were also increased by 86% in the siSun GM group compared to the siCntl GM group ($p < 0.05$, Fig. 7b). H3K27me3 decreased by 48% in the siSun AM group compared to the siCntl AM group ($p < 0.05$, Fig. 7c). H3K27me3 had a trend of decrease (27%, $p = 0.37$) in siSun GM treated MSCs when compared to siCntl GM treated MSCs. Euchromatin marker H3K4me3 experienced no significant changes in global protein levels between siSun and siCntl treated cells during adipogenesis or culture in growth media (Fig. 7d). To further investigate the observed increases of H3K9me3

confocal imaging of H3K9me3 (green) and DNA (blue) was analyzed for both siSun and SiCntl groups either GM (Fig. 7e) and AM conditions (Fig. 7h). H3K9me3 foci count per cell in siSun cells compared to siCntl cells in GM increased by 9% ($p < 0.01$, Fig. 7f). H3K9me3 foci area increased by 7% in siSun GM cells compared to siCntl GM cells ($p < 0.001$, Fig. 7g). H3K9me3 foci count per cell in the siSun AM group compared to the siCntl AM group increased by 43% ($p < 0.0001$, Fig. 7i). No detectable increase of H3k9me3 foci area was found in siSun AM groups (Fig. 7j). Next, CUT&RUN extraction targeting H3K9me3 was done on siSun and siCntl treatment groups during adipogenesis to detect any increased H3K9me3 enrichment on adipogenesis marker gene Adipoq. Shown in Fig. 7k, H3K9me3 enrichment on Adipoq was increased by 156% in the siSun AM group compared to the siCntl AM group ($p < 0.05$).

H3K9me3 Levels and Enrichment at Adipogenic Gene Adipoq Remains Unaltered during dnKASH Disruption of the LINC Complex

Investigating the increase of adipogenesis during dnKASH expression heterochromatin and euchromatin marker levels were also measured during culture in growth media (GM) or adipogenic media (AM) (Fig. 8a). Contrasting to Sun1/2 depletion, western blot analysis showed H3K9me3 levels decreased by 51% when comparing AM+Dox samples to AM samples ($p < 0.01$, Fig. 8b). GM+Dox H3K9me3 decreased by 37% compared to GM samples but was statistically not significant ($p = 0.07$, Fig. 8b). Similar to siSun AP treatment groups H3K27me3 levels also decreased by 56% in AM+Dox samples compared to AM samples ($p < 0.05$, Fig. 8c). Additionally, there were no observable significant differences in H3K4me3 in western analysis (Fig. 8d). Confocal imaging of H3K9me3 (green) and DNA (Blue) in growth media (Fig. 8e)

and adipogenesis (Fig. 8h) revealed no significant increases of H3K9me3 foci count per cell in the doxycycline treatment groups in both growth media (Fig. 8f) and adipogenesis (Fig. 8i). H3K9me3 foci area increased by 5% in GM+Dox samples compared to GM samples ($p < 0.05$, Fig. 8g) and decreased during adipogenesis in the AM+Dox samples compared to AM samples by 7% ($p < 0.01$). Enrichment of H3K9me3 on Adipoq was also measure in during adipogenesis in both AM+Dox and AM treatment groups (Fig. 8k). H3K9me3 enrichment was not found to be significantly increased between AM+Dox and AM groups during adipogenesis.

Discussion and Conclusion

Proper functioning of the LINC complex has been shown to be required for mechanical sensing and mechanoregulation of differentiation in MSCs. Studies have shown that upon loss of the LINC complex actin-cap formation is inhibited, osteogenesis is inhibited, and translocation of important mechanosensitive biomolecules such as YAP and β -Catenin into the nucleus is inhibited^{71,72,89-91}. While the importance of the LINC complex is known, independent effects of the Sun1/2 proteins in regulating the internal nuclear functions of differentiation and chromatin organization, remains underexplored. Previous research has shown that loss of Sun1/2 inhibits metabolism gene expression and metabolism proteomics⁹⁰. During loss of mechanical sensing MSCs experience rapid differentiation into adipocytes while osteogenesis is inhibited. Our findings support these previous studies. We show that while disabling LINC function via a dominant negative KASH domain biases MSC differentiation towards adipogenesis, depleting Sun1/2 proteins inhibits adipogenic differentiation as shown through western blot analysis, RNA-seq analysis, and lipid droplet amount. This suggests that Sun proteins may have a role in

directing internal nuclear functions, such as differentiation and chromatin organization, independent of LINC complex function.

Previous works have shown that depletion Sun1/2 reduces tethering of chromosomes to the nuclear envelope^{65,92,93}, alters nucleolus morphology⁹⁴, and increases trimethylated K9 histone (H3K9me3) levels in hTERT-RPE1 and MCF10A cells⁹⁵. Our results show similar trends as Sun1/2 depletion in MSCs increased both H3K9me3 protein levels and number of H3K9me3 heterochromatic foci while no H3K9me3 protein levels or foci number increases were observed under dnKASH expression. Further, we report that depleting Sun1/2 proteins at the inner nuclear envelope increases H3K9me3 heterochromatin formation on the adipogenic gene *Adipoq* in MSCs and that dnKASH expression does not alter H3K9me3 enrichment on *Adipoq*. These results reveal that Sun1/2 proteins regulates H3K9me3 heterochromatin organization independent of the LINC complex. Additionally, this observed increase of the H3K9me3, a constitutive form of heterochromatin, marks a strong response from the nucleus, indicating a potential mechanism by which adipogenesis is inhibited during depletion of Sun1/2. As a constitutive heterochromatin form, H3K9me3 forms constitutive heterochromatin that is tightly bound to DNA⁹⁶⁻⁹⁸, and is not easily removed. H3K27me3, on the other hand, is a facultative heterochromatin marker that is more easily modulated for differentiation⁹⁸⁻¹⁰⁰. The observed lack of H3K9me3 increase along with the corresponding decrease of H3K27me3 during dnKASH expression indicates that decoupling the LINC complex via dnKASH does not increase heterochromatin formation in MSCs. As observed in other studies, decreased heterochromatin, especially H3K27me3, is associated with increased adipogenesis. Decreases in H3K27me3 and its methyltransferase EZH2 corresponds with

increased adipogenesis in MSCs⁸³ which EZH2 expression is directly regulated by the mechanosensitive, LINC complex regulated⁷⁴ biomolecule β -Catenin⁸³. Therefore, our observed decreases of H3K27me3 during dnKASH expression with no increase in H3K9me3 may provide a mechanism by which acceleration of adipogenesis in MSCs occurs.

During depletion of Sun1/2 mechanosuppression of osteolytic factors such as PTHLH and Il-11 is inhibited. In our study we also found a tumorigenic and osteolytic effect from Sun1/2 depletion. During Sun1/2 depletion increases in the tumorigenic and osteolytic factors *Cxcl10*, *Cxcl1*, and *Cxcl5* were observed (Table S1). Increases in these markers are associated with increased cancer metastasis in breast cancer¹⁰¹ and prostate cancer¹⁰². Additionally, increases of *Cxcl10*, *Cxcl5* and *Cxcl1*¹⁰² recruit cancer cell metastasis to bone¹⁰²⁻¹⁰⁴, induce osteoclast differentiation^{103,105} and angiogenesis¹⁰⁶. Importantly, osteolysis has a direct relationship with tumorigenesis. For metastasis of cancer to occur cancer must be able to migrate out of bone or into bone¹⁰⁷. Thus, osteoclasts are needed to degrade the bone matrix. Depletion of Sun1/2 leads to an upregulation of *Cxcl10*, *Cxcl5*, and *Cxcl1*, However, dnKASH expression during adipogenesis saw these same genes down regulated (Table S4) indicating a reduction in the osteolytic signaling. While the underlying mechanism for these observed differences between Sun1/2 and dnKASH are unknown these results indicate that regulation of these proto-oncogenes and the resulting osteolytic signaling is dependent upon Sun1/2 mediated connection to the internal nucleus.

This work supports previous observations^{74,108,109} that inhibiting the LINC complex via siSun and dnKASH expression reduces overall nuclear structural integrity as

indicated by reduced nuclear circularity or aspect ratio. Our observed increase in nuclear area and perimeter seen during Sun1/2 depletion is similar to that of our previous observations of nuclear morphology changes during Lamin A/C depletion⁸⁶. Both Sun1/2 and Lamin A/C are important inner nuclear membrane nucleoskeleton elements that associate with other structural proteins and elements such as chromatin. Previous research has shown that during both depletion of Lamin A/C and Nesprin-Sun1 association inhibition Sun1 via Sun1-KDEL expression have large deformations during micropipette direct force application, indicating a softer nuclei¹¹⁰. However, during dnKASH expression deformation of the nucleus is reduced but nucleus displacement is not recovered after removal of micropipette force¹¹⁰. Thus, showing that dnKASH expression does not significantly reduce nuclear stiffness and nuclear morphology similar to that of internuclear proteins such as Sun1/2 and Lamin A/C. Chromatin does provide structural functions in the nucleus forces during low mechanical load^{111,112} and increasing heterochromatin formation has been shown to partially recover alter nuclear morphology¹¹². However, we have previously shown that depletion of Sun1/2 causes a reduction in nuclear stiffness and increased chromatin area size⁸². Thus, our data in combination with previous works indicates that depletion of Sun1/2 is potentially able to alter nuclear integrity independent of chromatin condensation. Additionally, our results indicate that the dnKASH expression effects on nuclear integrity is similar to other studies as seen by a reduction in nuclear area^{74,108,109}, indicating dnKASH regulates nuclear morphology and function without reducing nuclear stiffness.

In conclusion, this work reveals new insight into the role of Sun1/2 proteins in the nuclear interior and its effects on the nuclear functions of differentiation and chromatin

organization. Depletion of Sun1/2 not only inhibited adipogenesis, but promoted osteolytic and tumorigenic signaling. Chromatin organization was also altered, increasing H3K9me3 heterochromatin. Our findings show that these effects are independent of the LINC complex function. These results have potential impacts on our understanding of how envelopopathies targeting the nuclear envelope, such as Emery-Dreifuss muscular dystrophy (EDMD) and Progeria, become more severe during mutations in Sun1⁶⁸. Which, as shown here, may be caused by the misregulation of chromatin organization and differentiation regulation during Sun1/2 depletion. Thus, these results expand our understandings of the important role inner nuclear membrane proteins have in regulating proper nuclear functions and ultimately human health.

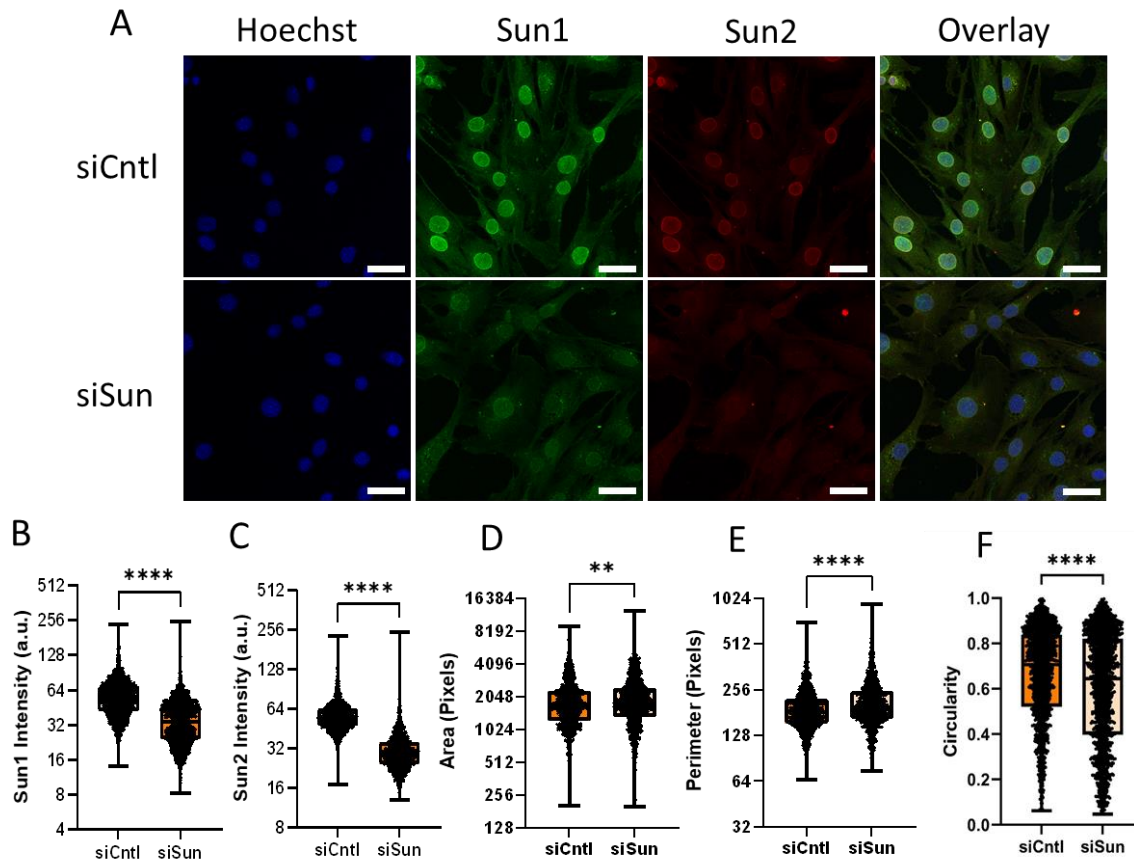


Figure 3.1 Sun1/2 Depletion Alters Nuclear Morphology

A Representative images of MSCs treated with siRNA targeting Sun1/2 (siSun) which were stained for Sun1 (green), Sun2 (red), and DNA (blue). B siSun treated cells had 47% decrease of Sun1 intensity (n = 1478, $p < 0.0001$). C Sun2 intensity levels were decreased by 52% in siSun treated cells (n = 1478, $p < 0.0001$). D MSCs treated with siSun had an increase in nuclear area by 7% (n = 1478, $p < 0.01$). E Nucleus perimeter decreased in siSun treated MSCs by 8% (n = 1478, $p < 0.0001$). F Nuclear circularity decreased by 9% in siSun treated cells (n = 1478, $p < 0.001$). Comparisons were made against control using non-parametric Mann-Whitney Test where * $p < 0.05$, ** $p < 0.01$, *** $p < 0.001$, **** $p < 0.0001$. Scale bar represents $50\mu\text{m}$.

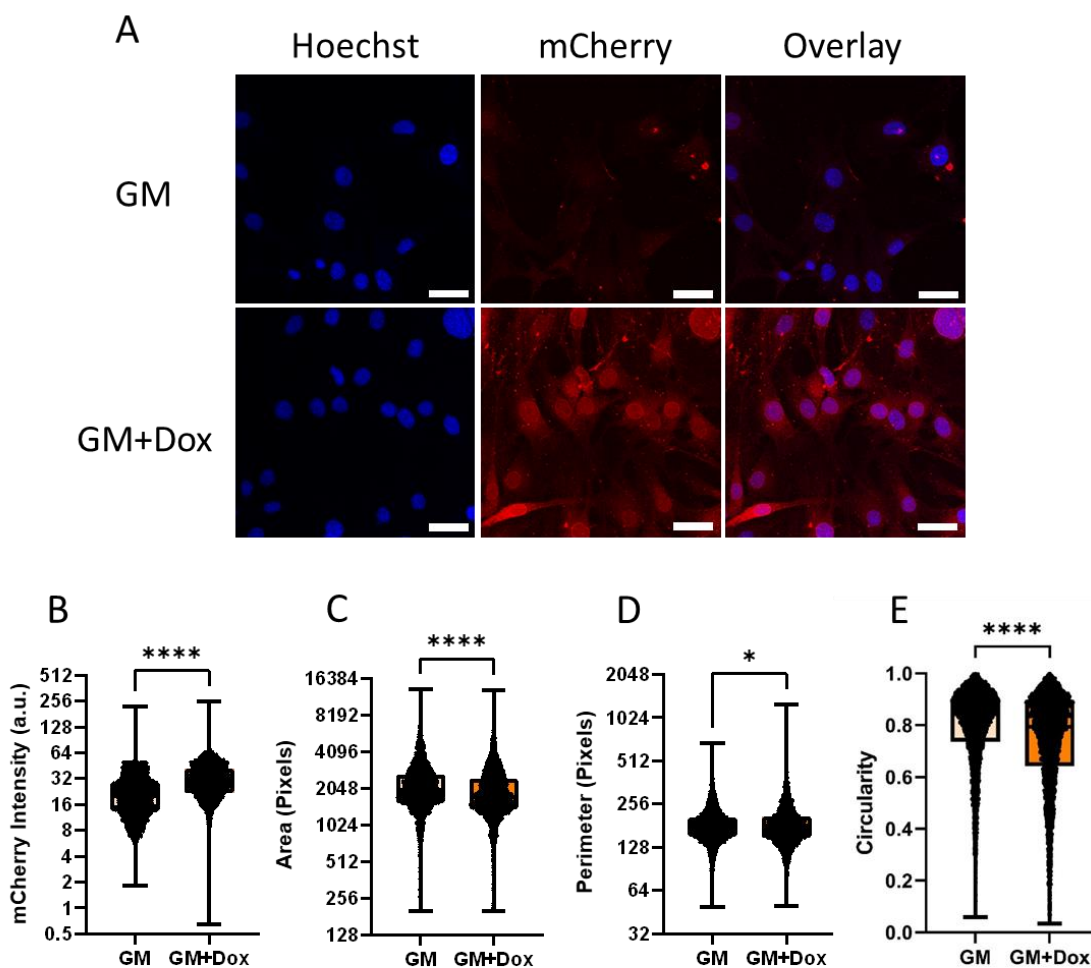


Figure 3.2 Dominant-Negative KASH Disruption of the LINC Complex Reduces Nuclear Area

A Representative photos of doxycycline induced DNKASH cells. Images show DNKASH tagged with mCherry (Red) and DNA (Blue). B mCherry intensity levels increased by 133% in doxycycline treated MSCs ($n = 5332$, $p < 0.0001$). C Doxycycline treated MSCs experienced a 14% decrease of nuclear area ($n = 5322$, $p = 0.001$). D Nuclear perimeter had a slight decrease of 1% in doxycycline treatment group ($n = 5322$, $p < 0.05$). E The circularity experienced a decrease of 6% in doxycycline treatment group ($n = 5322$, $p < 0.0001$). Comparisons were made against control using non-parametric Mann-Whitney Test where * $p < 0.05$, **** $p < 0.0001$. Scale bar represents $50\mu\text{m}$.

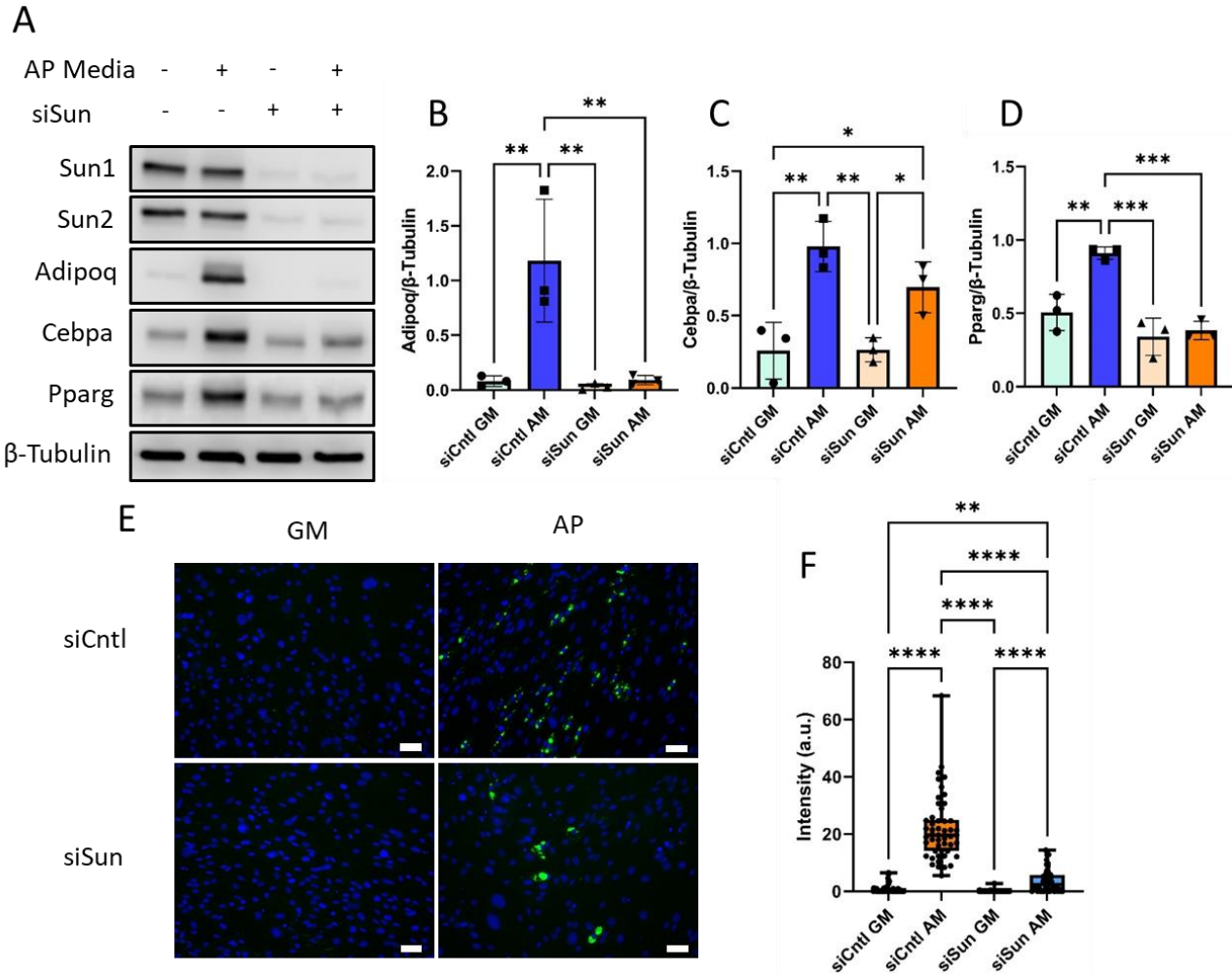


Figure 3.3 Depletion of Sun1/2 Inhibits Adipogenesis

A Western analysis of adipogenesis markers Adipoq, Cebpa, and Pparg in growth media and adipogenic media during siSun and siCntl treatment. B Analysis of Adipoq protein levels. Comparison of adipogenic siSun and siCntl groups showed a 92% reduction of Adipoq ($n = 3$, $p < 0.01$). C Cebpa experienced a non-significant reduction of 38% in protein levels in siSun cells compared to siCntl cells during adipogenesis ($n = 3$, $p = 0.22$). D Pparg levels decreased by 58% in adipogenic siSun compared to siCntl ($n = 3$, $p < 0.001$). E Representative images of lipid droplet fluorescence images where MSCs are stained for lipid droplets (green) and DNA (blue). F Quantification of the mean fluorescent lipid droplet intensity per cell from individual imaging fields shows a significant reduction of 83% in lipid droplet amounts in adipogenic siSun treatment compared to siCntl ($n = 50$, $p < 0.0001$). Western analysis group comparisons were One-Way Anova. Lipid droplet intensity group comparisons were made using Kruskal-Wallis test. * $p < 0.05$, ** $p < 0.01$, *** $p < 0.001$, **** $p < 0.0001$. Scale bar represents $50\mu\text{m}$.

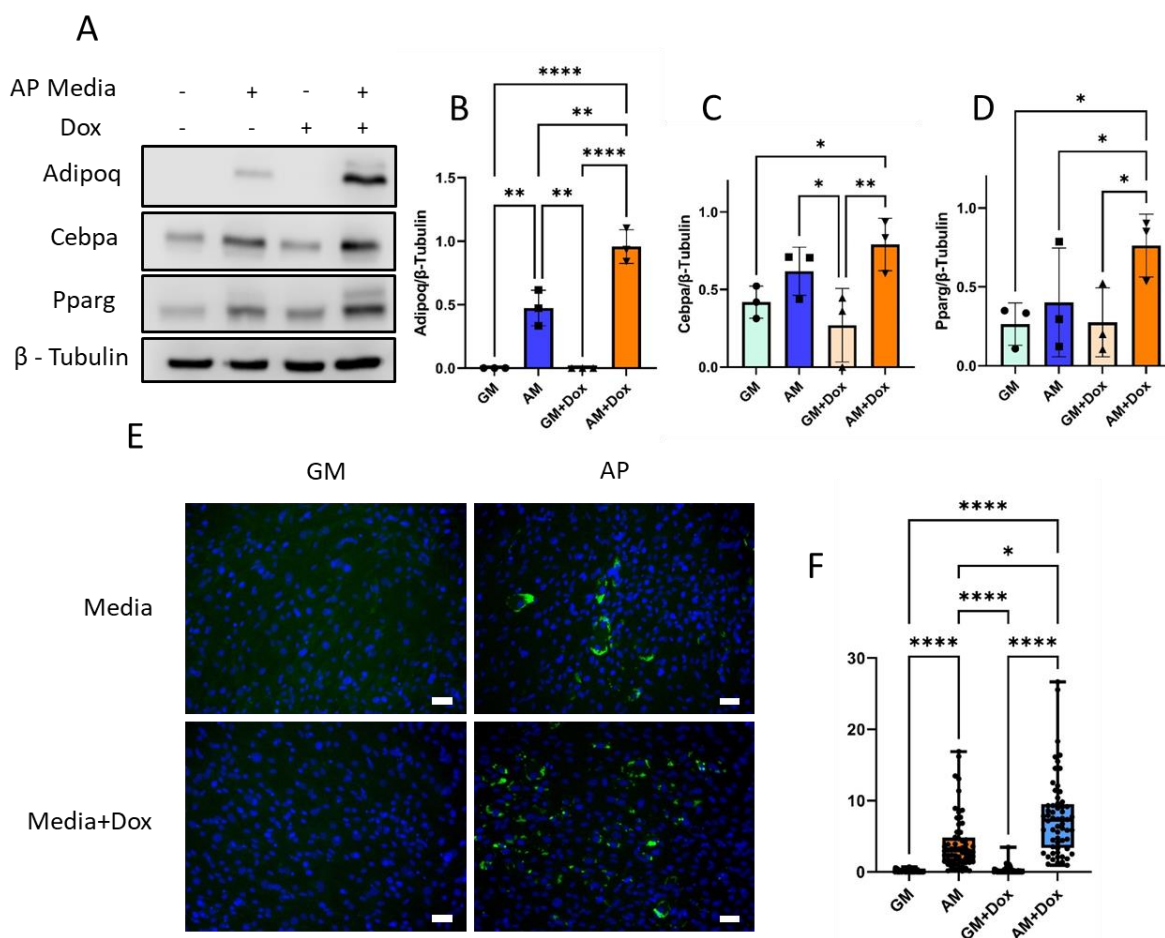


Figure 3.4 dnKASH Expression Induces Accelerated Adipogenesis in MSCs

A Representative western images of doxycycline induced dnKASH cells and control cells grown in growth media and adipogenic media. B During adipogenesis doxycycline treated samples had 98% increased levels of Adipoq ($n = 3$, $p < 0.01$). C Cebpa experienced an increase of 27% but was not significant during adipogenesis in doxycycline treatment ($n = 3$, $p = 0.38$). D Pparg in doxycycline treatment group during adipogenesis increased by 90% ($n = 3$, $p < 0.05$). E Representative photos of lipid droplets (green) and DNA (blue). F Quantification of mean lipid droplet intensity per cell in each field of view showed an increase of lipid droplet amounts in doxycycline treated cells by 258% ($n = 50$, $p < 0.05$) during adipogenesis. Western analysis group comparisons were One-Way Anova. Lipid Droplet Intensity group comparisons were made using Kruskal-Wallis test. * $p < 0.05$, ** $p < 0.01$, *** $p < 0.001$, **** $p < 0.0001$. Scale bar represents $50\mu\text{m}$.

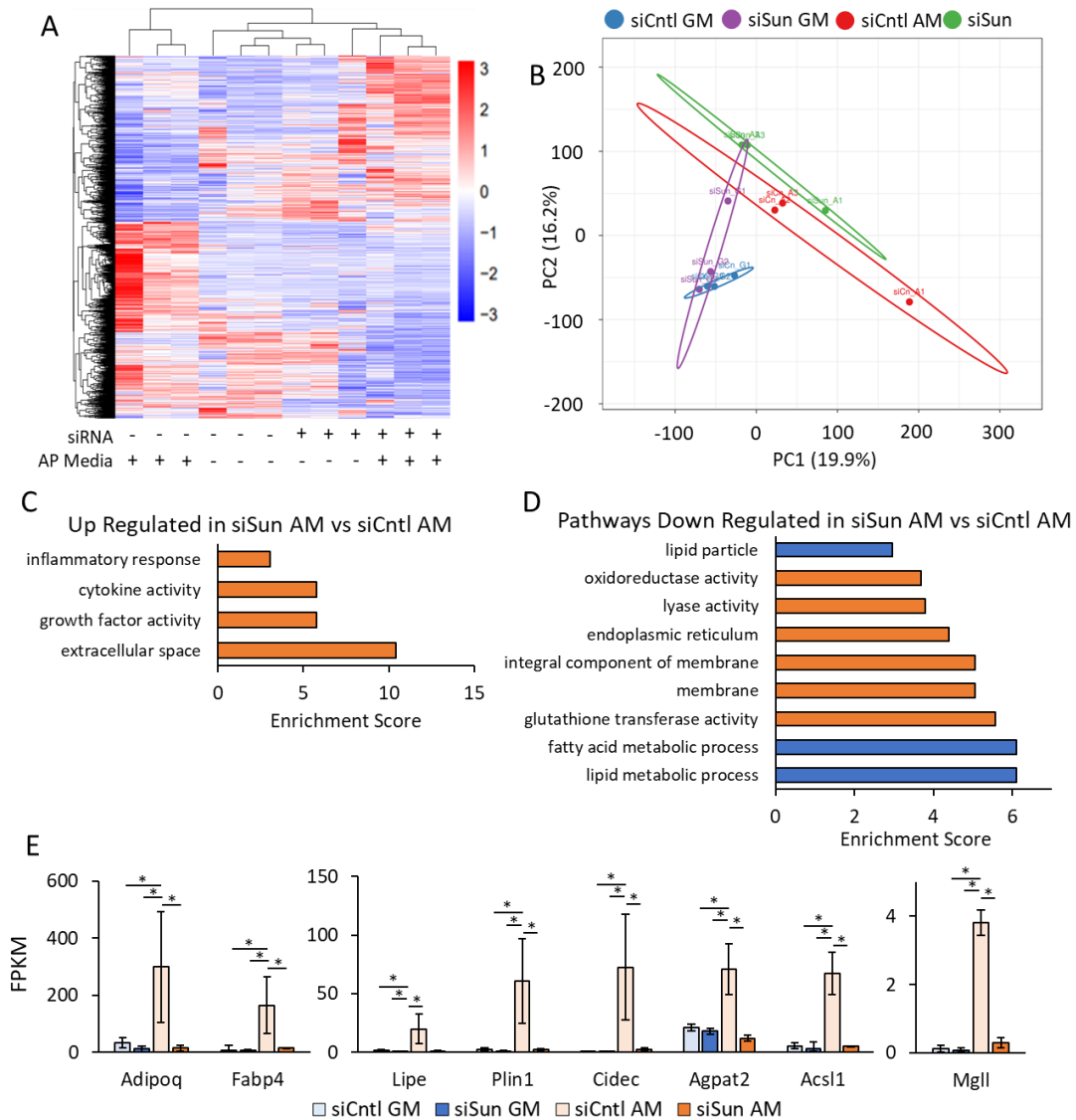


Figure 3.5 Sun1/2 Depletion Decreases Adipogenesis and Lipid Metabolism Related Genes

A Heatmap of genes with significant differential ($FC > 1$ and $p < 0.05$) gene expression during Sun1/2 depletion ($n = 24$). B Principle component plot where principal component 1 and principal component 2 explain 19.9% and 16.2% of the total variance, respectively. Prediction ellipses indicate that with a probability of 0.95, a new observation from the same group will fall inside the ellipse. $n = 24$ data points. C DAVID analysis of genes up regulated in siSun treatment compared to siCntl. Pathways selected have $FDR < 0.05$. D DAVID analysis of genes down regulated in siSun group compared to siCntl. Pathways selected have $FDR < 0.05$. Blue indicates pathways related to adipogenesis and lipid metabolism. E FPKM values for adipogenic and lipid metabolism related genes detected in both differential gene expression ($FC > 1$, $p < 0.05$) and in DAVID analysis ($FDR < 0.05$) ($n = 3/\text{grp}$). Group comparison was made using One-Way ANOVA where $* p < 0.05$.

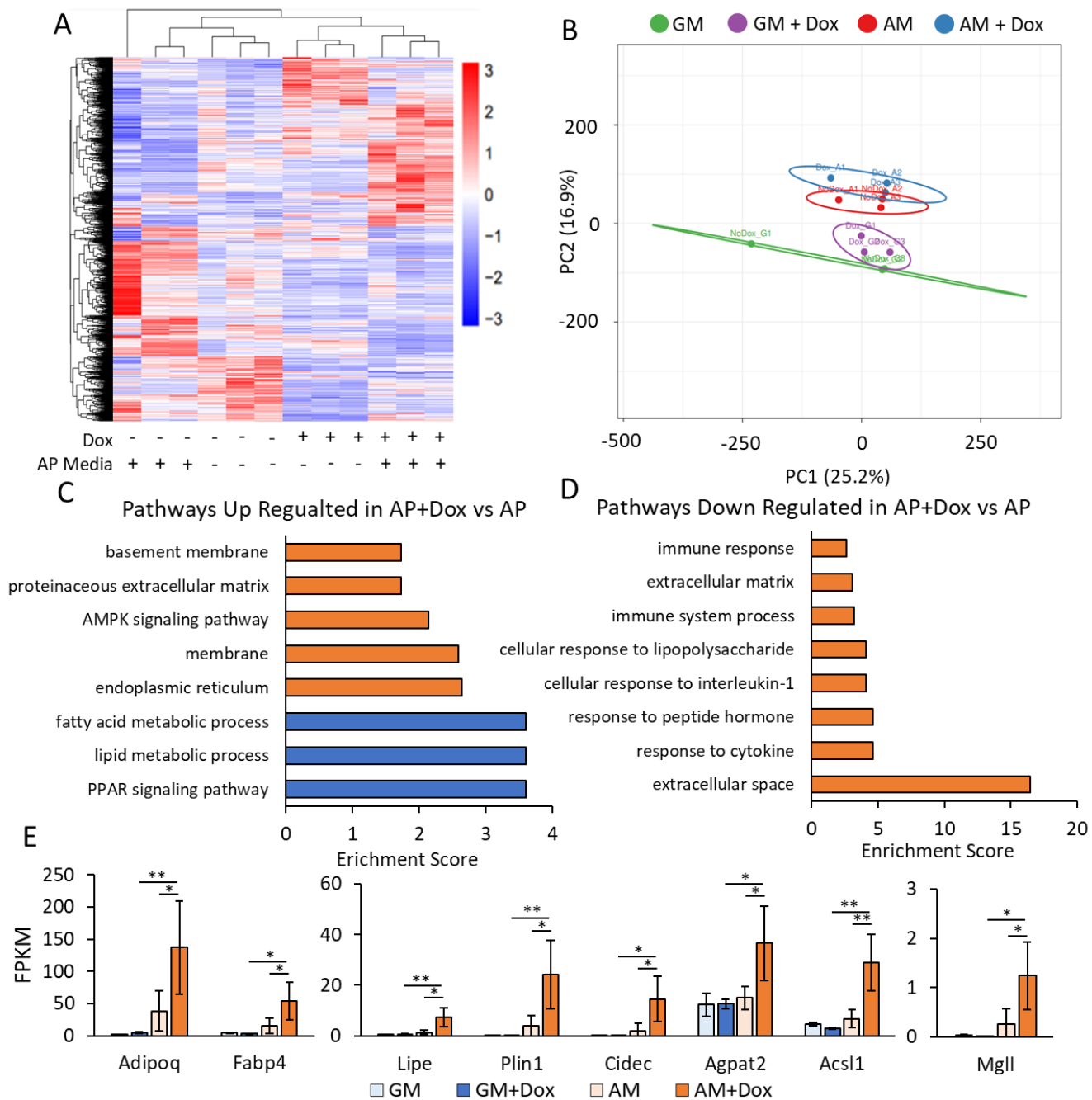


Figure 3.6 Dominant-Negative KASH Expression Upregulates Adipogenesis Related Pathways

A Heatmap of genes with significant differential ($FC > 1$ and $p < 0.05$) gene expression during doxycycline induced dnKASH expression ($n = 24$). B Principle component plot where principal component 1 and principal component 2 explain 25.2% and 16.9% of the total variance, respectively. Prediction ellipses indicate that with a probability of 0.95, a new observation from the same group will fall inside the ellipse. $n = 24$ data points. C

DAVID analysis of genes up regulated in doxycycline treatment compared to control. Blue indicates pathways related to adipogenesis and lipid metabolism. Pathways selected have $FDR < 0.05$. D DAVID analysis of genes down regulated in doxycycline group compared to control. Pathways selected have $FDR < 0.05$. E FPKM values for adipogenic and lipid metabolism related genes detected in both differential gene expression ($FC > 1$, $p < 0.05$) and in DAVID analysis ($FDR < 0.05$) ($n = 3/grp$). Group comparison was made using One-Way ANOVA. * $p < 0.05$, ** $p < 0.01$.

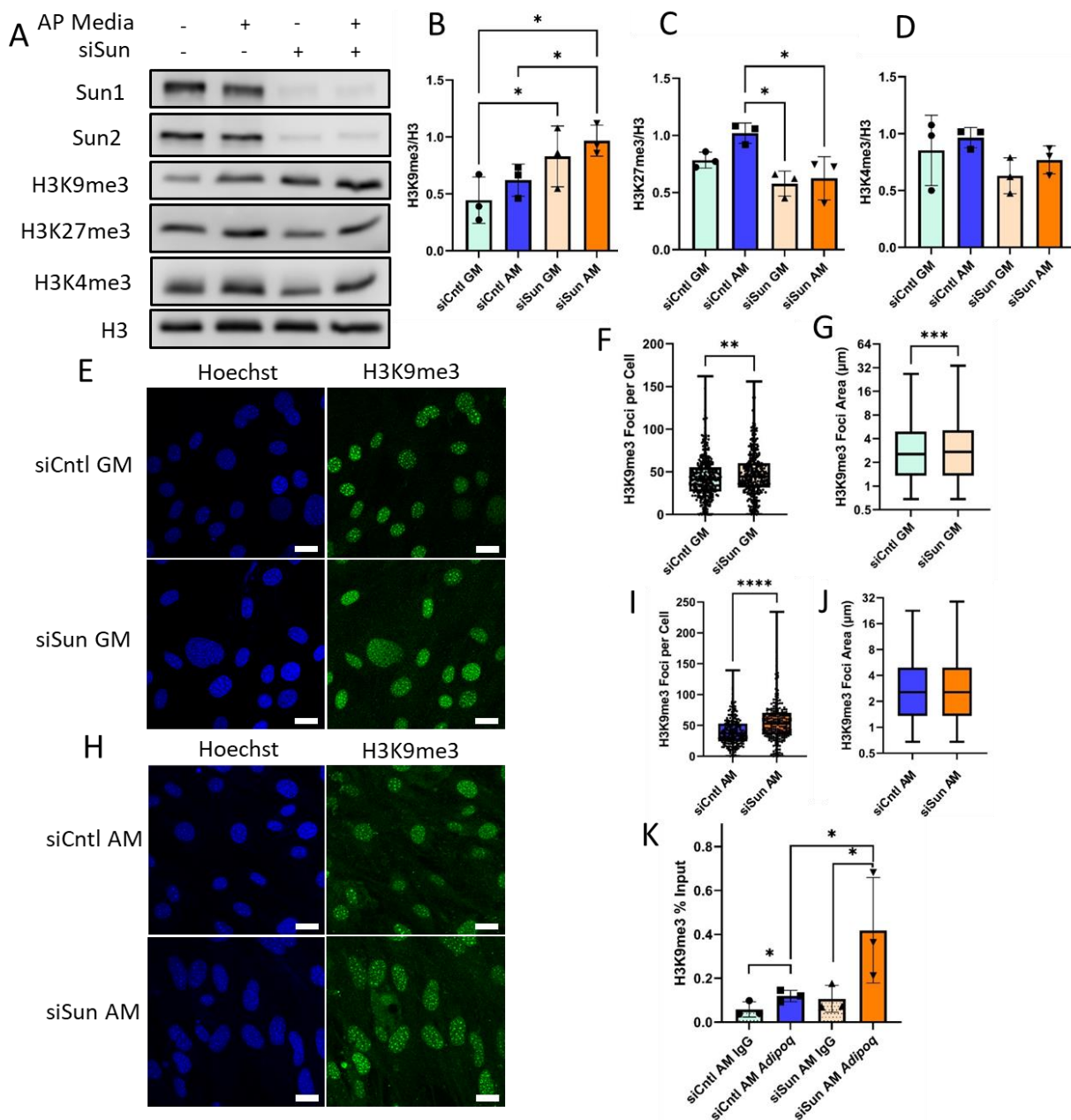


Figure 3.7 Global levels of H3K9me3 and Enrichment on Adipoq increases during Sun1/2 depletion

A Representative western images of heterochromatin markers H3K9me3 and H3K27me3 and euchromatin marker H3K4me3 in siSun and siCntl treatments during growth in growth media and adipogenic media. B Western analysis of heterochromatin marker H3K9me3 revealed an increase of 56% in siSun cells compared to siCntl during adipogenesis (n = 3, p < 0.05). C H3K27me3 had a decrease of 48% in siSun cells compared to siCntl cells during adipogenesis (n = 3, p < 0.05). D Euchromatin marker H3K4me3 experienced no significant changes in global protein levels between siSun and siCntl treated cells during adipogenesis. E Representative images of siCntl and siSun treated cells grown in growth

media staining for H3K9me3 (green) and Hoescht (blue). F H3K9me3 foci count per cell in siSun cells compared to siCntl cells in growth media increased by 9% (n = 338, p < 0.01). G H3K9me3 foci area increased by 7% in siSun cells compared to siCntl in growth media (n = 14560, p < 0.001). H Representative images of siSun and siCntl treated cells grown in adipogenic media and stained for H3K9me3 (green) and Hoechst (blue). I H3K9me3 foci count per cell in siSun cell compared to Sicontrol Cells during adipogenesis increased by 43% (n = 213, p < 0.0001). J No detectable increase of H3K9me3 foci area was found in siSun cells during adipogenesis (n = 8460). K CUR&RUN-qPCR targeting H3K9me3 localization on Adipoq showed an increased of 156% in siSun cells compared to siCntl (n = 3, p < 0.05). Western analysis group comparisons were One-Way Anova. H3K9me3 Foci count and area comparisons were made using Mann-Whitney Test. CUR&RUN-qPCR comparisons were done using One-Tailed Students T-Test. * p < 0.05, ** p < 0.01, *** p < 0.001, **** p < 0.0001. Scale bar represents 25µm.

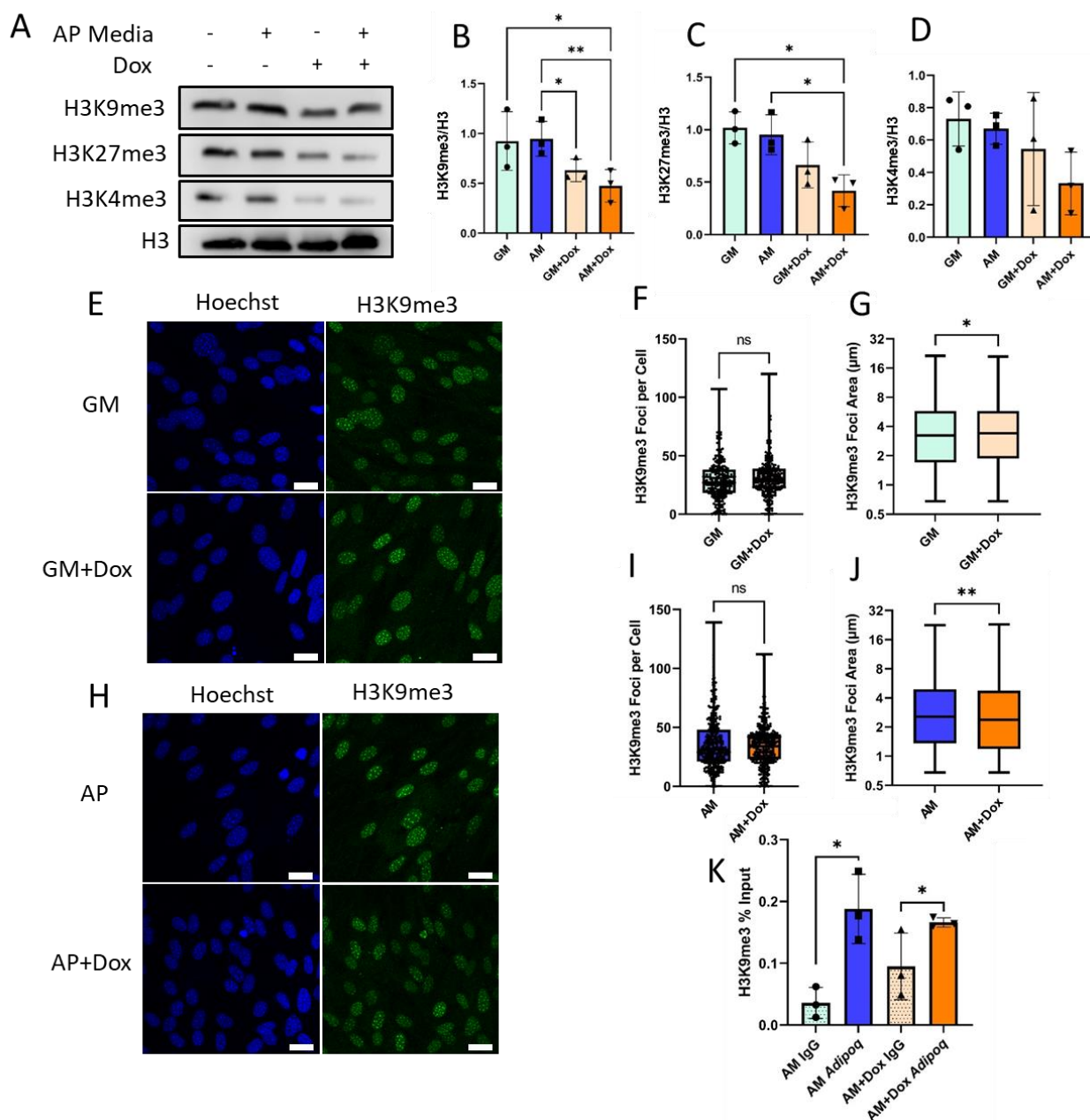


Figure 3.8 H3K9me3 Levels Are Unaltered During dnKASH Disruption of the LINC Complex

A Representative images of doxycycline induced dnKASH expression of heterochromatin markers H3K9me3 and H3K27me3 and euchromatin marker. B H3K9me3 levels decreased during adipogenesis in doxycycline treatment group compared to controls by 51% ($n = 3$, $p < 0.01$). C H3K27me3 levels decreased by 56% in doxycycline treatment group compared to control during adipogenesis ($n = 3$, $p < 0.05$). D H3K4me3 levels had no significant changes in doxycycline. E Representative confocal imaging of H3K9me3 (green) and DNA (Blue) in growth media. F Analysis of H3K9me3 foci count per cell in the doxycycline treatment group in growth media showed no significant changes in foci

count per cell (n= 246). g H3K9me3 foci area increased by 5% in doxycycline treatment group in growth media (n = 7350, p < 0.05). H Representative images of doxycycline treated cells and controls cells stained for H3K9me3 (green) and Hoescht (blue) during growth in adipogenic media. I H3K9me3 foci count per cell did not show significant changes between doxycycline treatment group and control group during growth in adipogenic media (n = 328). J Doxycycline treatment group had decreased H3k9me3 foci area during adipogenesis by 7% compared to control (n = 11317, p < 0.01). K CUR&RUN-qPCR targeting H3K9me3 localization on Adipoq showed no significant increase in doxycycline treatment cells compared to controls (n = 3). Western analysis group comparisons were One-Way Anova. H3K9me3 Foci count and area comparisons were made using Mann-Whitney Test. CUR&RUN-qPCR comparisons were done using One-Tailed Students T-Test. * p < 0.05, ** p < 0.01, *** p < 0.001, **** p < 0.0001. Scale bar represents 25 μ m.

CHAPTER FOUR: FUTURE DIRECTIONS AND CONCLUSIONS

Introduction

Mechanical sensing in the cell is critical to proper cellular and nuclear processes. Studies have shown the importance of transducing mechanical signals into the cell and nucleus. As mechanical signals, such as strain or extracellular stiffness, enter the cell and are transduced through biochemical pathways and physical forces, these signals encounter the nucleus where they must enter and induce a biological response. An important question arises, how do mechanical signals enter the nucleus? This has been of great interest to the field of mechanobiology and studies have highlighted multiple nuclear elements that could be significant in regulating the entrance and transduction of mechanical signals into the nucleus. Two main elements of the nucleoskeleton have been investigated: Lamin A/C and the LINC complex. Together they both help form the nucleoskeleton, but each has unique properties and functionality in the nucleoskeleton. In this dissertation I investigated both the Lamin A/C and LINC complex as important regulators of the mechanically sensitive function of adipogenesis in mesenchymal stem cells. Additionally, I investigated the differences between the LINC complex proteins Sun1/2 and Nesprins in regulating adipogenesis and chromatin dynamics.

In chapter 3 I investigated Lamin A/C and its role in mechanoregulation of adipogenesis in MSCs. Activation of focal adhesions during low intensity vibration were first investigated and was found to be activated independent of Lamin A/C. Additionally, Lamin A/C depletion also did not alter functionality of the LINC complex. Depletion of Lamin A/C negatively regulated adipogenesis compared to controls shown in protein levels of Adipoq, lipid droplets amounts, and RNA-seq data. LIV treatment in both control and Lamin A/C depleted cells inhibited adipogenesis in protein and lipid droplet amounts. However, RNA-seq data revealed only

interferon pathways to be affected by to LIV treatment. Together these data showed that Lamin A/C is not required for the activation of focal adhesions and mechanoregulation of adipogenesis.

The LINC complex was next investigated in chapter 4 as a key adipogenic and chromatin organization regulator. The LINC complex function was inhibited via two methods: depletion of Sun1/2 via siRNA and dominant-negative KASH domain expression (dnKASH). Depletion of Sun1/2 increased nuclear area and height while dnKASH expression decreased nuclear area. Adipogenesis was completely ablated by depleting Sun1/2 shown through adipogenesis protein markers, lipid droplet amounts, and RNA-seq. However, adipogenesis was accelerated during dnKASH expression. Heterochromatin markers H3K9me3 and H3K27me3 and euchromatin marker H3K4me3 were investigated to determine if loss of the LINC complex function effected the chromatin state. Depletion of Sun1/2 was found to increase H3K9me3 global levels while dnKASH expression decreased H3K9me3. Confocal imaging of H3K9me3 showed an increase of H3K9me3 foci per cell. Additionally, H3K9me3 enrichment on Adipoq was increased in Sun1/2 depleted cells while dnKASH cells had no significant changes in H3K9me3 enrichment. This data reveals new regulatory roles for the LINC complex proteins in regulating not only adipogenesis but also chromatin organization. Here I will present our experiments to investigate the role of LINC complex function during mechanical stimulation. Following these results, I will discuss the possible future direction to complete these preliminary studies.

Adipogenesis Commitment Depends upon Differentiation Time and Adipogenic

Media Strength

Preliminary data in Figure 4.1 shows that adipogenesis markers, Adipoq, Plin1 and Pparg protein levels increase due to increased time in adipogenic media and increased strength of adipogenic inducing drug indomethacin (**Fig. 4.1A** and **Fig. 4.1B**). Interestingly, mechanical strain reduces Adipoq levels in response to adipogenic media regardless of strength of indomethacin. However, strain has a stronger inhibition of adipogenesis in the weaker 1 ug/ml

indomethacin adipogenic media, indicating that mechanical regulation of adipogenesis is dependent upon strength of differentiation signals in MSCs.

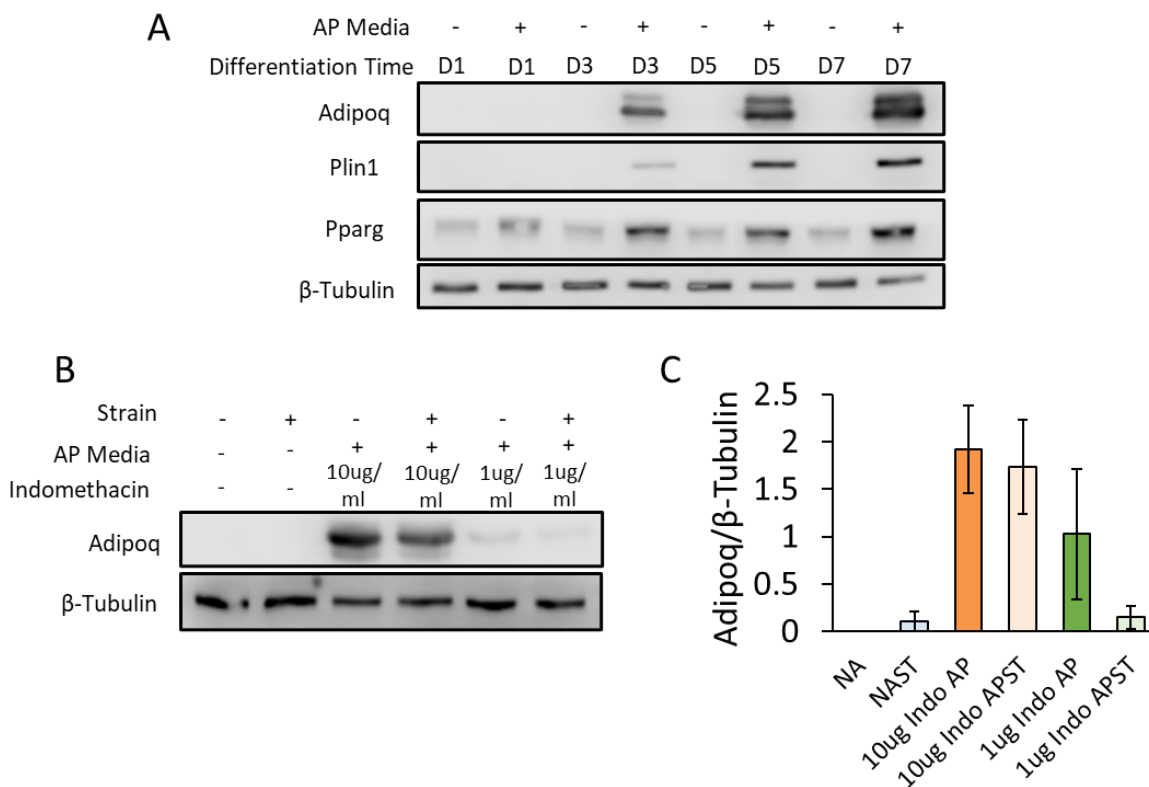


Figure 4.1 Adipogenesis Markers Increased Due to Differentiation Duration and Indomethacin Amounts.

A. Western image of time course of adipogenesis differentiation. MSCs were pulled down on 1, 3, 5, 7 days after adipogenic media was placed on MSCs. Adipogenesis markers, Adipoq, Plin1, and Pparg all experience increases due to elongated growth in adipogenic media. B. Representative western image of Adipoq during strain and differences in indomethacin amounts in adipogenic media. MSCs were grown in adipogenic media containing either 10 ug/ml or 1ug/ml of indomethacin, or growth media, and were then strained or left unstrained for 3 days. Adipoq levels had 47% reduction in 1 ug/ml indomethacin compared to 10 ug/ml indomethacin ($n = 3$). Strain reduced Adipoq by 10% ($n = 3$) when comparing unstrained to strained 10 ug/ml indomethacin and by 85% in 1 ug/ml indomethacin ($n = 3$).

Strain Induces Mechano-inhibition of Adipogenesis

In Figure 4.2 mechanical regulation of adipogenesis via strain in MSCs was further explored. Mechanical strain inhibits adipogenesis (**Fig. 4.2A**) as shown by reduction of adipogenesis markers Adipoq (**Fig. 4.2B**), Plin1 (**Fig. 4.2C**), and Cebpa (**Fig. 4.2D**) by 32%, 38%, and 21% respectively. This mechanical inhibition was conducted in weaker adipogenic media containing 1ug/ml indomethacin.

The next step in investigating the mechanical regulation of adipogenesis is to explore the role of the LINC complex in regulating mechanical repression of adipogenesis. In Figure 4.2B the LINC complex proteins Sun1/2 were depleted via siRNA. Depletion of Sun1/2 severely inhibited adipogenesis as seen by the reduction of Adipoq levels in siSun unstrained by 92% and strained cells by 96% compared to siCntl unstrained and strained cells respectively. While the inhibition of adipogenesis via Sun1/2 depletion was unexpected, the chapter 4 results reveal that expression of dominant-negative KASH effecting Nepsrin association with Sun proteins in the LINC complex accelerates adipogenesis. Therefore, further research is needed to investigate the role of the LINC complex during the mechanical regulation of adipogenesis during dnKASH expression and not depletion of Sun1/2. This will reveal whether the LINC complex is required for the mechanical regulation of adipogenesis. While mechanical forces are transduced through the LINC complex into the nucleus the LINC complex also has been shown to regulate translocation of mechanically sensitive biomolecules that also inhibit adipogenesis.

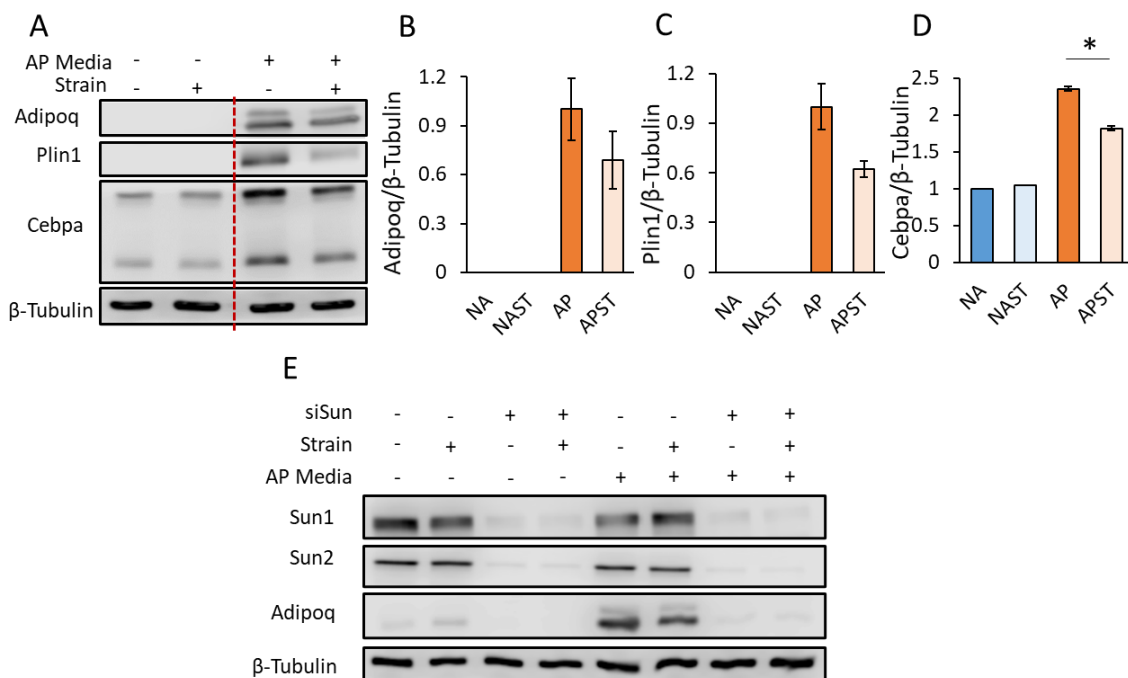


Figure 4.2 Strain Mechanoregulates Adipogenesis in MSCs.

A. Representative Western image of strain mechanoregulating adipogenesis markers Adipoq, Plin1, and Cebpa during growth in adipogenic media with 1 μ g/ml of indomethacin for 5 days. Mechanical strain reduces Adipoq levels by 32% ($n = 3$), Plin1 by 38% ($n = 3$), and Cebpa by 21% ($n = 3$, $p < 0.05$). B. Western image of strain application during adipogenesis and siSun treatment in MSCs. siSun treatment reduced Adipoq levels in strained and unstrained samples by 96% and 92%, respectively, compared to siCntl strained and unstrained samples. Strain reduced Adipoq in siCntl treated MSCs grown in adipogenic media by 22%. Group comparisons were made via Two-Tailed Students T-test. * $p < 0.05$.

Investigation Routes to Determine Mechanoregulatory Role of the LINC Complex

Mechanically activated biomolecular signals such as Yap and β -Catenin are translocated to nucleus following mechanical stimulation to regulate their respective gene targets which includes adipogenic repression¹¹³⁻¹¹⁷. Physical forces induced from mechanical stimulation are transduced through actin or microtubules, inducing contractile and compressive forces on the nucleus altering the nucleus shape and orientation^{115,117,118}. Mechanical stimulation increases nuclear β -Catenin and increased nuclear β -Catenin is correlated with inhibition of adipogenic differentiation. Depletion of Sun1/2 inhibits translocation of β -Catenin into the nucleus which strain and LIV cannot rescue, impeding of β -Catenin's role in anti-adipogenic differentiation regulation³⁵. Yap is a known driver of proliferation and has been shown to repress adipogenesis¹¹⁷. Increased nuclear Yap inhibits commitment to adipogenesis and maintains basal proliferation marker levels¹¹⁷. Additionally, cytosolic Yap/Taz associates with the GSK3 β degradation complex and is required for the degradation of cytosolic β -Catenin^{119,120}. Upon deactivation of the GSK3 β both Yap/Taz and β -Catenin are released allowing for the translocation of both proteins into the nucleus^{119,120}. This data indicates that both Yap/Taz and β -Catenin are regulated by mechanically induced inhibition of GSK3 β . Indeed, preliminary data from our lab shows that Yap nuclear levels also increase with mechanical stimulation like that of β -Catenin. Importantly, not only inhibition of the LINC complex reduces Yap nuclear levels which is not recovered during LIV treatment. RNA-seq done on adipogenic LINC-disabled MSCs indicate that both β -Catenin and Yap nuclear functionality is decreased, marked by altered expression of their respective downstream transcription targets of Myc, Ccnd1, and Ctgf (**Fig. 4.3**). This reduction of nuclear functionality during LINC complex function loss can stem from altered gene target association caused by changes in heterochromatin or reduced nuclear localization. Therefore, future research is needed to determine if the mechanical regulation of adipogenesis is dependent upon the LINC complex and if the loss of the LINC complex induces the loss of proper nuclear functionality of β -Catenin and Yap.

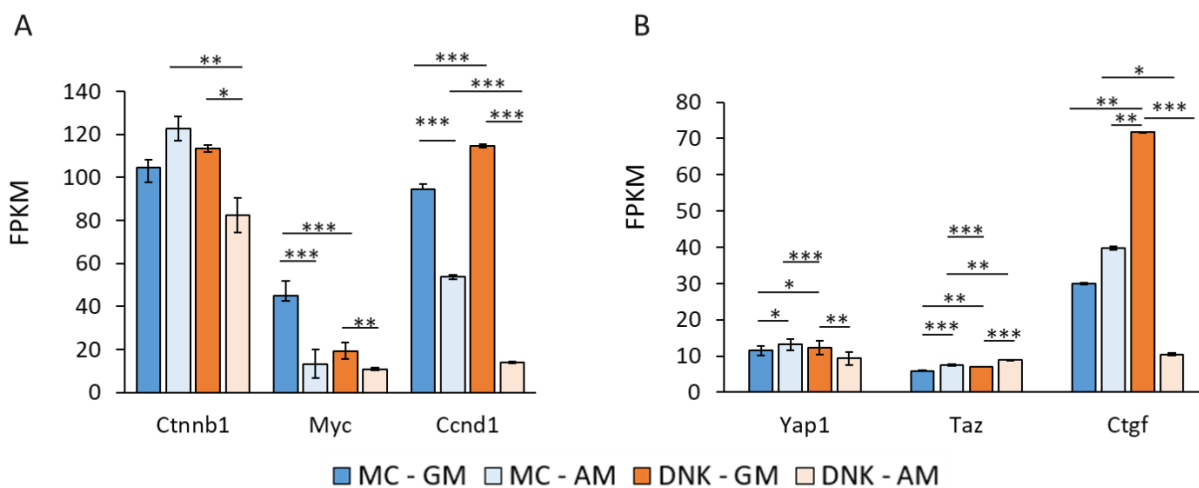


Figure 4.3 Loss of β -Catenin and Yap Nuclear functionality during loss of LINC Complex Function

A. Average FPKM values for β -Catenin (Ctnnb1) and β -Catenin gene targets Myc and Cyclin D1 (Ccnd1). Results are represented as mean \pm STE. B. Average FPKM of Yap1, Taz, and Yap1/Taz gene target Ctgf. Results are represented as mean \pm STE. Group comparison made using One-Way Anova. * $p < 0.05$, ** $p < 0.01$, *** $p < 0.001$.

Further research is also needed in visualizing and measuring the impact from mechanical forces on the nucleus. Current techniques of determining the impact from mechanical forces are limited to using fixed cells such as immunohistochemistry, RNA FISH, Western analysis, and RNA-seq. However, the impact of mechanical forces on the nucleus extends beyond fixed temporal points. Therefore, live cell techniques are needed to understand the dynamics of mechanical responses in the nucleus. Of great importance requiring live cell techniques is understanding how mechanical forces affect transcriptome and genome localization in the nucleus. Recent research has shown the ability to measure strain forces on the nucleus in live cells ¹²¹. Upon depletion of both the LINC complex and Lamin A/C strain forces in the nucleus were found to decrease compared to control cells ¹²¹. Indicating that the loss of the nucleoskeleton results in altered strain forces in the nucleus. Additionally, cardiomyocytes on stiff matrices experienced large differential strain forces in regions with high heterochromatin when compared to cardiomyocytes on soft matrices ¹²¹. Revealing that strain may cause alteration of transcriptome location based on strain forces localized around heterochromatin. Highlighting transcriptome localization changes, during adipogenesis the gene loci and mRNA transcripts of the adipogenic transcription activator PPAR- γ migrate from the periphery to the center of the nucleus shown through RNA and DNA FISH ¹²².

While these results are important, it is not known whether localization of adipogenic genes and transcripts at the center of the nucleus are the result of adipogenesis or is required for adipogenic gene expression. Additionally, it is not known whether this observation correlates with increased adipogenic gene transcripts migration velocity toward the center of the nucleus. While data shows that depletion of emerin reduces chromatin localization to the nuclear periphery ¹²³, it is not known whether the LINC complex also alters chromatin localization and whether mechanical stimulation can rescue altered chromatin localization. Therefore, determining transcriptome localization changes due to the mechanical repression of adipogenesis and the

effects of the loss of the LINC complex on transcript localization in live cells is needed. The new technology CRISPR cas13 is a new technique that promises to elucidate transcriptome alterations in live cells. CRISPR cas13 is a new class of CRISPR enzymes that targets RNA. CRISPR cas13 has been used to mutate mRNA^{124,125} and visualize mRNA localization in the nucleus in both live cells and fixed cells¹²⁶. Deactivated CRISPR cas13 (dCas13) allows for visualization of RNA targets using a guide RNA (gRNA) targeting a sequence of interest. Use of dCas13 tagged with RFP molecules was used to visualize RNA sequences for NEAT1, MUC4, and GLN4 in live cells¹²⁶. Therefore, future projects should aim to visualize RNA transcripts in the nucleus of cells undergoing mechanical repression of adipogenesis during loss of LINC complex function in both fixed cells using RNA FiSH and in live cells using dCas13.

Conclusion

The results presented in this dissertation highlight the importance of the nucleoskeleton in mechanotransduction and mechanical regulation of differentiation. Future research will be needed to further elucidate the interplay between the nucleoskeleton, mechanical signals, and differentiation and proliferation. Potential avenues for research include investigating how both β -Catenin and Yap1 regulate differentiation and proliferation under mechanical forces, indicating a unique balance between differentiation and proliferation which mechanical stimulus can modulate. Additionally, the dCas13 can be used to investigate many new systems. The dCas13 system could be used to determine the spatial and temporal changes of adipogenic mRNA transcripts during live cell strain mapping during the loss of nucleoskeleton proteins. Additionally, dCas13 could be used to determine potential post-transcriptional regulation of adipogenic genes. Overall, these data will indicate exciting, new research avenues that can further elucidate the interworking of the nucleus.

REFERENCES

1. Shumaker, D. K. *et al.* Mutant nuclear lamin A leads to progressive alterations of epigenetic control in premature aging. *Proceedings of the National Academy of Sciences* **103**, 8703-8708, doi:10.1073/pnas.0602569103 (2006).
2. Schreiber, K. H. & Kennedy, B. K. When lamins go bad: nuclear structure and disease. *Cell* **152**, 1365-1375, doi:10.1016/j.cell.2013.02.015 (2013).
3. De Sandre-Giovannoli, A. *et al.* Lamin a truncation in Hutchinson-Gilford progeria. *Science (New York, N.Y.)* **300**, 2055, doi:10.1126/science.1084125 (2003).
4. Constantinescu, D., Gray, H. L., Sammak, P. J., Schatten, G. P. & Csoka, A. B. Lamin A/C expression is a marker of mouse and human embryonic stem cell differentiation. *STEM CELLS* **24**, 474-474, doi:10.1634/stemcells.2006-erratum.2 (2006).
5. Rober, R. A., Weber, K. & Osborn, M. Differential timing of nuclear lamin A/C expression in the various organs of the mouse embryo and the young animal: a developmental study. *Development* **105**, 365-378 (1989).
6. Stewart, C. & Burke, B. Teratocarcinoma stem cells and early mouse embryos contain only a single major lamin polypeptide closely resembling lamin B. *Cell* **51**, 383-392, doi:10.1016/0092-8674(87)90634-9 (1987).
7. Underwood, J. M., Becker, K. A., Stein, G. S. & Nickerson, J. A. The Ultrastructural Signature of Human Embryonic Stem Cells. *Journal of cellular biochemistry* **118**, 764-774, doi:10.1002/jcb.25736 (2017).
8. Lammerding, J. *et al.* Lamins A and C but not lamin B1 regulate nuclear mechanics. *The Journal of biological chemistry* **281**, 25768-25780, doi:10.1074/jbc.M513511200 (2006).

9. Lee, J. S. *et al.* Nuclear lamin A/C deficiency induces defects in cell mechanics, polarization, and migration. *Biophysical journal* **93**, 2542-2552, doi:10.1529/biophysj.106.102426 (2007).
10. Lammerding, J. *et al.* Lamin A/C deficiency causes defective nuclear mechanics and mechanotransduction. *The Journal of Clinical Investigation* **113**, 370-378, doi:10.1172/JCI19670 (2004).
11. Verstraeten, V. L., Ji, J. Y., Cummings, K. S., Lee, R. T. & Lammerding, J. Increased mechanosensitivity and nuclear stiffness in Hutchinson-Gilford progeria cells: effects of farnesyltransferase inhibitors. *Aging cell* **7**, 383-393, doi:10.1111/j.1474-9726.2008.00382.x (2008).
12. Sullivan, T. *et al.* Loss of A-type lamin expression compromises nuclear envelope integrity leading to muscular dystrophy. *The Journal of cell biology* **147**, 913-920 (1999).
13. Sabatelli, P. *et al.* Nuclear alterations in autosomal-dominant Emery-Dreifuss muscular dystrophy. *Muscle & Nerve* **24**, 826-829, doi:10.1002/mus.1076 (2001).
14. Bronshtein, I. *et al.* Loss of lamin A function increases chromatin dynamics in the nuclear interior. *Nature Communications* **6**, 8044, doi:10.1038/ncomms9044 (2015).
15. Ranade, D., Pradhan, R., Jayakrishnan, M., Hegde, S. & Sengupta, K. Lamin A/C and Emerin depletion impacts chromatin organization and dynamics in the interphase nucleus. *BMC Molecular and Cell Biology* **20**, 11, doi:10.1186/s12860-019-0192-5 (2019).
16. Stephens, A. D., Banigan, E. J. & Marko, J. F. Separate roles for chromatin and lamins in nuclear mechanics. *Nucleus (Austin, Tex.)* **9**, 119-124, doi:10.1080/19491034.2017.1414118 (2018).
17. Moghadam, F. H. *et al.* Differentiation of bone marrow mesenchymal stem cells into chondrocytes after short term culture in alkaline medium. *International journal of hematology-oncology and stem cell research* **8**, 12-19 (2014).

18. Sen, B. *et al.* Mechanical signal influence on mesenchymal stem cell fate is enhanced by incorporation of refractory periods into the loading regimen. *Journal of biomechanics* **44**, 593-599, doi:10.1016/j.jbiomech.2010.11.022 (2011).
19. Sen, B. *et al.* Mechanical strain inhibits adipogenesis in mesenchymal stem cells by stimulating a durable beta-catenin signal. *Endocrinology* **149**, 6065-6075, doi:10.1210/en.2008-0687 (2008).
20. Sen, B. *et al.* Mechanically induced focal adhesion assembly amplifies anti-adipogenic pathways in mesenchymal stem cells. *Stem Cells* **29**, 1829-1836, doi:10.1002/stem.732 (2011).
21. Uzer, G., Pongkitwitoon, S., Ete Chan, M. & Judex, S. Vibration induced osteogenic commitment of mesenchymal stem cells is enhanced by cytoskeletal remodeling but not fluid shear. *Journal of biomechanics* **46**, 2296-2302, doi:10.1016/j.jbiomech.2013.06.008 (2013).
22. Bas, G. *et al.* Low Intensity Vibrations Augment Mesenchymal Stem Cell Proliferation and Differentiation Capacity during in vitro Expansion. *Scientific Reports* **10**, 9369, doi:10.1038/s41598-020-66055-0 (2020).
23. Akter, R., Rivas, D., Geneau, G., Drissi, H. & Duque, G. Effect of lamin A/C knockdown on osteoblast differentiation and function. *Journal of bone and mineral research : the official journal of the American Society for Bone and Mineral Research* **24**, 283-293, doi:10.1359/jbmr.081010 (2009).
24. Oldenburg, A. *et al.* A lipodystrophy-causing lamin A mutant alters conformation and epigenetic regulation of the anti-adipogenic MIR335 locus. *The Journal of cell biology* **216**, 2731-2743, doi:10.1083/jcb.201701043 (2017).
25. Bermeo, S., Vidal, C., Zhou, H. & Duque, G. Lamin A/C Acts as an Essential Factor in Mesenchymal Stem Cell Differentiation Through the Regulation of the Dynamics of the Wnt/ β -Catenin Pathway. *Journal of cellular biochemistry* **116**, 2344-2353, doi:10.1002/jcb.25185 (2015).
26. Li, W. *et al.* Decreased bone formation and osteopenia in lamin a/c-deficient mice. *PloS one* **6**, e19313, doi:10.1371/journal.pone.0019313 (2011).

27. Geiger, B., Spatz, J. P. & Bershadsky, A. D. Environmental sensing through focal adhesions. *Nature Reviews Molecular Cell Biology* **10**, 21-33, doi:10.1038/nrm2593 (2009).
28. Hamadi, A. *et al.* Regulation of focal adhesion dynamics and disassembly by phosphorylation of FAK at tyrosine 397. *Journal of Cell Science* **118**, 4415-4425, doi:10.1242/jcs.02565 (2005).
29. Uzer, G. *et al.* Cell Mechanosensitivity to Extremely Low-Magnitude Signals Is Enabled by a LINCed Nucleus. *STEM CELLS* **33**, 2063-2076, doi:10.1002/stem.2004 (2015).
30. Uzer, G., Fuchs, R. K., Rubin, J. & Thompson, W. R. Concise Review: Plasma and Nuclear Membranes Convey Mechanical Information to Regulate Mesenchymal Stem Cell Lineage. *Stem Cells* **34**, 1455-1463, doi:10.1002/stem.2342 (2016).
31. Sen, B. *et al.* mTORC2 regulates mechanically induced cytoskeletal reorganization and lineage selection in marrow-derived mesenchymal stem cells. *Journal of bone and mineral research : the official journal of the American Society for Bone and Mineral Research* **29**, 78-89, doi:10.1002/jbmr.2031 (2014).
32. Thompson, W. R. *et al.* LARG GEF and ARHGAP18 orchestrate RhoA activity to control mesenchymal stem cell lineage. *Bone* **107**, 172-180, doi:10.1016/j.bone.2017.12.001 (2018).
33. Tontonoz, P. & Spiegelman, B. M. Fat and Beyond: The Diverse Biology of PPAR γ . *Annual Review of Biochemistry* **77**, 289-312, doi:10.1146/annurev.biochem.77.061307.091829 (2008).
34. Pagnotti, G. M. *et al.* Combating osteoporosis and obesity with exercise: leveraging cell mechanosensitivity. *Nature reviews. Endocrinology* **15**, 339-355, doi:10.1038/s41574-019-0170-1 (2019).
35. Uzer, G. *et al.* Sun-mediated mechanical LINC between nucleus and cytoskeleton regulates β catenin nuclear access. *Journal of biomechanics* **74**, 32-40, doi:10.1016/j.jbiomech.2018.04.013 (2018).

36. Sen, B. *et al.* Mechanical signal influence on mesenchymal stem cell fate is enhanced by incorporation of refractory periods into the loading regimen. *Journal of biomechanics* **44**, 593-599, doi:10.1016/j.jbiomech.2010.11.022 (2011).
37. Metsalu, T. & Vilo, J. ClustVis: a web tool for visualizing clustering of multivariate data using Principal Component Analysis and heatmap. *Nucleic acids research* **43**, W566-570, doi:10.1093/nar/gkv468 (2015).
38. Peister, A. *et al.* Adult stem cells from bone marrow (MSCs) isolated from different strains of inbred mice vary in surface epitopes, rates of proliferation, and differentiation potential. *Blood* **103**, 1662-1668, doi:10.1182/blood-2003-09-3070 (2004).
39. Dobin, A. *et al.* STAR: ultrafast universal RNA-seq aligner. *Bioinformatics (Oxford, England)* **29**, 15-21, doi:10.1093/bioinformatics/bts635 (2013).
40. Love, M. I., Huber, W. & Anders, S. Moderated estimation of fold change and dispersion for RNA-seq data with DESeq2. *Genome biology* **15**, 550, doi:10.1186/s13059-014-0550-8 (2014).
41. Dudakovic, A. *et al.* High-resolution molecular validation of self-renewal and spontaneous differentiation in clinical-grade adipose-tissue derived human mesenchymal stem cells. *Journal of cellular biochemistry* **115**, 1816-1828, doi:10.1002/jcb.24852 (2014).
42. Wang, H. & Rodríguez, A. Identifying pediatric cancer clusters in Florida using loglinear models and generalized lasso penalties. *Stat Public Policy (Phila)* **1**, 86-96, doi:10.1080/2330443x.2014.960120 (2014).
43. Dudakovic, A. *et al.* Enhancer of zeste homolog 2 (Ezh2) controls bone formation and cell cycle progression during osteogenesis in mice. *The Journal of biological chemistry* **293**, 12894-12907, doi:10.1074/jbc.RA118.002983 (2018).
44. Dennison, E. & Cooper, C. Epidemiology of osteoporotic fractures. *Hormone research* **54 Suppl 1**, 58-63, doi:63449 (2000).
45. Kalari, K. R. *et al.* MAP-RSeq: Mayo Analysis Pipeline for RNA sequencing. *BMC bioinformatics* **15**, 224, doi:10.1186/1471-2105-15-224 (2014).

46. Kim, D. *et al.* TopHat2: accurate alignment of transcriptomes in the presence of insertions, deletions and gene fusions. *Genome biology* **14**, R36, doi:10.1186/gb-2013-14-4-r36 (2013).
47. Anders, S., Pyl, P. T. & Huber, W. HTSeq--a Python framework to work with high-throughput sequencing data. *Bioinformatics (Oxford, England)* **31**, 166-169, doi:10.1093/bioinformatics/btu638 (2015).
48. Raharjo, W. H., Enarson, P., Sullivan, T., Stewart, C. L. & Burke, B. Nuclear envelope defects associated with LMNA mutations cause dilated cardiomyopathy and Emery-Dreifuss muscular dystrophy. *J Cell Sci* **114**, 4447-4457 (2001).
49. Kim, J.-K. *et al.* Nuclear lamin A/C harnesses the perinuclear apical actin cables to protect nuclear morphology. *Nature Communications* **8**, 2123, doi:10.1038/s41467-017-02217-5 (2017).
50. Corne, T. D. J. *et al.* Deregulation of focal adhesion formation and cytoskeletal tension due to loss of A-type lamins. *Cell Adh Migr* **11**, 447-463, doi:10.1080/19336918.2016.1247144 (2017).
51. Chancellor, T. J., Lee, J., Thodeti, C. K. & Lele, T. Actomyosin tension exerted on the nucleus through nesprin-1 connections influences endothelial cell adhesion, migration, and cyclic strain-induced reorientation. *Biophysical journal* **99**, 115-123, doi:10.1016/j.bpj.2010.04.011 (2010).
52. Wang, W. *et al.* Structural insights into SUN-KASH complexes across the nuclear envelope. *Cell Research* **22**, 1440-1452, doi:10.1038/cr.2012.126 (2012).
53. Haque, F. *et al.* SUN1 Interacts with Nuclear Lamin A and Cytoplasmic Nesprins To Provide a Physical Connection between the Nuclear Lamina and the Cytoskeleton. *Molecular and Cellular Biology* **26**, 3738-3751, doi:10.1128/mcb.26.10.3738-3751.2006 (2006).
54. Liang, Y., Chiu, P. H., Yip, K. Y. & Chan, S. Y. Subcellular Localization of SUN2 Is Regulated by Lamin A and Rab5. *PloS one* **6**, e20507, doi:10.1371/journal.pone.0020507 (2011).

55. Naito, M., Omoteyama, K., Mikami, Y., Takagi, M. & Takahashi, T. Suppression of lamin A/C by short hairpin RNAs promotes adipocyte lineage commitment in mesenchymal progenitor cell line, ROB-C26. *Histochemistry and cell biology* **137**, 235-247, doi:10.1007/s00418-011-0890-3 (2012).
56. Khan, K. A. *et al.* Fine-Tuning of the RIG-I-Like Receptor/Interferon Regulatory Factor 3-Dependent Antiviral Innate Immune Response by the Glycogen Synthase Kinase 3/ β -Catenin Pathway. *Molecular and Cellular Biology* **35**, 3029-3043, doi:10.1128/mcb.00344-15 (2015).
57. Smith, J. L., Jeng, S., McWeeney, S. K. & Hirsch, A. J. A MicroRNA Screen Identifies the Wnt Signaling Pathway as a Regulator of the Interferon Response during Flavivirus Infection. *Journal of Virology* **91**, e02388-02316, doi:10.1128/jvi.02388-16 (2017).
58. Cartwright, T., Senussi, O. & Grady, M. D. The Mechanism of the Inactivation of Human Fibroblast Interferon by Mechanical Stress. *Journal of General Virology* **36**, 317-321, doi:<https://doi.org/10.1099/0022-1317-36-2-317> (1977).
59. Crisp, M. *et al.* Coupling of the nucleus and cytoplasm: role of the LINC complex. *J Cell Biol* **172**, 41-53, doi:10.1083/jcb.200509124 (2006).
60. Zhang, Q. *et al.* Nesprins: a novel family of spectrin-repeat-containing proteins that localize to the nuclear membrane in multiple tissues. *J Cell Sci* **114**, 4485-4498 (2001).
61. Bouzid, T. *et al.* The LINC complex, mechanotransduction, and mesenchymal stem cell function and fate. *J Biol Eng* **13**, 68, doi:10.1186/s13036-019-0197-9 (2019).
62. Mellad, J. A., Warren, D. T. & Shanahan, C. M. Nesprins LINC the nucleus and cytoskeleton. *Curr Opin Cell Biol* **23**, 47-54, doi:10.1016/j.ceb.2010.11.006 (2011).
63. Wilhelmsen, K. *et al.* Nesprin-3, a novel outer nuclear membrane protein, associates with the cytoskeletal linker protein plectin. *J Cell Biol* **171**, 799-810, doi:10.1083/jcb.200506083 (2005).

64. Haque, F. *et al.* SUN1 interacts with nuclear lamin A and cytoplasmic nesprins to provide a physical connection between the nuclear lamina and the cytoskeleton. *Mol Cell Biol* **26**, 3738-3751, doi:10.1128/MCB.26.10.3738-3751.2006 (2006).
65. Ding, X. *et al.* SUN1 is required for telomere attachment to nuclear envelope and gametogenesis in mice. *Dev Cell* **12**, 863-872, doi:10.1016/j.devcel.2007.03.018 (2007).
66. Lee, K. K. *et al.* Distinct functional domains in emerin bind lamin A and DNA-bridging protein BAF. *J Cell Sci* **114**, 4567-4573 (2001).
67. Caputo, S. *et al.* The carboxyl-terminal nucleoplasmic region of MAN1 exhibits a DNA binding winged helix domain. *J Biol Chem* **281**, 18208-18215, doi:10.1074/jbc.M601980200 (2006).
68. Janin, A., Bauer, D., Ratti, F., Millat, G. & Mejat, A. Nuclear envelopathies: a complex LINC between nuclear envelope and pathology. *Orphanet J Rare Dis* **12**, 147, doi:10.1186/s13023-017-0698-x (2017).
69. Emery, A. E. Emery-Dreifuss muscular dystrophy - a 40 year retrospective. *Neuromuscul Disord* **10**, 228-232, doi:10.1016/s0960-8966(00)00105-x (2000).
70. Anno, T., Sakamoto, N. & Sato, M. Role of nesprin-1 in nuclear deformation in endothelial cells under static and uniaxial stretching conditions. *Biochem Biophys Res Commun* **424**, 94-99, doi:10.1016/j.bbrc.2012.06.073 (2012).
71. Chambliss, A. B. *et al.* The LINC-anchored actin cap connects the extracellular milieu to the nucleus for ultrafast mechanotransduction. *Sci Rep* **3**, 1087, doi:10.1038/srep01087 (2013).
72. Killaars, A. R., Walker, C. J. & Anseth, K. S. Nuclear mechanosensing controls MSC osteogenic potential through HDAC epigenetic remodeling. *Proc Natl Acad Sci U S A* **117**, 21258-21266, doi:10.1073/pnas.2006765117 (2020).
73. Uzer, G. *et al.* Cell Mechanosensitivity to Extremely Low-Magnitude Signals Is Enabled by a LINCed Nucleus. *Stem Cells* **33**, 2063-2076, doi:10.1002/stem.2004 (2015).

74. Uzer, G. *et al.* Sun-mediated mechanical LINC between nucleus and cytoskeleton regulates betacatenin nuclear access. *Journal of biomechanics* **74**, 32-40, doi:10.1016/j.jbiomech.2018.04.013 (2018).
75. Benham-Pyle, B. W., Pruitt, B. L. & Nelson, W. J. Cell adhesion. Mechanical strain induces E-cadherin-dependent Yap1 and beta-catenin activation to drive cell cycle entry. *Science* **348**, 1024-1027, doi:10.1126/science.aaa4559 (2015).
76. Shen, X. *et al.* YAP promotes the proliferation of neuroblastoma cells through decreasing the nuclear location of p27(Kip1) mediated by Akt. *Cell Prolif* **53**, e12734, doi:10.1111/cpr.12734 (2020).
77. Pan, J. X. *et al.* YAP promotes osteogenesis and suppresses adipogenic differentiation by regulating beta-catenin signaling. *Bone Res* **6**, 18, doi:10.1038/s41413-018-0018-7 (2018).
78. Lorthongpanich, C. *et al.* YAP as a key regulator of adipo-osteogenic differentiation in human MSCs. *Stem Cell Res Ther* **10**, 402, doi:10.1186/s13287-019-1494-4 (2019).
79. Driscoll, T. P., Cosgrove, B. D., Heo, S. J., Shurden, Z. E. & Mauck, R. L. Cytoskeletal to Nuclear Strain Transfer Regulates YAP Signaling in Mesenchymal Stem Cells. *Biophys J* **108**, 2783-2793, doi:10.1016/j.bpj.2015.05.010 (2015).
80. Salpingidou, G., Smertenko, A., Hausmanowa-Petrucewicz, I., Hussey, P. J. & Hutchison, C. J. A novel role for the nuclear membrane protein emerin in association of the centrosome to the outer nuclear membrane. *J Cell Biol* **178**, 897-904, doi:10.1083/jcb.200702026 (2007).
81. Haque, F. *et al.* Mammalian SUN protein interaction networks at the inner nuclear membrane and their role in laminopathy disease processes. *J Biol Chem* **285**, 3487-3498, doi:10.1074/jbc.M109.071910 (2010).
82. Newberg, J. *et al.* Isolated nuclei stiffen in response to low intensity vibration. *J Biomech* **111**, 110012, doi:10.1016/j.jbiomech.2020.110012 (2020).

83. Sen, B. *et al.* β -Catenin Preserves the Stem State of Murine Bone Marrow Stromal Cells Through Activation of EZH2. *Journal of bone and mineral research : the official journal of the American Society for Bone and Mineral Research* **35**, 1149-1162, doi:10.1002/jbmr.3975 (2020).
84. Tajik, A. *et al.* Transcription upregulation via force-induced direct stretching of chromatin. *Nat Mater* **15**, 1287-1296, doi:10.1038/nmat4729 (2016).
85. Lombardi, M. L. *et al.* The interaction between nesprins and sun proteins at the nuclear envelope is critical for force transmission between the nucleus and cytoskeleton. *J Biol Chem* **286**, 26743-26753, doi:10.1074/jbc.M111.233700 (2011).
86. Goelzer, M. *et al.* Lamin A/C Is Dispensable to Mechanical Repression of Adipogenesis. *Int J Mol Sci* **22**, doi:10.3390/ijms22126580 (2021).
87. Dennis, G., Jr. *et al.* DAVID: Database for Annotation, Visualization, and Integrated Discovery. *Genome Biol* **4**, P3 (2003).
88. Thompson, M., Woods, K., Newberg, J., Oxford, J. T. & Uzer, G. Low-intensity vibration restores nuclear YAP levels and acute YAP nuclear shuttling in mesenchymal stem cells subjected to simulated microgravity. *NPJ Microgravity* **6**, 35, doi:10.1038/s41526-020-00125-5 (2020).
89. Zhang, Q. *et al.* N-terminal nesprin-2 variants regulate beta-catenin signalling. *Exp Cell Res* **345**, 168-179, doi:10.1016/j.yexcr.2016.06.008 (2016).
90. Gilbert, H. T. J. *et al.* Nuclear decoupling is part of a rapid protein-level cellular response to high-intensity mechanical loading. *Nat Commun* **10**, 4149, doi:10.1038/s41467-019-11923-1 (2019).
91. Denis, K. B. *et al.* The LINC complex is required for endothelial cell adhesion and adaptation to shear stress and cyclic stretch. *Mol Biol Cell* **32**, 1654-1663, doi:10.1091/mbc.E20-11-0698 (2021).
92. Cain, N. E. *et al.* Conserved SUN-KASH Interfaces Mediate LINC Complex-Dependent Nuclear Movement and Positioning. *Current biology : CB* **28**, 3086-3097.e3084, doi:10.1016/j.cub.2018.08.001 (2018).

93. Meinke, P. *et al.* Muscular dystrophy-associated SUN1 and SUN2 variants disrupt nuclear-cytoskeletal connections and myonuclear organization. *PLoS Genet* **10**, e1004605, doi:10.1371/journal.pgen.1004605 (2014).
94. Matsumoto, A. *et al.* Loss of the integral nuclear envelope protein SUN1 induces alteration of nucleoli. *Nucleus (Austin, Tex.)* **7**, 68-83, doi:10.1080/19491034.2016.1149664 (2016).
95. Satomi, E., Ueda, M., Katahira, J. & Hieda, M. The SUN1 splicing variants SUN1_888 and SUN1_916 differentially regulate nucleolar structure. *Genes to cells : devoted to molecular & cellular mechanisms* **25**, 730-740, doi:10.1111/gtc.12807 (2020).
96. Nakayama, J., Rice, J. C., Strahl, B. D., Allis, C. D. & Grewal, S. I. Role of histone H3 lysine 9 methylation in epigenetic control of heterochromatin assembly. *Science* **292**, 110-113, doi:10.1126/science.1060118 (2001).
97. Martens, J. H. *et al.* The profile of repeat-associated histone lysine methylation states in the mouse epigenome. *EMBO J* **24**, 800-812, doi:10.1038/sj.emboj.7600545 (2005).
98. Becker, J. S., Nicetto, D. & Zaret, K. S. H3K9me3-Dependent Heterochromatin: Barrier to Cell Fate Changes. *Trends Genet* **32**, 29-41, doi:10.1016/j.tig.2015.11.001 (2016).
99. Cheng, L. *et al.* Chromatin Assembly Factor 1 (CAF-1) facilitates the establishment of facultative heterochromatin during pluripotency exit. *Nucleic Acids Res* **47**, 11114-11131, doi:10.1093/nar/gkz858 (2019).
100. Yi, S. A., Han, J. & Han, J. W. Epigenetic role of nuclear S6K1 in early adipogenesis. *BMB Rep* **49**, 401-402, doi:10.5483/bmbrep.2016.49.8.116 (2016).
101. Wu, X., Sun, A., Yu, W., Hong, C. & Liu, Z. CXCL10 mediates breast cancer tamoxifen resistance and promotes estrogen-dependent and independent proliferation. *Molecular and cellular endocrinology* **512**, 110866, doi:10.1016/j.mce.2020.110866 (2020).

102. Hardaway, A. L., Herroon, M. K., Rajagurubandara, E. & Podgorski, I. Marrow adipocyte-derived CXCL1 and CXCL2 contribute to osteolysis in metastatic prostate cancer. *Clinical & experimental metastasis* **32**, 353-368, doi:10.1007/s10585-015-9714-5 (2015).
103. Lee, J. H. *et al.* CXCL10 promotes osteolytic bone metastasis by enhancing cancer outgrowth and osteoclastogenesis. *Cancer research* **72**, 3175-3186, doi:10.1158/0008-5472.can-12-0481 (2012).
104. Romero-Moreno, R. *et al.* The CXCL5/CXCR2 axis is sufficient to promote breast cancer colonization during bone metastasis. *Nat Commun* **10**, 4404, doi:10.1038/s41467-019-12108-6 (2019).
105. Onan, D. *et al.* The chemokine Cxcl1 is a novel target gene of parathyroid hormone (PTH)/PTH-related protein in committed osteoblasts. *Endocrinology* **150**, 2244-2253, doi:10.1210/en.2008-1597 (2009).
106. Chen, C. *et al.* CXCL5 induces tumor angiogenesis via enhancing the expression of FOXD1 mediated by the AKT/NF- κ B pathway in colorectal cancer. *Cell death & disease* **10**, 178, doi:10.1038/s41419-019-1431-6 (2019).
107. Goltzman, D. Osteolysis and cancer. *The Journal of clinical investigation* **107**, 1219-1220, doi:10.1172/jci13073 (2001).
108. Luke, Y. *et al.* Nesprin-2 Giant (NUANCE) maintains nuclear envelope architecture and composition in skin. *J Cell Sci* **121**, 1887-1898, doi:10.1242/jcs.019075 (2008).
109. Alam, S. G. *et al.* The mammalian LINC complex regulates genome transcriptional responses to substrate rigidity. *Sci Rep* **6**, 38063, doi:10.1038/srep38063 (2016).
110. Neelam, S. *et al.* Direct force probe reveals the mechanics of nuclear homeostasis in the mammalian cell. *Proc Natl Acad Sci U S A* **112**, 5720-5725, doi:10.1073/pnas.1502111112 (2015).

111. Stephens, A. D., Banigan, E. J., Adam, S. A., Goldman, R. D. & Marko, J. F. Chromatin and lamin A determine two different mechanical response regimes of the cell nucleus. *Mol Biol Cell* **28**, 1984-1996, doi:10.1091/mbc.E16-09-0653 (2017).
112. Stephens, A. D. *et al.* Chromatin histone modifications and rigidity affect nuclear morphology independent of lamins. *Mol Biol Cell* **29**, 220-233, doi:10.1091/mbc.E17-06-0410 (2018).
113. Driscoll, Tristan P., Cosgrove, Brian D., Heo, S.-J., Shurden, Zach E. & Mauck, Robert L. Cytoskeletal to Nuclear Strain Transfer Regulates YAP Signaling in Mesenchymal Stem Cells. *Biophysical Journal* **108**, 2783-2793, doi:10.1016/j.bpj.2015.05.010.
114. Elosegui-Artola, A. *et al.* Force Triggers YAP Nuclear Entry by Regulating Transport across Nuclear Pores. *Cell* **171**, 1397-1410.e1314, doi:10.1016/j.cell.2017.10.008 (2017).
115. Hoffman, L. M. *et al.* Mechanical stress triggers nuclear remodeling and the formation of transmembrane actin nuclear lines with associated nuclear pore complexes. *Molecular biology of the cell* **31**, 1774-1787, doi:10.1091/mbc.E19-01-0027 (2020).
116. Sen, B. *et al.* Mechanical Strain Inhibits Adipogenesis in Mesenchymal Stem Cells by Stimulating a Durable β -Catenin Signal. *Endocrinology* **149**, 6065-6075, doi:10.1210/en.2008-0687 (2008).
117. Oliver-De La Cruz, J. *et al.* Substrate mechanics controls adipogenesis through YAP phosphorylation by dictating cell spreading. *Biomaterials* **205**, 64-80, doi:10.1016/j.biomaterials.2019.03.009 (2019).
118. Sen, B. *et al.* Intranuclear Actin Structure Modulates Mesenchymal Stem Cell Differentiation. *Stem Cells* **35**, 1624-1635, doi:10.1002/stem.2617 (2017).
119. Azzolin, L. *et al.* Role of TAZ as mediator of Wnt signaling. *Cell* **151**, 1443-1456, doi:10.1016/j.cell.2012.11.027 (2012).

120. Azzolin, L. *et al.* YAP/TAZ incorporation in the β -catenin destruction complex orchestrates the Wnt response. *Cell* **158**, 157-170, doi:10.1016/j.cell.2014.06.013 (2014).
121. Ghosh, S. *et al.* Deformation Microscopy for Dynamic Intracellular and Intranuclear Mapping of Mechanics with High Spatiotemporal Resolution. *Cell reports* **27**, 1607-1620.e1604, doi:10.1016/j.celrep.2019.04.009 (2019).
122. Stachecka, J., Nowacka-Woszek, J., Kolodziejcki, P. A. & Szczerbal, I. The importance of the nuclear positioning of the PPAR γ gene for its expression during porcine in vitro adipogenesis. *Chromosome research : an international journal on the molecular, supramolecular and evolutionary aspects of chromosome biology* **27**, 271-284, doi:10.1007/s10577-019-09604-2 (2019).
123. Demmerle, J., Koch, A. J. & Holaska, J. M. The nuclear envelope protein emerin binds directly to histone deacetylase 3 (HDAC3) and activates HDAC3 activity. *The Journal of biological chemistry* **287**, 22080-22088, doi:10.1074/jbc.M111.325308 (2012).
124. Cox, D. B. T. *et al.* RNA editing with CRISPR-Cas13. *Science (New York, N.Y.)* **358**, 1019-1027, doi:10.1126/science.aaq0180 (2017).
125. Abudayyeh, O. O. *et al.* RNA targeting with CRISPR-Cas13. *Nature* **550**, 280-284, doi:10.1038/nature24049 (2017).
126. Yang, L. Z. *et al.* Dynamic Imaging of RNA in Living Cells by CRISPR-Cas13 Systems. *Molecular cell* **76**, 981-997.e987, doi:10.1016/j.molcel.2019.10.024 (2019).
127. Lemke, S. B. & Schnorrer, F. Mechanical forces during muscle development. *Mechanisms of Development* **144**, 92-101, doi:<https://doi.org/10.1016/j.mod.2016.11.003> (2017).
128. Fung, Y. C. *Biomechanics : mechanical properties of living tissues*. 2nd edn, (Springer-Verlag, 1993).

129. Pagnotti, G. M. *et al.* Combating osteoporosis and obesity with exercise: leveraging cell mechanosensitivity. *Nature Reviews Endocrinology*, doi:10.1038/s41574-019-0170-1 (2019).
130. Riddle, R. C. & Donahue, H. J. From Streaming Potentials to Shear Stress: 25 Years of Bone Cell Mechanotransduction. *Journal of Orthopaedic Research* **27**, 143-149, doi:10.1002/jor.20723 (2009).
131. Pittenger, M. F. *et al.* Multilineage Potential of Adult Human Mesenchymal Stem Cells. *Science (New York, N.Y.)* **284**, 143-147, doi:10.1126/science.284.5411.143 (1999).
132. Rusinol, A. E. & Sinensky, M. S. Farnesylated lamins, progeroid syndromes and farnesyl transferase inhibitors. *J Cell Sci* **119**, 3265-3272, doi:10.1242/jcs.03156 (2006).
133. Broers, J. L., Ramaekers, F. C., Bonne, G., Yaou, R. B. & Hutchison, C. J. Nuclear lamins: laminopathies and their role in premature ageing. *Physiol Rev* **86**, 967-1008, doi:10.1152/physrev.00047.2005 (2006).
134. Hale, C. M. *et al.* Dysfunctional connections between the nucleus and the actin and microtubule networks in laminopathic models. *Biophysical journal* **95**, 5462-5475, doi:10.1529/biophysj.108.139428 (2008).
135. Haque, F. *et al.* Mammalian SUN Protein Interaction Networks at the Inner Nuclear Membrane and Their Role in Laminopathy Disease Processes. *Journal of Biological Chemistry* **285**, 3487-3498, doi:10.1074/jbc.M109.071910 (2010).
136. Chen, C.-Y. *et al.* Accumulation of the Inner Nuclear Envelope Protein Sun1 Is Pathogenic in Progeric and Dystrophic Laminopathies. *Cell* **149**, 565-577, doi:<http://dx.doi.org/10.1016/j.cell.2012.01.059> (2012).
137. Wang, H., Leng, Y. & Gong, Y. Bone Marrow Fat and Hematopoiesis. *Frontiers in endocrinology* **9**, 694, doi:10.3389/fendo.2018.00694 (2018).
138. Muruganandan, S. & Sinal, C. J. The impact of bone marrow adipocytes on osteoblast and osteoclast differentiation. *IUBMB life* **66**, 147-155, doi:10.1002/iub.1254 (2014).

139. Sen, B. *et al.* β -Catenin Preserves the Stem State of Murine Bone Marrow Stromal Cells Through Activation of EZH2. *Journal of Bone and Mineral Research* **35**, 1149-1162, doi:10.1002/jbmr.3975 (2020).
140. Farmer, S. R. Regulation of PPAR γ activity during adipogenesis. *International journal of obesity (2005)* **29 Suppl 1**, S13-16, doi:10.1038/sj.ijo.0802907 (2005).
141. Tolwinski, N. S. & Wieschaus, E. A nuclear function for armadillo/beta-catenin. *PLoS biology* **2**, E95, doi:10.1371/journal.pbio.0020095 (2004).
142. Case, N. *et al.* Mechanical activation of β -catenin regulates phenotype in adult murine marrow-derived mesenchymal stem cells. *Journal of Orthopaedic Research* **28**, 1531-1538, doi:10.1002/jor.21156 (2010).
143. Yoshigi, M., Hoffman, L. M., Jensen, C. C., Yost, H. J. & Beckerle, M. C. Mechanical force mobilizes zyxin from focal adhesions to actin filaments and regulates cytoskeletal reinforcement. *The Journal of Cell Biology* **171**, 209-215, doi:10.1083/jcb.200505018 (2005).
144. Hu, S. H., Chen, J. X., Butler, J. P. & Wang, N. Prestress mediates force propagation into the nucleus. *Biochemical and Biophysical Research Communications* **329**, 423-428, doi:10.1016/j.bbrc.2005.02.026 (2005).
145. Hotulainen, P. & Lappalainen, P. Stress fibers are generated by two distinct actin assembly mechanisms in motile cells. *J Cell Biol* **173**, 383-394, doi:10.1083/jcb.200511093 (2006).
146. Hirata, H., Tatsumi, H. & Sokabe, M. Mechanical forces facilitate actin polymerization at focal adhesions in a zyxin-dependent manner. *Journal of cell science* **121**, 2795-2804, doi:10.1242/jcs.030320 (2008).
147. Blanchoin, L., Boujemaa-Paterski, R., Sykes, C. & Plastino, J. Actin Dynamics, Architecture, and Mechanics in Cell Motility. *Physiological Reviews* **94**, 235-263, doi:10.1152/physrev.00018.2013 (2014).

148. Kutscheidt, S. *et al.* FHOD1 interaction with nesprin-2G mediates TAN line formation and nuclear movement. *Nat Cell Biol* **16**, 708-715, doi:10.1038/ncb2981 (2014).
149. Hwang, J. H. *et al.* Nanotopological plate stimulates osteogenic differentiation through TAZ activation. *Sci Rep* **7**, 3632, doi:10.1038/s41598-017-03815-5 (2017).
150. Liu, R. & Ding, J. Chromosomal Repositioning and Gene Regulation of Cells on a Micropillar Array. *ACS applied materials & interfaces* **12**, 35799-35812, doi:10.1021/acsami.0c05883 (2020).
151. Arnsdorf, E. J., Tummala, P., Kwon, R. Y. & Jacobs, C. R. Mechanically induced osteogenic differentiation - the role of RhoA, ROCKII and cytoskeletal dynamics. *Journal of cell science* **122**, 546-553, doi:10.1242/jcs.036293 (2009).
152. McBeath, R., Pirone, D. M., Nelson, C. M., Bhadriraju, K. & Chen, C. S. Cell shape, cytoskeletal tension, and RhoA regulate stem cell lineage commitment. *Developmental cell* **6**, 483-495, doi:10.1016/s1534-5807(04)00075-9 (2004).
153. Chen, L., Hu, H., Qiu, W., Shi, K. & Kassem, M. Actin depolymerization enhances adipogenic differentiation in human stromal stem cells. *Stem cell research* **29**, 76-83, doi:10.1016/j.scr.2018.03.010 (2018).
154. Swift, J. *et al.* Nuclear lamin-A scales with tissue stiffness and enhances matrix-directed differentiation. *Science (New York, N.Y.)* **341**, 1240104, doi:10.1126/science.1240104 (2013).
155. Hwang, J. H. *et al.* Extracellular Matrix Stiffness Regulates Osteogenic Differentiation through MAPK Activation. *PloS one* **10**, e0135519, doi:10.1371/journal.pone.0135519 (2015).
156. Crisp, M. *et al.* Coupling of the nucleus and cytoplasm: role of the LINC complex. *The Journal of Cell Biology* **172**, 41-53, doi:10.1083/jcb.200509124 (2006).

157. Padmakumar, V. C. *et al.* The inner nuclear membrane protein Sun1 mediates the anchorage of Nesprin-2 to the nuclear envelope. *Journal of Cell Science* **118**, 3419-3430, doi:10.1242/jcs.02471 (2005).
158. Luxton, G. W., Gomes, E. R., Folker, E. S., Worman, H. J. & Gundersen, G. G. TAN lines: a novel nuclear envelope structure involved in nuclear positioning. *Nucleus (Austin, Tex.)* **2**, 173-181, doi:10.4161/nucl.2.3.16243 (2011).
159. Burridge, K. & Guilly, C. Focal adhesions, stress fibers and mechanical tension. *Experimental cell research* **343**, 14-20, doi:10.1016/j.yexcr.2015.10.029 (2016).
160. Katsumi, A., Orr, A. W., Tzima, E. & Schwartz, M. A. Integrins in mechanotransduction. *Journal of Biological Chemistry* **279**, 12001-12004, doi:10.1074/jbc.R300038200 (2004).
161. Thompson, W. R., Rubin, C. T. & Rubin, J. Mechanical regulation of signaling pathways in bone. *Gene* **503**, 179-193, doi:10.1016/j.gene.2012.04.076 (2012).
162. Schaller, M. D. The focal adhesion kinase. *Journal of Endocrinology* **150**, 1-7, doi:10.1677/joe.0.1500001 (1996).
163. Tamkun, J. W. *et al.* Structure of integrin, a glycoprotein involved in the transmembrane linkage between fibronectin and actin. *Cell* **46**, 271-282 (1986).
164. del Rio, A. *et al.* Stretching single talin rod molecules activates vinculin binding. *Science* **323**, 638-641, doi:10.1126/science.1162912 (2009).
165. Subauste, M. C. *et al.* Vinculin modulation of paxillin-FAK interactions regulates ERK to control survival and motility. *The Journal of Cell Biology* **165**, 371-381, doi:10.1083/jcb.200308011 (2004).
166. Sawada, Y. *et al.* Force sensing by mechanical extension of the Src family kinase substrate p130Cas. *Cell* **127**, 1015-1026, doi:10.1016/j.cell.2006.09.044 (2006).
167. Gallant, N. D., Michael, K. E. & Garcia, A. J. Cell adhesion strengthening: contributions of adhesive area, integrin binding, and focal adhesion assembly. *Mol Biol Cell* **16**, 4329-4340, doi:10.1091/mbc.e05-02-0170 (2005).

168. Engler, A. J., Sen, S., Sweeney, H. L. & Discher, D. E. Matrix elasticity directs stem cell lineage specification. *Cell* **126**, 677-689, doi:10.1016/j.cell.2006.06.044 (2006).
169. Zhang, P., Wu, Y., Jiang, Z., Jiang, L. & Fang, B. Osteogenic response of mesenchymal stem cells to continuous mechanical strain is dependent on ERK1/2-Runx2 signaling. *International journal of molecular medicine* **29**, 1083-1089, doi:10.3892/ijmm.2012.934 (2012).
170. Thompson, W. R. *et al.* Mechanically activated Fyn utilizes mTORC2 to regulate RhoA and adipogenesis in mesenchymal stem cells. *Stem cells* **31**, 2528-2537, doi:10.1002/stem.1476 (2013).
171. Case, N. *et al.* Mechanical regulation of glycogen synthase kinase 3beta (GSK3beta) in mesenchymal stem cells is dependent on Akt protein serine 473 phosphorylation via mTORC2 protein. *The Journal of biological chemistry* **286**, 39450-39456, doi:10.1074/jbc.M111.265330 (2011).
172. Burridge, K. & Wennerberg, K. Rho and Rac take center stage. *Cell* **116**, 167-179 (2004).
173. Bos, J. L., Rehmann, H. & Wittinghofer, A. GEFs and GAPs: critical elements in the control of small G proteins. *Cell* **129**, 865-877, doi:10.1016/j.cell.2007.05.018 (2007).
174. Patel, V. S. *et al.* Incorporating Refractory Period in Mechanical Stimulation Mitigates Obesity-Induced Adipose Tissue Dysfunction in Adult Mice. *Obesity (Silver Spring)* **25**, 1745-1753, doi:10.1002/oby.21958 (2017).
175. Machesky, L. M. & Insall, R. H. Scar1 and the related Wiskott–Aldrich syndrome protein, WASP, regulate the actin cytoskeleton through the Arp2/3 complex. *Current Biology* **8**, 1347-1356 (1998).
176. Machesky, L. M. *et al.* Scar, a WASp-related protein, activates nucleation of actin filaments by the Arp2/3 complex. *Proceedings of the National Academy of Sciences of the United States of America* **96**, 3739-3744, doi:10.1073/pnas.96.7.3739 (1999).

177. Rohatgi, R., Nollau, P., Ho, H.-Y. H., Kirschner, M. W. & Mayer, B. J. Nck and Phosphatidylinositol 4,5-Bisphosphate Synergistically Activate Actin Polymerization through the N-WASP-Arp2/3 Pathway. *Journal of Biological Chemistry* **276**, 26448-26452, doi:10.1074/jbc.M103856200 (2001).
178. Marchand, J.-B., Kaiser, D. A., Pollard, T. D. & Higgs, H. N. Interaction of WASP/Scar proteins with actin and vertebrate Arp2/3 complex. *Nature cell biology* **3**, 76-82, doi:http://www.nature.com/ncb/journal/v3/n1/supinfo/ncb0101_76_S1.html (2001).
179. Mullins, R. D., Heuser, J. A. & Pollard, T. D. The interaction of Arp2/3 complex with actin: Nucleation, high affinity pointed end capping, and formation of branching networks of filaments. *Proceedings of the National Academy of Sciences* **95**, 6181-6186 (1998).
180. Jaffe, A. B. & Hall, A. Rho GTPases: Biochemistry and Biology. *Annual Review of Cell & Developmental Biology* **21**, 247-269, doi:10.1146/annurev.cellbio.21.020604.150721 (2005).
181. Riddick, N., Ohtani, K. & Surks, H. K. Targeting by myosin phosphatase-RhoA interacting protein mediates RhoA/ROCK regulation of myosin phosphatase. *Journal of Cellular Biochemistry* **103**, 1158-1170, doi:10.1002/jcb.21488 (2008).
182. Khatiwala, C. B., Kim, P. D., Peyton, S. R. & Putnam, A. J. ECM Compliance Regulates Osteogenesis by Influencing MAPK Signaling Downstream of RhoA and ROCK. *Journal of Bone and Mineral Research* **24**, 886-898, doi:10.1359/jbmr.081240 (2009).
183. Horikawa, A., Okada, K., Sato, K. & Sato, M. Morphological changes in osteoblastic cells (MC3T3-E1) due to fluid shear stress: Cellular damage by prolonged application of fluid shear stress. *Tohoku Journal of Experimental Medicine* **191**, 127-137, doi:10.1620/tjem.191.127 (2000).

184. Greiner, A. M., Chen, H., Spatz, J. P. & Kemkemer, R. Cyclic Tensile Strain Controls Cell Shape and Directs Actin Stress Fiber Formation and Focal Adhesion Alignment in Spreading Cells. *PLoS ONE* **8**, e77328, doi:10.1371/journal.pone.0077328 (2013).
185. Chancellor, T. J., Lee, J., Thodeti, C. K. & Lele, T. Actomyosin Tension Exerted on the Nucleus through Nesprin-1 Connections Influences Endothelial Cell Adhesion, Migration, and Cyclic Strain-Induced Reorientation. *Biophysical journal* **99**, 115-123 (2010).
186. Uzer, G., Pongkitwitoon, S., Ete Chan, M. & Judex, S. Vibration induced osteogenic commitment of mesenchymal stem cells is enhanced by cytoskeletal remodeling but not fluid shear. *Journal of biomechanics* **46**, 2296-2302, doi:10.1016/j.jbiomech.2013.06.008 (2013).
187. Ingber, D. E., Wang, N. & Stamenovic, D. Tensegrity, cellular biophysics, and the mechanics of living systems. *Rep Prog Phys* **77**, 046603, doi:10.1088/0034-4885/77/4/046603 (2014).
188. Cooper, L. F., Harris, C. T., Bruder, S. P., Kowalski, R. & Kadiyala, S. Incipient Analysis of Mesenchymal Stem-cell-derived Osteogenesis. *Journal of Dental Research* **80**, 314-320, doi:10.1177/00220345010800010401 (2001).
189. Wang, N., Butler, J. P. & Ingber, D. E. Mechanotransduction Across the Cell-surface and Through the Cytoskeleton. *Science (New York, N.Y.)* **260**, 1124-1127, doi:10.1126/science.7684161 (1993).
190. McGarry, J. G. & Prendergast, P. J. A three-dimensional finite element model of an adherent eukaryotic cell. *European cells & materials* **7**, 27-33; discussion 33-24 (2004).
191. Wang, X. & Ha, T. Defining Single Molecular Forces Required to Activate Integrin and Notch Signaling. *Science (New York, N.Y.)* **340**, 991-994, doi:10.1126/science.1231041 (2013).

192. Nagayama, K., Yamazaki, S., Yahiro, Y. & Matsumoto, T. Estimation of the mechanical connection between apical stress fibers and the nucleus in vascular smooth muscle cells cultured on a substrate. *Journal of biomechanics*, doi:<http://dx.doi.org/10.1016/j.jbiomech.2014.01.042> (2014).
193. Smith, M. A. *et al.* A Zyxin-Mediated Mechanism for Actin Stress Fiber Maintenance and Repair. *Developmental Cell* **19**, 365-376, doi:<http://dx.doi.org/10.1016/j.devcel.2010.08.008> (2010).
194. Reinhard, M. *et al.* An α -Actinin Binding Site of Zyxin Is Essential for Subcellular Zyxin Localization and α -Actinin Recruitment. *Journal of Biological Chemistry* **274**, 13410-13418, doi:10.1074/jbc.274.19.13410 (1999).
195. Smith, M., Blankman, E., Deakin, N. O., Hoffman, L. M. & Jensen, C. C. LIM domains target actin regulators paxillin and zyxin to sites of stress fiber strain. *PLoS one* **8**, e69378, doi:10.1371/journal.pone.0069378 (2013).
196. Flitney, E. W., Kuczmarski, E. R., Adam, S. A. & Goldman, R. D. Insights into the mechanical properties of epithelial cells: the effects of shear stress on the assembly and remodeling of keratin intermediate filaments. *The FASEB Journal* **23**, 2110-2119, doi:10.1096/fj.08-124453 (2009).
197. Maniotis, A. J., Chen, C. S. & Ingber, D. E. Demonstration of mechanical connections between integrins cytoskeletal filaments, and nucleoplasm that stabilize nuclear structure. *Proceedings of the National Academy of Sciences of the United States of America* **94**, 849-854 (1997).
198. Brangwynne, C. P. *et al.* Microtubules can bear enhanced compressive loads in living cells because of lateral reinforcement. *The Journal of Cell Biology* **173**, 733-741, doi:10.1083/jcb.200601060 (2006).
199. Odde, D. J., Ma, L., Briggs, A. H., DeMarco, A. & Kirschner, M. W. Microtubule bending and breaking in living fibroblast cells. *Journal of cell science* **112**, 3283-3288 (1999).
200. Ingber, D. E. Tensegrity: The architectural basis of cellular mechanotransduction. *Annual Review of Physiology* **59**, 575-599 (1997).

201. McGarry, J. G., Klein-Nulend, J. & Prendergast, P. J. The effect of cytoskeletal disruption on pulsatile fluid flow-induced nitric oxide and prostaglandin E2 release in osteocytes and osteoblasts. *Biochemical and Biophysical Research Communications* **330**, 341-348, doi:DOI: 10.1016/j.bbrc.2005.02.175 (2005).
202. Norvell, S. M., Ponik, S. M., Bowen, D. K., Gerard, R. & Pavalko, F. M. Fluid shear stress induction of COX-2 protein and prostaglandin release in cultured MC3T3-E1 osteoblasts does not require intact microfilaments or microtubules. *Journal of Applied Physiology* **96**, 957-966, doi:10.1152/jappphysiol.00869.2003 (2004).
203. De Magistris, P. & Antonin, W. The Dynamic Nature of the Nuclear Envelope. *Current biology : CB* **28**, R487-r497, doi:10.1016/j.cub.2018.01.073 (2018).
204. Rubin, J., Styner, M. & Uzer, G. Physical Signals May Affect Mesenchymal Stem Cell Differentiation via Epigenetic Controls. *Exercise and sport sciences reviews* **46**, 42-47, doi:10.1249/jes.0000000000000129 (2018).
205. Ketema, M. & Sonnenberg, A. Nesprin-3: a versatile connector between the nucleus and the cytoskeleton. *Biochemical Society Transactions* **39**, 1719-1724, doi:10.1042/bst20110669 (2011).
206. Padmakumar, V. C. *et al.* Enaptin, a giant actin-binding protein, is an element of the nuclear membrane and the actin cytoskeleton. *Experimental cell research* **295**, 330-339, doi:<http://dx.doi.org/10.1016/j.yexcr.2004.01.014> (2004).
207. Zhen, Y.-Y., Libotte, T., Munck, M., Noegel, A. A. & Korenbaum, E. NUANCE, a giant protein connecting the nucleus and actin cytoskeleton. *Journal of cell science* **115**, 3207-3222 (2002).
208. Wilson, M. H. & Holzbaur, E. L. Nesprins anchor kinesin-1 motors to the nucleus to drive nuclear distribution in muscle cells. *Development (Cambridge, England)* **142**, 218-228, doi:10.1242/dev.114769 (2015).
209. Roux, K. J. *et al.* Nesprin 4 is an outer nuclear membrane protein that can induce kinesin-mediated cell polarization. *Proceedings of the National Academy of Sciences* **106**, 2194-2199, doi:10.1073/pnas.0808602106 (2009).

210. Simpson, J. G. & Roberts, R. G. Patterns of evolutionary conservation in the nesprin genes highlight probable functionally important protein domains and isoforms. *Biochemical Society Transactions* **36**, 1359-1367, doi:10.1042/bst0361359 (2008).
211. Autore, F. *et al.* Large-Scale Modelling of the Divergent Spectrin Repeats in Nesprins: Giant Modular Proteins. *PLoS ONE* **8**, e63633, doi:10.1371/journal.pone.0063633 (2013).
212. Antoku, S. & Gundersen, G. G. Analysis of Nesprin-2 Interaction with Its Binding Partners and Actin. *Methods Mol Biol* **1840**, 35-43, doi:10.1007/978-1-4939-8691-0_4 (2018).
213. Arsenovic, P. T. *et al.* Nesprin-2G, a Component of the Nuclear LINC Complex, Is Subject to Myosin-Dependent Tension. *Biophysical journal* **110**, 34-43, doi:10.1016/j.bpj.2015.11.014 (2016).
214. Lu, W. *et al.* Nesprin interchain associations control nuclear size. *Cellular and Molecular Life Sciences* **69**, 3493-3509, doi:10.1007/s00018-012-1034-1 (2012).
215. Duong, N. T. *et al.* Nesprins: Tissue-Specific Expression of Epsilon and Other Short Isoforms. *PLoS ONE* **9**, e94380, doi:10.1371/journal.pone.0094380 (2014).
216. Rajgor, D., Mellad, J. A., Autore, F., Zhang, Q. & Shanahan, C. M. Multiple Novel Nesprin-1 and Nesprin-2 Variants Act as Versatile Tissue-Specific Intracellular Scaffolds. *PLoS ONE* **7**, e40098, doi:10.1371/journal.pone.0040098 (2012).
217. Starr, D. A. & Han, M. Role of ANC-1 in tethering nuclei to the actin cytoskeleton. *Science (New York, N.Y.)* **298**, 406-409, doi:10.1126/science.1075119 (2002).
218. Dreger, M., Bengtsson, L., Schöneberg, T., Otto, H. & Hucho, F. Nuclear envelope proteomics: Novel integral membrane proteins of the inner nuclear membrane. *Proceedings of the National Academy of Sciences* **98**, 11943-11948, doi:10.1073/pnas.211201898 (2001).

219. Hodzic, D. M., Yeater, D. B., Bengtsson, L., Otto, H. & Stahl, P. D. Sun2 Is a Novel Mammalian Inner Nuclear Membrane Protein. *Journal of Biological Chemistry* **279**, 25805-25812, doi:10.1074/jbc.M313157200 (2004).
220. Sosa, B. A., Kutay, U. & Schwartz, T. U. Structural insights into LINC complexes. *Curr Opin Struct Biol* **23**, 285-291, doi:10.1016/j.sbi.2013.03.005 (2013).
221. Cain, N. E. & Starr, D. A. SUN proteins and nuclear envelope spacing. *Nucleus (Austin, Tex.)* **6**, 2-7, doi:10.4161/19491034.2014.990857 (2015).
222. Cain, N. E., Tapley, E. C., McDonald, K. L., Cain, B. M. & Starr, D. A. The SUN protein UNC-84 is required only in force-bearing cells to maintain nuclear envelope architecture. *J Cell Biol* **206**, 163-172, doi:10.1083/jcb.201405081 (2014).
223. Sosa, B. A., Rothballer, A., Kutay, U. & Schwartz, T. U. LINC Complexes Form by Binding of Three KASH Peptides to the Interfaces of Trimeric SUN proteins. *Cell* **149**, 1035-1047, doi:10.1016/j.cell.2012.03.046 (2012).
224. Liu, Q. *et al.* Functional association of Sun1 with nuclear pore complexes. *J Cell Biol* **178**, 785-798, doi:10.1083/jcb.200704108 (2007).
225. Link, J. *et al.* Analysis of Meiosis in SUN1 Deficient Mice Reveals a Distinct Role of SUN2 in Mammalian Meiotic LINC Complex Formation and Function. *PLoS Genet* **10**, e1004099, doi:10.1371/journal.pgen.1004099 (2014).
226. Chang, W. *et al.* Imbalanced nucleocytoskeletal connections create common polarity defects in progeria and physiological aging. *Proceedings of the National Academy of Sciences of the United States of America* **116**, 3578-3583, doi:10.1073/pnas.1809683116 (2019).
227. Sen, B. *et al.* Mechanical Strain Inhibits Adipogenesis in Mesenchymal Stem Cells by Stimulating a Durable beta-Catenin Signal. *Endocrinology* **149**, 6065-6075, doi:10.1210/en.2008-0687 (2008).

228. Codelia, Veronica A., Sun, G. & Irvine, Kenneth D. Regulation of YAP by Mechanical Strain through Jnk and Hippo Signaling. *Current Biology* **24**, 2012-2017, doi:<http://dx.doi.org/10.1016/j.cub.2014.07.034> (2014).
229. Koike, M. *et al.* β -Catenin Shows an Overlapping Sequence Requirement but Distinct Molecular Interactions for Its Bidirectional Passage through Nuclear Pores. *Journal of Biological Chemistry* **279**, 34038-34047, doi:10.1074/jbc.M405821200 (2004).
230. Neumann, S. *et al.* Nesprin-2 Interacts with α -Catenin and Regulates Wnt Signaling at the Nuclear Envelope. *Journal of Biological Chemistry* **285**, 34932-34938, doi:10.1074/jbc.M110.119651 (2010).
231. Uzer, G. *et al.* Sun-mediated mechanical LINC between nucleus and cytoskeleton regulates β catenin nuclear access. *Journal of biomechanics* **74**, 32-40, doi:<https://doi.org/10.1016/j.jbiomech.2018.04.013> (2018).
232. Horn, H. F. *et al.* The LINC complex is essential for hearing. *The Journal of Clinical Investigation* **123**, 740-750, doi:10.1172/JCI66911 (2013).
233. Rubin, C., Turner, A. S., Bain, S., Mallinckrodt, C. & McLeod, K. Anabolism. Low mechanical signals strengthen long bones. *Nature* **412**, 603-604, doi:10.1038/35088122 (2001).
234. Gilsanz, V. *et al.* Low-Level, High-Frequency Mechanical Signals Enhance Musculoskeletal Development of Young Women With Low BMD. *Journal of Bone and Mineral Research* **21**, 1464-1474, doi:10.1359/jbmr.060612 (2006).
235. Sen, B. *et al.* mTORC2 Regulates Mechanically Induced Cytoskeletal Reorganization and Lineage Selection in Marrow-Derived Mesenchymal Stem Cells. *Journal of Bone and Mineral Research* **29**, 78-89, doi:10.1002/jbmr.2031 (2014).
236. Graham, D. M. *et al.* Enucleated cells reveal differential roles of the nucleus in cell migration, polarity, and mechanotransduction. *J Cell Biol* **217**, 895-914, doi:10.1083/jcb.201706097 (2018).

237. Lombardi, M. L. *et al.* The Interaction between Nesprins and Sun Proteins at the Nuclear Envelope Is Critical for Force Transmission between the Nucleus and Cytoskeleton. *Journal of Biological Chemistry* **286**, 26743-26753, doi:10.1074/jbc.M111.233700 (2011).
238. Banerjee, I. *et al.* Targeted Ablation of Nesprin 1 and Nesprin 2 from Murine Myocardium Results in Cardiomyopathy, Altered Nuclear Morphology and Inhibition of the Biomechanical Gene Response. *PLoS Genet* **10**, e1004114, doi:10.1371/journal.pgen.1004114 (2014).
239. Touchstone, H. *et al.* Recovery of stem cell proliferation by low intensity vibration under simulated microgravity requires intact LINC complex *npj. Microgravity* *in press (2019).
240. Pongkitwitoon, S., Uzer, G., Rubin, J. & Judex, S. Cytoskeletal Configuration Modulates Mechanically Induced Changes in Mesenchymal Stem Cell Osteogenesis, Morphology, and Stiffness. *Scientific reports* **6**, 34791, doi:10.1038/srep34791 (2016).
241. Manilal, S., Man, N. t., Sewry, C. A. & Morris, G. E. The Emery-Dreifuss Muscular Dystrophy Protein, Emerin, is a Nuclear Membrane Protein. *Human molecular genetics* **5**, 801-808, doi:10.1093/hmg/5.6.801 (1996).
242. Holaska, J. M., Kowalski, A. K. & Wilson, K. L. Emerin caps the pointed end of actin filaments: evidence for an actin cortical network at the nuclear inner membrane. *PLoS biology* **2**, E231, doi:10.1371/journal.pbio.0020231 (2004).
243. Le, H. Q. *et al.* Mechanical regulation of transcription controls Polycomb-mediated gene silencing during lineage commitment. *Nature cell biology* **18**, 864-875, doi:10.1038/ncb3387 (2016).
244. Stubenvoll, A., Rice, M., Wietelmann, A., Wheeler, M. & Braun, T. Attenuation of Wnt/beta-catenin activity reverses enhanced generation of cardiomyocytes and cardiac defects caused by the loss of emerin. *Human molecular genetics* **24**, 802-813, doi:10.1093/hmg/ddu498 (2015).

245. Tilgner, K., Wojciechowicz, K., Jahoda, C., Hutchison, C. & Markiewicz, E. Dynamic complexes of A-type lamins and emerin influence adipogenic capacity of the cell via nucleocytoplasmic distribution of β -catenin. *Journal of cell science* **122**, 401-413, doi:10.1242/jcs.026179 (2009).
246. Markiewicz, E. *et al.* The inner nuclear membrane protein Emerin regulates [beta]-catenin activity by restricting its accumulation in the nucleus. *EMBO J* **25**, 3275-3285, doi:http://www.nature.com/emboj/journal/v25/n14/suppinfo/7601230a_S1.html (2006).
247. Guilluy, C. *et al.* Isolated nuclei adapt to force and reveal a mechanotransduction pathway in the nucleus. *Nature cell biology* **16**, 376-381, doi:10.1038/ncb2927 (2014).
248. Tanabe, L. M., Kim, C. E., Alagem, N. & Dauer, W. T. Primary dystonia: molecules and mechanisms. *Nat Rev Neurol* **5**, 598-609 (2009).
249. Jungwirth, M., Kumar, D., Jeong, D. & Goodchild, R. The nuclear envelope localization of DYT1 dystonia torsinA-DeltaE requires the SUN1 LINC complex component. *BMC Cell Biology* **12**, 24 (2011).
250. Nery, F. C. *et al.* TorsinA binds the KASH domain of nesprins and participates in linkage between nuclear envelope and cytoskeleton. *Journal of cell science* **121**, 3476-3486, doi:10.1242/jcs.029454 (2008).
251. Sosa, B. A. *et al.* How lamina-associated polypeptide 1 (LAP1) activates Torsin. *Elife* **3**, e03239, doi:10.7554/eLife.03239 (2014).
252. Shin, J. Y. *et al.* Lamina-associated polypeptide-1 interacts with the muscular dystrophy protein emerin and is essential for skeletal muscle maintenance. *Dev Cell* **26**, 591-603, doi:10.1016/j.devcel.2013.08.012 (2013).
253. Saunders, C. A. *et al.* TorsinA controls TAN line assembly and the retrograde flow of dorsal perinuclear actin cables during rearward nuclear movement. *J Cell Biol* **216**, 657-674, doi:10.1083/jcb.201507113 (2017).

254. Cook, P. R. The nucleoskeleton: artefact, passive framework or active site? *Journal of cell science* **90** (Pt 1), 1-6 (1988).
255. Grosse, R. & Vartiainen, M. K. To be or not to be assembled: progressing into nuclear actin filaments. *Nature reviews. Molecular cell biology* **14**, 693-697, doi:10.1038/nrm3681 (2013).
256. Baarlink, C., Wang, H. & Grosse, R. Nuclear actin network assembly by formins regulates the SRF coactivator MAL. *Science (New York, N.Y.)* **340**, 864-867, doi:10.1126/science.1235038 (2013).
257. Belin, B. J., Cimini, B. A., Blackburn, E. H. & Mullins, R. D. Visualization of actin filaments and monomers in somatic cell nuclei. *Molecular biology of the cell* **24**, 982-994, doi:10.1091/mbc.E12-09-0685 (2013).
258. Munsie, L. N., Desmond, C. R. & Truant, R. Cofilin nuclear-cytoplasmic shuttling affects cofilin-actin rod formation during stress. *Journal of cell science* **125**, 3977-3988, doi:10.1242/jcs.097667 (2012).
259. Plessner, M., Melak, M., Chinchilla, P., Baarlink, C. & Grosse, R. Nuclear F-actin formation and reorganization upon cell spreading. *J Biol Chem* **290**, 11209-11216, doi:10.1074/jbc.M114.627166 (2015).
260. Sen, B. *et al.* Intranuclear Actin Regulates Osteogenesis. *Stem Cells*, doi:10.1002/stem.2090 (2015).
261. Samsonraj, R. M. *et al.* Validation of Osteogenic Properties of Cytochalasin D by High-Resolution RNA-Sequencing in Mesenchymal Stem Cells Derived from Bone Marrow and Adipose Tissues. *Stem cells and development*, doi:10.1089/scd.2018.0037 (2018).
262. Serebryanny, L. A. *et al.* Persistent nuclear actin filaments inhibit transcription by RNA polymerase II. *Journal of cell science* **129**, 3412-3425, doi:10.1242/jcs.195867 (2016).
263. Zhu, X., Zeng, X., Huang, B. & Hao, S. Actin is closely associated with RNA polymerase II and involved in activation of gene transcription. *Biochemical and biophysical research communications* **321**, 623-630 (2004).

264. Spichal, M. *et al.* Evidence for a dual role of actin in regulating chromosome organization and dynamics in yeast. *Journal of cell science* **129**, 681-692, doi:10.1242/jcs.175745 (2016).
265. Crabbe, L., Cesare, A. J., Kasuboski, J. M., Fitzpatrick, J. A. & Karlseder, J. Human telomeres are tethered to the nuclear envelope during postmitotic nuclear assembly. *Cell reports* **2**, 1521-1529, doi:10.1016/j.celrep.2012.11.019 (2012).
266. Czapiewski, R., Robson, M. I. & Schirmer, E. C. Anchoring a Leviathan: How the Nuclear Membrane Tethers the Genome. *Frontiers in genetics* **7**, 82, doi:10.3389/fgene.2016.00082 (2016).
267. Lottersberger, F., Karssemeijer, R. A., Dimitrova, N. & de Lange, T. 53BP1 and the LINC Complex Promote Microtubule-Dependent DSB Mobility and DNA Repair. *Cell* **163**, 880-893, doi:10.1016/j.cell.2015.09.057 (2015).
268. Oshidari, R. *et al.* Nuclear microtubule filaments mediate non-linear directional motion of chromatin and promote DNA repair. *Nature communications* **9**, 2567, doi:10.1038/s41467-018-05009-7 (2018).
269. Schreiber, Katherine H. & Kennedy, Brian K. When Lamins Go Bad: Nuclear Structure and Disease. *Cell* **152**, 1365-1375, doi:10.1016/j.cell.2013.02.015 (2013).
270. Eckersley-Maslin, M. A., Bergmann, J. H., Lazar, Z. & Spector, D. L. Lamin A/C is expressed in pluripotent mouse embryonic stem cells. *Nucleus (Austin, Tex.)* **4**, 53-60, doi:10.4161/nucl.23384 (2013).
271. Lammerding, J. *et al.* Lamins A and C but Not Lamin B1 Regulate Nuclear Mechanics. *Journal of Biological Chemistry* **281**, 25768-25780, doi:10.1074/jbc.M513511200 (2006).
272. Swift, J. *et al.* Nuclear Lamin-A Scales with Tissue Stiffness and Enhances Matrix-Directed Differentiation. *Science (New York, N.Y.)* **341**, doi:10.1126/science.1240104 (2013).

273. Buxboim, A. *et al.* Matrix elasticity regulates lamin-A,C phosphorylation and turnover with feedback to actomyosin. *Current biology : CB* **24**, 1909-1917, doi:10.1016/j.cub.2014.07.001 (2014).
274. Verstraeten, V. L. R. M., Ji, J. Y., Cummings, K. S., Lee, R. T. & Lammerding, J. Increased mechanosensitivity and nuclear stiffness in Hutchinson–Gilford progeria cells: effects of farnesyltransferase inhibitors. *Aging Cell* **7**, 383-393, doi:10.1111/j.1474-9726.2008.00382.x (2008).
275. Gaspar-Maia, A., Alajem, A., Meshorer, E. & Ramalho-Santos, M. Open chromatin in pluripotency and reprogramming. *Nat Rev Mol Cell Biol* **12**, 36-47 (2011).
276. Chiang, F. P. & Uzer, G. Mapping full field deformation of auxetic foams using digital speckle photography. *Physica Status Solidi B-Basic Solid State Physics* **245**, 2391-2394, doi:DOI 10.1002/pssb.200880254 (2008).
277. Pagliara, S. *et al.* Auxetic nuclei in embryonic stem cells exiting pluripotency. *Nat Mater* **13**, 638-644, doi:10.1038/nmat3943 (2014).
278. Matsumoto, A. *et al.* Global loss of a nuclear lamina component, lamin A/C, and LINC complex components SUN1, SUN2, and nesprin-2 in breast cancer. *Cancer Med*, doi:10.1002/cam4.495 (2015).
279. Liu, Q. *et al.* Dynamics of Lamin-A Processing Following Precursor Accumulation. *PLOS ONE* **5**, e10874, doi:10.1371/journal.pone.0010874 (2010).
280. Mounkes, L. C., Kozlov, S., Hernandez, L., Sullivan, T. & Stewart, C. L. A progeroid syndrome in mice is caused by defects in A-type lamins. *Nature* **423**, 298-301, doi:http://www.nature.com/nature/journal/v423/n6937/supinfo/nature01631_S1.html (2003).
281. Scaffidi, P. & Misteli, T. Lamin A-Dependent Nuclear Defects in Human Aging. *Science (New York, N.Y.)* **312**, 1059-1063, doi:10.1126/science.1127168 (2006).

282. Mulvihill, B. M. & Prendergast, P. J. An algorithm for bone mechanoresponsiveness: implementation to study the effect of patient-specific cell mechanosensitivity on trabecular bone loss. *Computer methods in biomechanics and biomedical engineering* **11**, 443-451, doi:10.1080/10255840802136150 (2008).
283. Hernandez, L. *et al.* Functional Coupling between the Extracellular Matrix and Nuclear Lamina by Wnt Signaling in Progeria. *Developmental Cell* **19**, 413-425, doi:<http://dx.doi.org/10.1016/j.devcel.2010.08.013> (2010).
284. Padiath, Q. S. *et al.* Lamin B1 duplications cause autosomal dominant leukodystrophy. *Nat Genet* **38**, 1114-1123, doi:10.1038/ng1872 (2006).
285. Hegele, R. A. *et al.* Sequencing of the reannotated LMNB2 gene reveals novel mutations in patients with acquired partial lipodystrophy. *Am J Hum Genet* **79**, 383-389, doi:10.1086/505885 (2006).
286. Osmanagic-Myers, S., Dechat, T. & Foisner, R. Lamins at the crossroads of mechanosignaling. *Genes & development* **29**, 225-237, doi:10.1101/gad.255968.114 (2015).
287. de Leeuw, R., Gruenbaum, Y. & Medalia, O. Nuclear Lamins: Thin Filaments with Major Functions. *Trends in cell biology* **28**, 34-45, doi:10.1016/j.tcb.2017.08.004 (2018).
288. Hozak, P., Sasseville, A. M., Raymond, Y. & Cook, P. R. Lamin proteins form an internal nucleoskeleton as well as a peripheral lamina in human cells. *Journal of cell science* **108 (Pt 2)**, 635-644 (1995).
289. Mattout-Drubezki, A. & Gruenbaum, Y. Dynamic interactions of nuclear lamina proteins with chromatin and transcriptional machinery. *Cellular and molecular life sciences : CMLS* **60**, 2053-2063, doi:10.1007/s00018-003-3038-3 (2003).
290. Solovei, I. *et al.* LBR and lamin A/C sequentially tether peripheral heterochromatin and inversely regulate differentiation. *Cell* **152**, 584-598, doi:10.1016/j.cell.2013.01.009 (2013).

291. Bode, J., Goetze, S., Heng, H., Krawetz, S. A. & Benham, C. From DNA structure to gene expression: mediators of nuclear compartmentalization and dynamics. *Chromosome research : an international journal on the molecular, supramolecular and evolutionary aspects of chromosome biology* **11**, 435-445 (2003).
292. Dahl, K. N., Engler, A. J., Pajerowski, J. D. & Discher, D. E. Power-Law Rheology of Isolated Nuclei with Deformation Mapping of Nuclear Substructures. *Biophysical journal* **89**, 2855-2864, doi:10.1529/biophysj.105.062554 (2005).
293. Ugarte, F. *et al.* Progressive Chromatin Condensation and H3K9 Methylation Regulate the Differentiation of Embryonic and Hematopoietic Stem Cells. *Stem Cell Reports* **5**, 728-740, doi:<https://doi.org/10.1016/j.stemcr.2015.09.009> (2015).
294. Dudakovic, A. *et al.* Epigenetic Control of Skeletal Development by the Histone Methyltransferase Ezh2. *Journal of Biological Chemistry* **290**, 27604-27617, doi:10.1074/jbc.M115.672345 (2015).
295. Pajerowski, J. D., Dahl, K. N., Zhong, F. L., Sammak, P. J. & Discher, D. E. Physical plasticity of the nucleus in stem cell differentiation. *Proceedings of the National Academy of Sciences of the United States of America* **104**, 15619-15624, doi:10.1073/pnas.0702576104 (2007).
296. Heo, S. J. *et al.* Biophysical Regulation of Chromatin Architecture Instills a Mechanical Memory in Mesenchymal Stem Cells. *Scientific reports* **5**, 16895, doi:10.1038/srep16895 (2015).
297. Poh, Y.-C. *et al.* Dynamic force-induced direct dissociation of protein complexes in a nuclear body in living cells. *Nature communications* **3**, 866, doi:http://www.nature.com/ncomms/journal/v3/n5/supinfo/ncomms1873_S1.html (2012).
298. Makhija, E., Jokhun, D. S. & Shivashankar, G. V. Nuclear deformability and telomere dynamics are regulated by cell geometric constraints. *Proceedings of the National Academy of Sciences of the United States of America* **113**, E32-40, doi:10.1073/pnas.1513189113 (2016).

APPENDIX**Mesenchymal Stem Cells as Mechanically Sensitive Cell Models**

As the smallest unit in the body, cells both sense and adapt to dynamic mechanical environments to drive tissue level adaptations. The type and intensity of forces to which cells are subjected depends on the tissue type and physiologic function. For example, myocytes, found in cardiac and skeletal muscles, are exposed to tensile and shear forces generated by sarcomeres that slide against each other within myofibrils¹²⁷. Endothelial cells, which line the inner layer of blood vessels, are subjected to pulsatile fluid shear stress as blood is pumped¹²⁸. The ability to adapt to the mechanical demands conveyed by these unique environments is best embodied in stem cells that can differentiate into a multitude of cell types based on physical environmental cues¹²⁹. Stem cells are multipotent cells that can self-renew and differentiate into terminally differentiated cell types of the tissues that they reside in. For example, mesenchymal stem cells (MSC) are subjected to oscillatory fluid shear as a result of deformation of bone during locomotion, guiding differentiation into osteocytes or chondrocytes which the lack of mechanical signals drives MSC fate towards adipocytes^{19,130,131}. Therefore, as stem cells replace and regenerate tissues by replenishing resident cell populations, they not only hold great therapeutic promise for tissue engineering and regenerative approaches, but also provide a robust model for studying how mechanical forces are sensed and adapt at the cellular level.

Clinical relevance of Nucleoskeleton in Mesenchymal Stem Cell function

Mutations of the nuclear proteins Lamin A/C have been linked to Hutchinson Gilford Progeria syndrome (HGPS), also known as progeria^{3,11,132}. Progeria is hallmarked by advanced aging, causing age related disease such as osteoporosis and cardiovascular diseases in affected people between the ages of 2-18 years old. As a result of progeria all

patients diagnosed with this disease do not survive past the age of 18 years old. Progeria, along with other diseases such as Emery–Dreyfuss muscular dystrophy, are the result of mutated Lamin A/C and are termed opathies. Laminopathies highlight the importance of MSCs as these diseases diminish the ability of MSCs to regulate differentiation, predisposing MSCs to accelerated aging and adipogenesis^{2,133-136}.

Mechanical Regulation of Adipogenesis in Mesenchymal Stem Cells

Residing in the bone marrow, mesenchymal stem cells (MSC) differentiate into chondrocytes, osteocytes, and adipocytes. In mammals the bone marrow is 70% fat tissue by volume, which bone marrow fat is comprised of the MSC derivative adipocytes¹³⁷. The role of bone marrow adipocytes has been linked to energy storage for hematopoietic cells and promotion of HSC proliferation through secretion of adiponectin and other adipocyte factors¹³⁷. However, the imbalance of adipocytes in the bone marrow has been linked to reduced bone mass associated with osteoporosis, diabetes, and aging¹³⁸. MSC differentiation towards adipocytes has been linked to overexpression of the transcription activator PPAR- γ and inhibition of β -Catenin nuclear localization^{19,117,138}. In MSCs translocation of cytosolic β -Catenin into the nucleus inhibits PPAR- γ and adipogenesis. Additionally, nuclear β -Catenin promotes proliferation and osteogenesis differentiation^{33,138-140}. However, GSK3 β complex degrades cytosolic β -Catenin which stops translocation of β -Catenin into the nucleus, inducing adipogenesis in MSCs^{19,140}. This degradation of β -Catenin via GSK3 β is halted by mechanical activation of focal adhesions. Activation of the cell membrane bound focal adhesions (FA) initiates Akt phosphorylation of GSK3 β , inhibiting GSK3 β and causing the release of β -Catenin from GSK3 β . β -Catenin is then translocated into the nucleus through association with nuclear

pore complexes, inhibiting PPAR- γ and activating proliferation transcription targets such as Myc, Axin2, and Cyclin D1 (Ccnd1) ¹³⁹⁻¹⁴².

Activation of FAs not only activate biomolecular signaling pathways like β -Catenin, but also increases formation of the actin cytoskeleton network and actin stress fibers ^{29,115,143-148}. Activation of focal adhesions induces the formation of actin stress fibers that both applies and transduces physical forces upon the nucleus altering nucleus orientation and shape, inhibiting adipogenesis and promoting osteogenesis in MSCs ^{21,115,145,149-151}. However, inhibition of actin cytoskeleton tension induces adipogenesis and inhibits osteogenesis, resulting in a spherical cell shape ^{152,153}. Re-introduction of actin tension and inducement of actin stress fibers inhibits adipogenesis and causes elongation of MSCs ^{21,29,152,153}. Activation of biomolecular signaling pathways and the actin cytoskeleton network at focal adhesions occurs through mechanical stimulation of MSCs. Mechanical stimulation of strain, low intensity vibration (LIV), and growth on stiff extracellular matrices activate FAs triggering mechanically induce biomolecular signaling pathways such as the Akt/ β -Catenin pathway, increasing actin cytoskeleton tension, and formation of actin stress fibers ^{18,19,30,154,155}. Mechanical activation of these FA pathways transduces the mechanical signal from the FA into the nucleus repressing adipogenesis. For these mechanically induced signals to enter the nucleus they first must be transferred through the Linker of the nucleoskeleton and cytoskeleton (LINC) complex located in the nuclear membrane.

The LINC complex spans the nuclear envelope and connects to intra-nuclear networks such as nuclear pore complexes (NPC) and the nuclear a. The LINC complex is comprised of the proteins: nesprin-1, nesprin-2, nesprin-3, nesprin-4, Sun1, and Sun2

^{53,135,156}. The LINC complex binds to F-actin via the N-termini of nesprin-1/2, connecting the actin cytoskeleton network to the nucleus. The Sun1 and Sun2 proteins have a C-terminal luminal domain that associates with the KASH domain of nesprin-1/2 in the perinuclear space, anchoring nesprin-1/2 to the outer nuclear membrane in the nuclear envelope ^{35,157}. The importance of the LINC complex can be seen during the depletion of Sun1/2 and nesprin-1/2. Inhibition of Sun1/2 and nesprin-1/2 inhibits translocation of the β -Catenin into the nucleus, nuclear orientation, centrosome orientation, and lack of mechanical suppression of adipogenesis ^{29,35,158}. Further research is required to understand the mechanism by which the loss of the LINC complex function impacts mechanical suppression of adipogenesis. Therefore, using the ability of MSCs to mechanically regulate adipogenesis we can further understand the impact of mechanical signals on the cell. However, to understand how mechanical signals are sensed in the cell, the underlying cellular and nuclear structures must be further explained as mechanical sensing in the cell occurs through its cytoskeletal proteins as well through the nuclear skeleton proteins.

Role of Cell Structure in Mechanical Sensing

Cellular mechanosensation is accomplished through a variety of structures and proteins that reside within the plasma membrane, the cytoskeleton, and the nucleus. Depending on the sensory element, mechanical signals are either converted into biochemical signaling cascades or directly transduced to inner cellular structures. This conversion of extracellular forces into intracellular signals is called mechanotransduction.

However, the process of mechanotransduction cannot be reduced to passive sensory functioning of these structures. As a functioning unit, cells adapt to alterations in

mechanical stress, resulting in remodeling of internal structures. In turn, these structural adaptations, provide another level of control by regulating the effectiveness of subsequent mechanotransduction events. In this way, maladaptation to mechanical stress is a common etiologic factor in many debilitating diseases. This chapter discusses the function of different sensing elements in cells. The major mechanotransduction pathways and signaling elements activated by these structures will also be discussed. When appropriate we will discuss how these cellular structures adapt to mechanical force in both health and disease. Our examples will focus on the influence of mechanical force on bone marrow mesenchymal stem cell (MSC) differentiation, as it relates to the osteogenic and adipogenic lineages. While stem cells in other tissue compartments are subjected to different mechanical environments, information presented in this chapter can be easily generalized to these stem cells and to other cell types.

Focal Adhesions

Located in the cellular membrane, focal adhesions (FAs) enable direct connections between the ECM and signaling effectors. FAs are made up of numerous proteins, forming mechanical signaling “platforms”¹⁵⁹. Central to the formation of these signaling platforms are integrins, which both bind to the extracellular matrix and enable initiation of intracellular signaling cascades.

Integrins are heterodimeric structures made up of α and β subunits, both of which contain small cytoplasmic domains¹⁶⁰. Integrin activation induces a conformational change in the β subunit, such as occurs following stretching of the matrix substrate. Integrin activation enables direct transmission of mechanical signals through the cell membrane, which results in recruitment of signaling adapters at the cytoplasmic regions

¹⁶⁰. These linker proteins contain both structural and biochemical functions, which further propagates mechanical signals through direct structural interactions with the cytoskeleton and by activating downstream signaling cascades ¹⁶¹. These adapter proteins include talin, paxillin, vinculin, p130Cas, and focal adhesion kinase (FAK). Talin and paxillin bind to FAK via the focal adhesion targeting sequence ¹⁶². Association of talin with the cytoplasmic tail of β integrins brings FAK to the FA complex¹⁶³. Additional adapter protein binding may be initiated by conformational changes in talin in response to mechanical force. These conformational changes are thought to unmask binding sites for adapter proteins ¹⁶⁴. Paxillin binds FAK and Src kinase ¹⁶⁵, while p130Cas enhances association of Src kinases with FAs following mechanical strain ¹⁶⁶. Src and FAK kinases not only initiate downstream signaling events but are also essential for the composition of the FA complex. In particular, accumulation of FAK at FA sites reinforces structure of the FA through integrin clustering ¹⁶². Importantly, the number of integrins is directly proportional to the strength of adhesion binding to the ECM ¹⁶⁷, a property that strongly influences MSC differentiation.

Lineage allocation of mesenchymal progenitors is strongly influenced by the stiffness of the underlying substrate ¹⁶⁸, which is directly related to FA attachment. Transmission of mechanical signals through integrin-based FAs, and the subsequent activation of intracellular signaling, directs the lineage fate of marrow-derived MSCs, partly through an increased number of FAs following mechanical input ²⁰. Mechanical force activates pathways that restrict adipogenesis while promoting osteogenic differentiation ³⁰. Extracellular regulated kinase (ERK1/2) is one such signal that promotes osteogenesis through activation of Runx2 ¹⁶⁹. Another distinctly regulated

pathway is initiated by recruitment of FAK and Fyn (a Src-like kinase) to FAs¹⁷⁰. Mechanical strain of MSCs enhanced the association of Fyn with vinculin at FAs, resulting in co-activation of FAK and Fyn through phosphorylation of tyrosines 397 and 418 respectively. FAK and Fyn were both necessary for mTORC2-dependent phosphorylation of Akt at serine 473. While, both pharmacological and siRNA-mediated knockdown confirmed that mTORC2 is necessary for Fyn/FAK activation of Akt, the regulatory sites of mTORC2 responsible for mechanical activation of Akt remain unclear. Importantly, mechanical force also recruits mTORC2 and Akt to FA sites, where it presumably is positioned to amplify additional mechanical input³¹.

Activation of mTORC2 in MSCs, by mechanical force, culminates in repression of adipogenesis through two distinct pathways, one through regulation of adipogenic genes and the other through enhancement of cytoskeletal structure, leading to increased cellular stiffness. In the former case, transcription of adipogenic genes is altered through nuclear translocation of GSK3 β . mTORC2-mediated activation of pAkt phosphorylates GSK3 β at serine 9, leading to inactivation and subsequent release of β -catenin from the proteasomal degradation complex¹⁷¹. Release of β -catenin from proteasomal targeting enables nuclear translocation, allowing for activation of LEF and TCF targeted transcription factors, or through direct repression of PPAR- γ activity, ultimately resulting in decreased adipogenesis¹⁴².

In addition to regulating adipogenic gene transcription via GSK3 β , mechanical activation of mTORC2 also influences actin cytoskeletal structure through activation of RhoA¹⁷⁰. Inhibition of both mTORC2 and Fyn resulted in abrogation of strain-induced actin stress fiber formation in MSCs, as well as increased adipogenic commitment^{31,170}.

Formation of actin stress fibers in response to mechanical force requires RhoA²⁰, a GTPase that organizes actin monomers into filamentous structures¹⁷². The on/off balance of RhoA is controlled by guanine nucleotide exchange factors (GEFs) and GTPase activating proteins (GAPs)¹⁷³. GEFs enable the exchange of GDP for GTP, resulting in activation of RhoA GTPase activity. Conversely, GAPs facilitate release of GTP from the active RhoA. This balance controls the formation of structural components of the actin cytoskeleton, which are particularly important in cell that rely on actin structures for motility, where the leading and lagging edges need to be dynamically remodeled. Juxtaposed to the on/off dynamics required for cell motility, mechanical forces imposed on the skeleton during exercise are delivered in a dynamic fashion. As such, GEFs and GAPs provide a means by which the cellular mechanostat can regulate the necessary stiffness of the cell to respond to additional mechanical stimuli, or to prepare for entry into the appropriate lineage programming. In MSCs, mechanical strain activates RhoA through a GEF called leukemia-associated Rho guanine nucleotide exchange factor (Larg)³². Knockdown of Larg impaired the mechanical activation of RhoA, while also preventing the ability of mechanical strain to suppress adipogenesis. Furthermore, the Rho GAP, ARHGAP18, was found to be essential for lineage allocation of MSCs as well. While ARHGAP18 did not influence the ability of RhoA to be activated in response to force, knockdown of ARHGAP18 reduced the tonic suppression of RhoA activity, resulting in increased actin cytoskeletal structure with enhanced osteogenesis and decreased adipogenesis³².

The increased accumulation of FA platforms following mechanical force not only brings signaling effectors to the sites of force transmission but provides a signaling hub

capable of amplifying signal transmission. This effect can be seen in the substantial increase in activation of Akt and β -catenin signaling following the insertion of a rest period between bouts of mechanical force¹⁸. As such, in response to the initial mechanical stimulus, signals are recruited to FA platforms³¹, where the enhanced cytoskeletal structure provides the necessary scaffolding to retain such signals where they are amplified in response to the second bout of mechanical input^{20,170}. The increased efficacy of a rest period in between two bouts of loading is also evident in tissue responses *in vivo* where twice-daily mechanical input, separated by five hours, attenuated adipose accumulation and improved glucose metabolism in response to high fat diet compared to a once-daily mechanical regimen of equal overall duration¹⁷⁴.

Cytoskeleton

The cytoskeleton provides a highly adaptable dynamic scaffolding by which cells move and interact with their environment. Remodeling of cytoskeletal elements, in response to mechanical force, not only provide a mechanism by which cell structure adapts to its physical environment but also repositions the mechanosensitive machinery in cells to amplify the activation of downstream mechanotransduction cascades upon subsequent loading events. In this section we will discuss the force bearing cytoskeletal networks including actin, microtubules and intermediate filaments. We will focus on how force alters the structure and signaling in these networks.

Polymerization of new actin filaments is largely modulated by actin related protein (Arp) 2/3 complex which acts as a nucleation core¹⁷⁵. Arp2/3 complex mediated actin branching events are also assisted by nucleation promoting factors from Wiskott-Aldrich syndrome (WAS) family of proteins including WASP, N-WASP and SCAR

which enable rapid polymerization¹⁷⁵⁻¹⁷⁷. Arp/23 complex and WAS family proteins also play a role in binding newly formed actin filaments to the WAS family proteins also play a role in binding newly formed actin filaments to the existing actin network^{178,179}.

Formins on the other hand regulate the end to end polymerization of F-actin. Formins are classified by the presence of formin homology 1 (FH1) and 2 (FH2) domains¹⁴⁷. Myosin related cytoskeletal contractility in stem cells is regulated by small Rho GTPases such as RhoA, Ras and CDC42A¹⁸⁰. RhoA activity increases the cell tension through its effector protein Rock, activating myosin light chain kinase, which in turn, activates the dimerized motor protein myosin II¹⁸¹. RhoA can be activated by variety of mechanical cues such as fluid flow, extracellular matrix (ECM), ECM compliance and vibrations^{20,151,182}. End result for RhoA activation is stress fiber formation in cells. Formation of these RhoA mediated stress fibers is context dependent. Under a fluid shear for example, stress fiber formation is parallel to flow direction^{151,183}. Under cyclic strain cells re-orient their stress fibers perpendicular to principal stretch direction^{184,185}. Different than both fluid shear and strain, Low Intensity Vibrations (LIV) result in robust F-actin bundling at the perinuclear region of cells²⁹. This perinuclear F-actin formation is concomitant to activation of F-actin modulators such as RhoA stimulator ARHGGEF11 (Rho Guanine Nucleotide Exchange Factor 11, +6-fold) and Arp2/3 complex regulatory protein WAS (+43-fold)¹⁸⁶. Therefore, F-actin cytoskeleton is not only load bearing but can adapt to mechanical force in a context dependent manner.

Aside from the “slow” adaptations of cytoskeletal networks through RhoGTPases, cytoskeleton also functions to transmit mechanical signals within the cell and this transmittance appears to be dependent on the cellular tension. In airway smooth muscle

cells for example, integrin bound surface deformation of $0.4\mu\text{m}$ (peak) deformed the nucleus and stress propagation within the cell was controlled by intracellular stress levels¹⁴⁴. This effect of intracellular stress levels on force propagation can be explained by the concept of tensegrity. Tensegrity dictates that cells are under a constant force-balance and thus even small local deformations to the cytoskeleton are compensated by the whole structure¹⁸⁷. Consistent with the hypothesis, fluid flow induced deformations in a single cell were weakly correlated with direction of the flow but instead propagated through cell structure in a multi-directional way¹⁸⁸. The tensegrity model also predicts instantaneous and non-linear cell stiffening under magnetically induced membrane deformations^{189,190}. These key studies open up a new perspective where mechanical signals are the first signals that propagate through the whole cell body even earlier than biochemical signals. These forces may use a pre-stressed cytoskeleton.

F-actin fibers are under constant stress, for example, initiation of F-actin polymerization and signaling requires forces in pN range ($\sim 10\text{-}50\text{pN}$)¹⁹¹. When F-actin fibers bundle, they generate more and more force. In smooth muscle cells, dissection of a single apical actin stress fiber generates a force of 65nN on the nucleus¹⁹². Similarly, switching between weak and strong actin coupling with nuclear envelope can generate up to 40nN force differentials. These forces generated by F-actin cytoskeleton results in micro/nano scale damage of individual fibers. One important molecule that play a role in repair of these small breaks is zyxin¹⁹³. Zyxin is a prominent member of focal adhesions but in contrast to other focal adhesion proteins that get recruited when force is present, zyxin leaves focal adhesion upon mechanical force and localizes to actin fibers that are damaged due to cellular contractions or extracellular deformation. This zyxin localization

to stress fibers then recruit other F-actin initiations such as α -actinin to fortify and repairs F-actin fibres ^{143,146,194,195} .

Intermediate filaments acts as stabilizers of the cytoskeleton, they play a role in resisting shear stress ¹⁹⁶ and provide stiffness to the cell nucleus ¹⁹⁷. We will discuss intermediate filaments in later sections within the context of nuclear structure.

Microtubules are the stiffest of the three building blocks of the cytoskeleton and can form long tracks that span the length the cell. During mitosis, these long and stiff networks assemble into radial arrays that function as central hubs and facilitate intracellular transport. It is not entirely clear if microtubules are directly involved in mechanosensory functions. However, microtubules are known to buckle under compressive loads in cells¹⁹⁸ and these compressive loads can increase the overall curvature and create fractures in microtubules. The relationship between microtubule fracture and intracellular forces suggests a regulatory mechanism ¹⁹⁹. Additionally, microtubules act to stabilize the cytoplasm and nucleus ²⁰⁰. When endothelial cells were stretched by pulling actin filaments, removal of functional microtubules resulted in the release of normal restriction of nuclear movement ¹⁹⁷, suggesting that microtubules may indirectly be involved in mechanosensory functions by protecting nucleus from extreme deformations.

Experimental evidence regarding the regulatory function of microtubule integrity on mechanosensing is not clear. For example, when microtubules were disrupted by colchicine, fluid flow increased cell sensitivity to further by increasing PGE₂ release in osteoblast cells ²⁰¹. A different study, however, showed muting of the PGE₂ response ²⁰². Showing that microtubules play a role in mechanotransduction but the mechanism by which the regulation is controlled is unknown.

Nucleus as a Mechanosensitive Organelle

The nucleus is the largest and most dense organelle found in our cells. In the last decade the understanding of nuclear functionality has shifted from a passive organelle to an active participant in the mechanisms of mechanosensing and mechanosignaling. In this section we will divide the nucleus into three main compartments: nuclear envelope, nucleoskeleton, and chromatin. First, the nuclear envelope will be discussed as the nuclear envelope is a unit that maintains a dynamic connectivity between the cytoskeleton and nucleoskeleton. Second, the nucleoskeleton will be discussed from the perspective of nuclear actins, microtubules and intermediate filaments (Lamin A/C and B). Finally, the chromatin will be introduced as a structural element and how chromatin organization may play a role in mechanosensing. Throughout these sections, the focus will be on both structural sensing mechanisms as well as identified signaling proteins that facilitate nuclear mechanotransduction. Additionally, important diseases that affect nuclear organization and mechanosignaling will be highlighted as modern medicine and science has been linking meachanosignaling and mehcanotransduction to known human pathologies.

Nuclear Envelope

The Nuclear envelope (NE) is a double membraned barrier that is composed of the outer nuclear membrane (ONM) and inner nuclear membrane (INM) which are separated by a 20-100nm perinuclear space. Despite continuity between the NE and the Endoplasmic Reticulum (ER), the ONM and INM house diverse protein groups that are not common to the ER ²⁰³. As the NE physically separates cytoplasmic and intra-nuclear compartments, a vital function of the NE is to interact with both the cytoskeleton and

chromatin to enable mechanical and biochemical communication between these two compartments²⁰⁴.

At the ONM the nucleus interacts with cytoskeletal networks via Linker of Nucleoskeleton and Cytoskeleton (LINC) complex¹⁵⁶. The LINC complex provides the physical coupling of the nucleus to the cytoskeleton by maintaining interactions with both actin, microtubule, and intermediate filament networks²⁰⁵. Giant isoforms of nesprin-1 and nesprin-2 reside at the cytoplasmic face of the ONM and provide the cytoskeletal tethering points for the LINC complex. N-termini of giant nesprins share a calponin homology (CH) domain that binds to actin with high affinity. The CH domains found in nesprin-1 and nesprin-2 giant isoforms are identical to that found in α -actinin^{206,207}. Presenting CH domain of nesprins to non-polymerized actin filaments promotes actin polymerization in-vitro²⁰⁷, suggesting that CH domains may act as initiation points for actin polymerization at the perinuclear region of the cytoplasm. Nesprins have been found to interact with microtubules through intermediate proteins such as dynein and kinesin^{208,209}. The N and C terminals of giant nesprin isoforms are connected together with larger spectrin repeat (SR) domains. Giant isoform of nesprin-1 has 72 SR domains while giant isoform of nesprin-2 has 56 SR domains²¹⁰, making the size of the proteins ~1000 and ~800 kDa, respectively. While these SR regions in giant nesprins are large, the role these regions play in mechanosensing is not well understood. It has been suggested that these regions may play a role in mechanical load transmission²¹¹. Interestingly, these SR domains are highly conserved across different species²¹⁰ and thus presenting putative binding sites for protein-protein interactions²¹¹ that maybe be important for mechanosensing. For example, FH1/FH2 domain-containing protein 1 (FHOD1), binds

to the SR region of giant isoform of nesprin-2. FHOD1 binding has been shown to increase the coupling strength between LINC complex and F-actin¹⁴⁸. Other cytoskeleton related binding partners of the LINC complex include actin bundling protein Fascin²¹². Indeed, recent findings via utilizing FRET based force sensors shown that giant nesprin-2 was under subject to myosin dependent tension²¹³. These force sensors are based on a so called nesprin-mini, a designed nesprin isoform that lacks SR repeat region. Overexpression of nesprin-mini increases the number of F-actin connections to nucleus and decreases nuclear size²¹⁴. There are number of naturally occurring isoforms of nesprin-1 and nesprin-2 that lack CH and large SR regions²¹⁵. These smaller α and β isoforms are found in both the cytoplasm and nucleus²¹⁶. The LINC complex also interacts with intermediate filaments through plectin, this interaction is however facilitated by Nesprin-3, a structurally distinct isoform of Nesprin²⁰⁵.

The C-termini of the nesprin proteins transverse the ONM and end in a conserved KASH (Klarsicht, ANC-1, Syne Homology) domain²¹⁷. The KASH domain interacts with Sun (Sad1p, UNC-84) proteins. In mammalian cells two isoforms are highly expressed, Sun1²¹⁸ and Sun2²¹⁹. The N terminal of Sun1 and Sun2 proteins start at the perinuclear space, transverses INM, and connects to nuclear a at the C terminal. The physical lengths of Sun1 and Sun2 are predicted to be similar to the distance between the ONM and INM^{220,221} and possibly play a role in maintaining the size of the perinuclear space. For example, shorter Sun isoforms shorten the distance between the INM and ONM, in contrast depleting Sun proteins increase the spacing between the INM and ONM²²². Proteins Sun1 and Sun2 are structurally similar and capable of forming strong trimeric structures that connect to the KASH domain of LINC complexes²²³. Further, depleting

either Sun1 or Sun2 is not sufficient to disrupt LINC complex connections¹⁵⁶. However, recent findings indicate that there are distinct functional differences between Sun1 and Sun2. For example, Sun2 anchorage to the INM requires Lamin A/C while Sun1 localization to the INM is less dependent of Lamin A/C¹³⁵. Instead, only Sun1 associates with the nuclear pore complexes (NPC)²²⁴. Functionally, Sun2 was found to be involved in actomyosin dependent nuclear connectivity while Sun1 function was preferentially important for meiosis²²⁵ and dynein mediated connectivity with microtubules²²⁶.

As discussed above, LINC complexes play a critical role in connecting the nucleus to the cytoskeleton. However, in recent years LINC complex connections emerged as important mechanotransduction elements for signaling molecules. The nucleus relies on both direct mechanical input as well as its molecular transducers to sense external stimuli and regulate gene expression. In mesenchymal stem cells (MSC) which reside in bone tissue, β catenin and Yap/Taz have been identified as two important molecular ‘transducers’ of mechanical information and rely on LINC-mediated connectivity to be functional. Residing in the cytoplasm, both β catenin and Yap/Taz are activated (de-phosphorylated) by mechanical strain^{227,228} and enter into the nucleus to function as transcription factors. Depleting nesprin-1 impairs strain-induced nuclear entry of Yap1 in MSCs¹¹³. It has been reported that the access of transcriptional coactivator Yap1 to the nucleus is facilitated through stretching of nuclear pore complexes (NPC) via F-actin contractility to facilitate its nuclear accumulation¹¹⁴. The LINC complex has an important role in β catenin nuclear access as well. β catenin does not possess a classic nuclear localization signal; instead, it transits through the nuclear leaflets via direct contact with the NPC^{141,229}. β catenin is localized on the LINC element nesprin-2 that

appears to provide a ‘launching-pad’ for subsequent nuclear entry²³⁰. It has been reported that untethering of nesprin-2 from the nuclear envelope displaces β catenin from the nuclear envelope, impeding its nuclear entry rate, reducing its nuclear levels and lowers the transcription of β catenin gene target Axin-2²³¹.

LINC-mediated physical coupling to the nucleus through the cytoskeleton is mechanoadaptive and plays a role in cell mechanosensitivity. Sun1 or nesprin-4 deficient mice fail to maintain the nuclear positioning in mechanosensory epithelial cells resulting in gradual hearing loss of the mice²³². This suggests that the LINC complex’s connections to the nucleus has a part to play in sensation of mechanical vibrations, such as those sensed as sound. When MSCs are subjected to high frequency (30-200Hz), low intensity (0.1-1g) vibrations that mimic muscle contractions^{233,234}, focal adhesion kinase (FAK) mediated RhoA activation and subsequent cytoskeletal remodeling are activated in MSCs²⁹. Depleting the LINC complex functionality via Sun1 and Sun2 specific siRNA sequences, or by overexpressing a dominant negative form of nesprin KASH domain, impairs vibration induced FAK and Akt phosphorylation²⁹. Importantly, stretching the substrate that the cells are attached to also activates FAK and Akt signaling²³⁵. However, depleting LINC function²⁹ or removing nuclei²³⁶ were not sufficient to inhibit strain activated FAK and Akt signaling. Strain-induced signaling was also intact in LINC deficient fibroblast²³⁷ but not in cardiomyocytes²³⁸. These findings suggest that the LINC complex may play a role in how cells sense certain mechanical information. Therefore, mechanical influences may cause gain or loss of function in the LINC complex to alter cell mechanosensitivity. In support of these observations, conditions that simulate unloading events such as microgravity results in the reduced expression of LINC

elements²³⁹. In contrast, LINC complex elements have increased expression in response to low intensity vibrations²⁴⁰. Ability of mechanical signals to regulate LINC complex implies that positive regulation of LINC complex elements through application of mechanical therapies such as low intensity vibrations may be leveraged to improve cell sensitivity to external mechanical and biochemical demands. Not surprisingly, application of low intensity vibration have been shown to amplify the response to other mechanical or biochemical factors in mice¹²⁹.

An important protein that plays a prominent role in nuclear envelope mechanotransduction is emerin²⁴¹. Functionally, emerin is an actin capping protein that binds to the pointed of ends of actin fibers and accelerate actin polymerization²⁴². When force is applied to epidermal stem cells, emerin enrichment at the ONM is accompanied by the recruitment of non-muscle myosin IIA to promote local actin polymerization at the perinuclear region²⁴³. Emerin also plays a role in nuclear export of β catenin as emerin depletion results in nuclear β catenin accumulation^{230,244-246}. Furthermore, direct application of force to isolated nuclei results in Src dependent emerin phosphorylation leading to increased nuclear stiffness in a Lamin A/C dependent manner²⁴⁷. Clinically, mutations of emerin are associated with Emery-Dreifuss muscular dystrophy (EDMD). EDMD is characterized by early contracture of the elbows and Achilles tendons, slow progressive muscle weakening and wasting, and cardiomyopathy with conduction block. There are two main genetic forms of EDMD: X-linked EMD (X-EDMD), and autosomal dominant EMD (AD-EDMD). The X-EDMD version is caused by a mutation in emerin while the AD-EDMD inherited version is caused by mutations in *LMNA*.

Another important regulator of mechanosensing is Torsin A. Torsin A is a nuclear envelope protein that belongs to AAA+ family (ATPases associated with various cellular activities) that utilizes ATP to unfold other proteins^{157,248}. Torsin A interacts with Sun1²⁴⁹, nesprin-3 α ²⁵⁰, a associated polypeptide 1 (LAP-1)²⁵¹, and emerin²⁵². While exact function of Torsin A in nuclear mechanotransduction is unclear it's functional role in the formation of perinuclear actin cables during rearward nuclear movement²⁵³ suggest that it is important in regulating the cytoskeletal dynamics at the nuclear envelope.

Nucleoskeleton

The term nucleoskeleton is used to describe the pellet of proteins that are precipitated during salt buffer extractions of cell nuclei²⁵⁴. This insoluble fraction of nuclear structure houses the nuclear a, chromatin, and cytoskeletal scaffolding. These proteins play a vital role in providing structural support to the nucleus, regulation of gene expression, and chromatin structure. Additionally, nucleoskeleton proteins have been linked to mechanical signal sensing and transduction. Nucleoskeleton proteins also affect human health as multiple human diseases have been linked to the misregulation and synthesis of nucleoskeleton proteins, causing a wide range of diseases ranging from deformed muscle tissue to inducing rapid premature aging. This section investigates the role of the nucleoskeleton proteins in mechanical sensing and signal transduction, human health, and regulation of chromatin.

Nuclear Actin and Microtubules

Although the role of actin within the nucleus is largely uncharted, the nucleus houses large number of regulators actin polymerization and depolymerization²⁵⁵. These components include mDia formins that catalyze end-on-end actin polymerization and

Arp2/3 complex elements necessary for actin branching¹⁴⁵. Actin can also be found in filamentous forms^{256,257} and as actin-cofilin rods²⁵⁸ within the nucleus. Importantly, during cell spreading, nuclear F-actin structures form in a LINC dependent manner²⁵⁹, suggesting actin polymerization as a potential target for mechanosignaling. In MSCs that are treated with cytochalasin D, cytoplasmic actin depolymerizes and rapidly enters into the nucleus²⁶⁰. The Influx of G-actin results in secondary intranuclear scaffolding that results in osteogenic differentiation in MSCs¹¹⁸. The effect of cytochalasin D can be abolished when actin branching is inhibited via arp2/3 ck666¹¹⁸. A consistent target for cytochalasin D targeted transcriptions is vestigial-Like 4 (VGLL4)²⁶¹ a regulator of the Hippo pathway that controls the interactions of Yap/Taz interaction with transcription factor TEAD. While cytochalasin D represents a chemically induced effect of actin influx into nucleus, persistent actin polymerization in the nucleus have been shown to reduce mRNA transcription²⁶², suggesting a common, actin-related pathway. Not surprisingly, nuclear actin has also directly been implicated in gene transcription through its association with RNA polymerases. Immunoprecipitation assays have shown that nuclear actin directly interacts with RNA polymerase II²⁶³. As such, the intranuclear state of actin controls both the availability of genes to their transcription factors, and the transcription.

Nuclear cytoskeletal elements, in conjunction with LINC complex elements play a role in directing DNA repair. For example, inhibiting actin polymerization alters telomere dynamics²⁶⁴. During post mitotic genome reorganization, the LINC protein Sun1 and GTPase rap1 (Ras-proximate-1 or Ras-related protein 1) mediate telomere tethering on to the nuclear envelope²⁶⁵. As telomeres function to protect ends of

chromatin from DNA repair machinery²⁶⁶, mechanically induced changes to the nuclear actin structure may play a role in cellular health. Microtubules also contribute to the DNA repair machinery from both inside and outside of the nucleus. It has been reported that microtubules, in conjunction with the LINC complex and double-strand break repair protein 53BP1, generates pockets within the nuclear interior to direct double stranded DNA break mobility²⁶⁷. While the extent of nuclear microtubule machinery and its responsiveness to mechanical cues is unknown, existence of DNA-damage inducible intranuclear microtubule filaments were recently discovered²⁶⁸, suggesting that traditional cytoskeletal proteins may play an important role in sensing and responding to mechanics within the cell nucleus.

Lamin A/C

A and C are part of the protein family which A and C can be further classified as A-type lamins. All proteins are considered intermediate filaments. A-types are expressed by the same gene called *LMNA*¹³³. Alternative splicing produces either A or C, most often termed Lamin A/C proteins. Both A-type s and B-types, which B-types will be discussed in the next section, share similar protein domains with other intermediate filaments as they are comprised of a N-terminal head domain, coiled-coil central rod domain, and a C-terminal domain. Both types also have unique features such as a nuclear localization signal (NLS), an immunoglobulin (Ig)-fold domain, and a chromatin binding site¹³². During maturation A undergoes posttranslational modification in the CAAX motif located in the C-terminal. The CAAX motif allows for modifications at the cysteine residues where farnesylation and proteolytic processing occurs. Other modifications include carboxymethylation of new C-terminal residues and isoprenylation. Finally, a

second proteolytic event occurs that is mediated by zinc metalloproteinase ZMPSTE24 which removes 15 amino acids from the end of the C-terminal. This secondary proteolytic cleavage removes any previously modified cysteines to form the mature A¹³². Interestingly, C escapes these modifications because it lacks a C-terminal due to the alternative splicing of the *LMNA* gene. These posttranslational modifications during maturation of A play an important role in human pathologies related to proteins, termed laminopathies, as most laminopathies are related to an altered posttranslational modification or a loss-of-function of ZMPSTE24²⁶⁹.

All A-types are not constitutively expressed but are expressed during and after differentiation into specific tissues. For example, Lamin A is not detected in the brain cells of mice until several days after birth⁵ and embryonic cells display very low levels of Lamin A/C²⁷⁰. One of the prominent roles of Lamin A/C is to maintaining the nuclear mechanical competency based on extracellular mechanosensing. Not only the depletion of A and C result in a softer nuclei²⁷¹ Lamin A/C levels in resident tissue types positively correlate with the tissue stiffness²⁷². One of the mechanisms that regulate Lamin A/C levels based on physical force appears to be its phosphorylation. Fluid shear stress for example have been shown to expose the Cys⁵²² residue of Lamin A/C Ig tail domain and Ser/Thr phosphorylation of these residues appear to be inversely correlated with Lamin A/C stability²⁷². In this way, increasing matrix stiffness reduces the Ser/Thr phosphorylation and result in increased protein levels of Lamin A/C²⁷³. This correlation between matrix stiffness and Lamin A/C levels may be seen as a protective mechanism to shield cell nuclei from excessive environmental force and may serve to blunt the effectiveness of mechanical force on the chromatin in order to maintain normal

transcriptional activity. Not only cells with Lamin A/C depletion or mutation are more sensitive to mechanical damage^{272,274} Lamin A/C was also shown to recruit perinuclear actin cables upon cyclic mechanical stretching to shield nucleus from mechanical damage⁴⁹. However, alternative protective mechanisms also exist to shield genome in embryonic stem cells with very low levels of Lamin A/C²⁷⁰. As embryonic stem cells have an open chromatin state with little or no heterochromatin²⁷⁵, during the transition phase between un-differentiated to a pre-differentiation states, the nucleus becomes auxetic, an intrinsic material behavior described by the ability to shrink transversely when compressed in longitudinal direction (i.e. negative Poisson's ratio)²⁷⁶. This auxetic property of embryonic nuclei increases the compression modulus considerably²⁷⁷ thus protecting the chromatin from mechanical perturbation.

Interestingly, cancer cells also display reduced levels of Lamin A/C and LINC complex elements²⁷⁸. As cancer cells are characterized by uncontrolled gene expression, loss of Lamin A/C in these cells supports the important role of Lamin A/C in regulating chromatin dynamics as well as the subsequent control of cell fate²⁶⁶.

Laminopathies describe a breadth of human pathologies. Currently, there are 15 known diseases that are directly linked to mutations in *LMNA* and altered synthesis of Lamin A/C²⁶⁹. Changes in Lamin A/C produce four main clinical phenotypes: striated muscle diseases, lipodystrophic syndromes, peripheral neuropathy, and accelerated aging diseases. One of the most well-known laminopathies is Hutchinson-Gilford progeria syndrome, also known as progeria. Progeria is an aging disease that induces premature aging. It is hallmarked by postnatal growth retardation, premature atherosclerosis, generalized osteodysplasia with osteolysis, micrognathia, absence of subcutaneous fat,

alopecia, and pathologic fractures. The cause of progeria is a dominant silent mutation in exon 11³. This silent mutation leads to a splicing defect and a generation of a smaller prelamin A variant, creating a new splice variant called progerin. Progerin has permanent farnesylation and carboxymethylation which causes a loss of the cleavage site, not allowing for the secondary proteolytic event to occur²⁷⁹. This induces progerin accumulation in the nuclear periphery. Interestingly, progerin accumulation also accompanied with upregulation of LINC element Sun1. For example, farnesylated producing mice¹³⁴ with *lmna*^{L530P/L530P} (*Lmna*Δ9) mutation²⁸⁰ shown increased presence of Sun1 in its nuclear NE and ER membranes and Sun1 depletion was sufficient to partially rescue the bone phenotype¹³⁶. While why Sun1 accumulation leads to decreased bone phenotype is unclear, fibroblasts from progeria patients as well as progerin expressing fibroblasts also show abnormal Sun1 accumulation. This accumulation of Sun1 preferentially results in cell polarity defects due to increased Sun1 interaction with microtubules²²⁶. Importantly, similar effect are also seen in fibroblasts from aged patients, that show low levels of the progerin production and display irregular nuclear geometry²⁸¹. Critically, during aging skeletal tissues display increased bone marrow fat and reduced bone quality²⁸². One possible mechanism that explains why both progeric and aged cells cannot respond to mechanical signaling may be the relation between βcatenin mobility and LINC complex. Both *Lmna*Δ9 mice as well as *Lmna*Δ50 cells display reduced effectiveness of Wnt activity and decreased βcatenin levels²⁸³. Our work *in vitro* further shown that disabling LINC function via depleting Sun1 and Sun2 results in decreased βcatenin function and increased adipogenic bias in

MSCs²⁹. These findings suggest that age related alteration in nuclear envelope and nucleoskeleton may result in how cells respond to their mechanical environments.

Lamin B

A second type of s are classified as B-type lamins which is made of two different proteins, Lamin B1 and B2 which are also intermediate filaments. Unlike Lamin A/C, Lamin B1 and B2 are expressed from two different genes *LMNB1* and *LMNB2* which are located on chromosome 5 and 19, respectively⁵. As noted previously B-type lamins also have the same domains as A-type lamins. Additionally, during maturation B-type lamins also experience similar posttranslational modifications such as farnesylation at cysteine residues, proteolytic processing, and carboxymethylation. However, B-type lamins do not have any secondary proteolytic processing where 15 amino acids are cleaved to remove the farnesylated and carboxymethylated sites. Instead, mature B-type lamins permanently maintain farnesylated and carboxymethylated tails. Known laminopathies are also linked to B-type lamin mutations²⁸⁴.

One B-type lamin disease is adult-onset leukodystrophy. This disease is linked to autosomal dominant mutations in the gene *LMNB1*. Adult-onset leukodystrophy is hallmarked by demyelination of the central nervous system. This disease is similar to multiple sclerosis as there is a widespread demyelination of the central nervous system. The cause of Adult-onset leukodystrophy is linked to duplication of the genomic region containing *LMNB1* leading to an increase in Lamin B1. While it is not known fully how overexpression of Lamin B1 leads to adult-onset leukodystrophy it is hypothesized that when Lamin B1 is overexpressed it causes abnormal nuclear shape that is more susceptible to physical disturbances to the nucleus²⁸⁵. Not to be left out, Lamin B2 is

indicated in acquired partial lipodystrophy²⁸⁴. Acquired partial lipodystrophy is the loss of subcutaneous adipose tissue in areas around the neck, face, arms, and legs. Recent studies have discovered that patients with heterozygous mutations in *LMNB2* are susceptible to acquiring partial lipodystrophy²⁸⁵. B-type lamins have an important role in the mechanical properties of the nucleus and in differentiation.

B-type lamins are associated with providing elastic properties to the nucleus. B lamin proteins confer these properties to the nucleus by being located underneath the inner nuclear membrane²⁸⁶. Unlike Lamin A/C, Lamin B proteins do not associate with the NPCs nor do they associate with Lamin A/C. Instead, Lamin B proteins bind to Lamin B receptor (LBR) located in the nuclear membrane²⁸⁷. B-type lamins role in mechanical signal sensing and transduction is contrastingly small compared to Lamin A/C. In cells with defects in Lamin B1 few changes in the cells mechanical sensitive genes are detected as well as changes in the nuclear mechanics when a mechanical force is applied²⁷¹. In relation to chromatin regulation, when chromatin was removed from cells Lamin A/C was uncovered but Lamin B was not²⁸⁸.

Chromatin

Chromatin is the level of DNA packaging where the DNA wrapped around histone proteins that are then wrapped more tightly to form into nucleosomes. Euchromatin and heterochromatin describe the origination of the nucleosomes. Euchromatin is lightly packed nucleosomes commonly referred to as “beads on a string” and allows for transcription to occur on exposed genes. Heterochromatin is tightly packed nucleosomes forming a 30-nm fiber that does not allow transcription of enclosed genes to occur. Chromatin binding domains have been found on both A-type and B-type lamins.

Chromatin close to s in the nucleoskeleton forms heterochromatin²⁸⁹. This is a result of the s along with a class of proteins called LEM proteins, as LEM proteins anchor the chromatin to the INM. The LBR and A-type lamins are very important to chromatin localization as loss of both the LBR and A-type lamins cause heterochromatin to localize in the interior of the nucleus²⁸⁹. This occurs because the LBR and associated polypeptides (LAP) tether the chromatin to s ²⁹⁰. s can also directly bind to DNA through matrix associated regions (MARs) in the DNA. These MARs are AT-rich and are located at the beginning and end of protein coding genes and organize the chromatin into distinct functional chromosomal territories²⁹¹.

Role of chromatin as a load bearing structure is a relatively new concept. Earlier studies with micropipette aspiration and atomic force microscopy assays shown that chromatin significantly contributes to the apparent nuclear modulus^{82,292}. As cells differentiate from embryonic state, they accumulate heterochromatin in order to silence unwanted gene regions²⁹³, consequently inhibiting heterochromatin regulators such as ezh2 to uncover histone embedded gene regions is a robust way to affect cell differentiation²⁹⁴. When stem cells differentiate, their nuclei become stiffer^{295,296}. Importantly, chromatin is directly subjected to mechanical force from extracellular environment. For example, deformation applied to cell membrane via magnetic beads, transmitted to nuclear surface through LINC complexes and directly regulate the displacements of coilin and SMN proteins in nuclear Cajal bodies²⁹⁷. Additionally, mechanical forces may cause detachment of the chromatin from s , allowing for genes to be accessible to transcription initiation factors²⁸⁷. In this way, not only pharmacological regulation of histone modifications regulate nuclear stiffness¹¹² but mechanical forces

applied to cell membrane directly alters heterochromatin dynamics²⁴³ and chromatin organization²⁹⁸. While the mechanisms by which heterochromatin altered by mechanical challenge is an underexplored question, chromatin should be considered as a load sensitive compartment with a self-regulatory functions.